UNIVERSITY OF ARKANSAS

Graduate Institute of Technology

Department of Electronics and Instrumentation

Research Grant NGL 04-001-007

National Aeronautics and Space Administration

September 30, 1969

Informal Status Progress Report

for

NASA Research Grant NGL 04-001-007

for the period ending

September 30, 1969

INVESTIGATION OF LASER PROPERTIES RELEVANT TO THE MEASUREMENT OF DIFFERENT PHYSICAL PARAMETERS

Department of Electronics and Instrumentation

University of Arkansas Graduate Institute of Technology

Little Rock

M. K. Testerman

M. K. Testerman
Principal Investigator

Date

TABLE OF CONTENTS

I. Measurement of Small Phase Variations in Static and Transient Optical Fields

G. S. Ballard and S. Sengupta

Introduction

A variation of the double-exposure holographic interferometer technique has been reported [1,2] in which a separate reference beam is used for each of the dual hologram exposures. This method possesses all of the well known advantages of the typical double-exposure hologram while combining the flexibility of information presentation found in conventional interferometers. It has further been shown that the separate reference beam hologram can be used to measure small phase variations in an interference field[2]. Phase shifts as small as 1/60 of a wavelength have been measured. The lower limit of these measurements was due to small path length changes in the two reconstructing beams, resulting in an uncertainty in the observed data.

It has been proposed that the separate reference beam method of double exposure holographic interferometry be further investigated in order to study new techniques which will make it possible to measure smaller phase changes in interference fields. One specific technique to be evaluated was as follows:

If the relative phase of the two reconstructing beams is varied in a periodic manner, a photo-detector placed at some point in the reconstructed interference field will produce a periodic signal as conditions of constructive and destructive interference are reached at that particular point. A second detector, placed at some other point in the field, will also produce a periodic signal. This second signal will exhibit a phase angle with respect to the first signal, the difference in phase of the signals being identical to the difference of phase of the two points in the interference field at which the

two detectors are located. If one of these detectors is kept stationary while the other is scanned throughout the field, the phase difference of the signals can be measured and a map of the relative phase of each point throughout the field can be obtained.

The periodic variation of the two reconstructing beams can be accomplished by utilizing a diffraction grating as a beam splitter. The grating will diffract the laser beam into a zero order and various higher orders. If the diffraction grating is moved laterally, the higher diffracted orders will experience a phase change with respect to the zero order beam. For the first diffracted order, this phase change will be 360 degrees each time the grating is moved a distance equivalent to the grating spacing. By continuously displacing the grating laterally, the phase of the diffracted beam will vary periodically with respect to the zero order. The zero order and a higher order diffracted beam can be used to form the two reconstructing beams in the separate reference beam technique. This should eliminate the effects of slight changes in path length between the two reconstructing beams which proved to be the limit of sensitivity encountered in the previously reported experiments. These small changes will affect the signal on both detectors in an identical manner. They will appear as a slight frequency modulation in both signals, but the relative phase will not be affected.

Work Performed

Work has proceeded in an effort to fabricate the system as described in the proposal and reviewed in the introduction of this section of the report.

The diffraction gratings to be used as beam-splitters were obtained by recording the interference pattern of two coherent beams with plane wavefronts

on Kodak 649-F high resolution glass plates. The two interfering beams were of equal intensity so as to achieve maximum fringe contrast, and the photographic exposure was chosen for maximum brightness of the first order diffracted beam. The two beams were made to interfere at an angle of approximately 55 degrees, which would give a fringe spacing of 1300 lines per millimeter. This angle was chosen only for convenience in using the available work area in later steps and is otherwise not critical.

In spite of the optimization of the grating recording, the first order diffracted beam was prohibitively dim. In order to increase diffraction efficiency of the gratings it was necessary to treat them with ammonium bichromate bleach. It is well known that bleached holograms or gratings exhibit a greater intensity in their diffracted orders than amplitude gratings[3].

The results of bleaching the gratings were very disappointing. In some cases the diffration efficiency of the bleached gratings were no greater than that of the amplitude gratings. The best results as far as efficiency is concerned were obtained when "old" gratings which had been processed as amplitude gratings some weeks previously were immersed in the bleaching solution, washed, and allowed to dry. Both the zero order and first order beams of the bleached gratings exhibited great non-uniformity of intensity after they were expanded and collimated. One particular grating was more uniform than the others and was chosen for use. A later attempt to make more gratings was even less successful as the resulting beams were more non-uniform and completely unuseable. It has been determined that the bleaching step is responsible for a deterioration of the emulsion. The reason for the completely adverse results of the latter bleaching efforts has not been determined. Photographically

produced diffraction gratings are ideal for this particular application, but the bleaching process must be optimized so that routine production of these gratings can be accomplished.

The periodic variation of the phase of the reconstructing beams is to be accomplished by displacing the grating laterally. The motion of the grating must be smooth and free of vibration, otherwise the output of the device will be distorted. Vibration, chatter, and tilt of the grating cannot be tolerated. A carriage was designed with which it was anticipated that the stringent motion requirements would be met. Precision shopwork and components were used in the fabrication of the carriage. The grating is moved by a lead screw which, in turn, is driven by a 4.7 rpm motor through a flexible coupling. The threads on the lead screw were cut so that the ultimate speed of translation, together with the line spacing of the grating, would give an output signal of approximately 220 Hz. This frequency was chosen because it lies within the allowable range of the phase meter to be used and is not a multiple of the line frequency (60 Hz).

In operation, it was determined that the carriage motion was not uniform and the resulting output signals and phase measurements were erratic. At least part of this particular problem has been traced back to motor vibration. These vibrations were transmitted to the carriage and grating through the flexible coupling. This coupling is currently being replaced by a belt and pully arrangement with which it is hoped the motor vibrations will no longer be a source of error.

The optical arrangement for recording a double-exposure hologram with separate reference beams is shown in Figure 1. The beam from a laser source is incident upon the bleached diffraction grating. The first order diffracted beam is expanded and collimated, forming reference beam R_1. The zero order

beam is likewise collimated and forms reference beam R_o. A portion of the brighter zero order is reflected by a beam splitter prior to collimation and used to form the object beam R_{obj}. Each of these three beams is adjusted so as to be of approximately equal intensity.

The double-exposure holographic interferogram is recorded by placing the test object in beam R_{obj} and blocking off beam R_o. A hologram is then recorded using R_1 as the reference. The object is then removed from R_{obj} and beam R_1 is blocked off. A second exposure is made, which is a hologram of beam R_{obj} without the test object using R_o as a reference. The hologram is then developed in the normal manner.

After development the hologram is replaced in its original position. If illuminated by beam R_1 alone, R_{obj} with the test object is reconstructed. Illumination by R_o alone reconstructs R_{obj} without the test object. Illumination by both the reference beams results in coincident reconstructions of both the test scene and the comparison beam and phase variations in the test object on the order of at least 1/2 wavelength are visible. These reconstructions proved to be quite dim, so the hologram was bleached to improve the brightness of the two beams. It was again noticed that the uniformity of the reconstructions deteriorated after bleaching. The effect here was not as severe as that noted earlier, as these reconstructions were not expanded. The effect appeared as small scale imperfections rather than the gross variations encountered with the gratings.

No test object was in the holograms used in these experiments. It was decided to record the same identical wavefront, R_{obj}, with each of the reference beams. In this way, the phase variation in the reconstructed scene could be changed at will from no phase variation to gross phase variations by

adjusting the angle of one of the reconstructing beams. Thus, one hologram could be made to serve as many objects by a simple adjustment.

The ultimate phase measurements are made on an AN/URM-67 phase monitor. This instrument measures the phase angle between two periodic signals over the range of 20 to 20,000 Hz to an accuracy of ±1.0 degree. The required amplitude of the input signals is 2.0 to 30 volts peak.

The detectors are two dentical LS-400-NPN silicon planar photo devices. The relative spectral response of these devices at 6328A is about 55%. The maximum sensitive area is approximately 0.082 inch, or essentially a point.

The outputs of the two detectors are amplified by identical operational amplifiers, Dual MC 17098. The gain of the amplifiers is adjusted to approximately 1000 so the minimum input requirements of the phase detector can be met. A circuit diagram of the detector-amplifier circuit is shown in Figure 2.

The method of measuring the small phase variations in the holographically recorded test scene is shown in Figure 3. With the grating in motion, the output from one of the detectors was displayed on an oscilloscope and is shown in Figure 4. Upon visually examining this signal, large variations in its amplitude were quite noticeable. These variations were due to the non-uniformity of the reconstructing beams, brought about by bleaching the grating. The signal was also seen to show little resemblance to a sine wave. Thus far two causes have been found for this. One cause is the motor vibration mentioned earlier; the second is a slight bend which has shown up in the carriage lead screw. Both of these are now being corrected. Upon applying the outputs of the two detectors to the phase monitor, it was observed that the indicated phase was not constant but fluctuated over a wide range. As noted before, it has been determined that the motor vibrations are a major contributing factor.

Conclusions

The ultimate sensitivity of this system for measuring very small phase changes has not as yet been determined. A number of problems have appeared which must be solved before the system can match the sensitivity of the phase meter, which is ±1 degree. One of these problems is the non-uniformity of the reference beams formed from bleached photographic gratings. Another problem is the fluctuation of the phase meter readout. Two contributors to this difficulty have been found, but whether their elimination will be effective in utilizing the inherent accuracy of the phase meter has yet to be determined. In spite of these difficulties, it has been shown that the system as described is generally performing as expected. The overall system is quite stable and simple to align and operate.

Future Work

The area of first importance is the stabilization of the phase measurement. The carriage drive is being changed in an effort to completely isolate the motor from the carriage. The carriage itself is being re-worked to improve its smoothness of operation. Also, an Ealing 22-9583 optical bench carrier with transverse travel is being modified to serve as the grating translator. Methods of varying the phase of the two reconstructing beams other than that described have been considered. The moving grating seems inherently more desirable than any of the other methods. However, if the output cannot be stabilized to the degree desired, these other methods will be tested.

Methods of obtaining high efficiency gratings of equally high quality will be investigated. The photographically recorded interference grating has several advantages over commercial diffraction gratings. One advantage is that

the photographic grating can be custom made for any situation. They are inexpensive, easy to produce, and appear to be of a quality at the very least as good as commercial replica gratings. After bleaching, the first order diffracted beam is slightly more intense than that obtained from a commercial grating. The one difficulty is that the present bleaching process deteriorates the emulsion. If this can be overcome or at least minimized, the photographic grating would be ideal.

At the present time, the detectors and their associated circuitry are mounted in rather bulky packages that prevent their scanning the entire reconstructed interference field. These will be mounted in a compact package that will allow the field to be scanned to a degree consistent with the small diameter of the detector itself.

It has been observed that if one of the collimators that forms the reconstructing beam is replaced with another component, interference fringes are observed in the reconstructed output. These fringes represent variations in the original wavefront with which the hologram was recorded and the wavefront with which it was replaced. The instrument therefore can be used to compare optical elements. This ability, coupled with the measurement of small phase variations, may lead to a simple device for testing optical components to great accuracy. This application will be investigated, as well as any other minute measurements for which the device may be adapted.

II. Measurement of Film Grain Noise

D. L. Wankum

Introduction

In the NGR 04-001-007 Progress Report of September 30, 1968, a limited discussion was given to some of the observed effects which film grain noise have upon the quality of photographic and holographic images. Reference was made to the fact that film grain noise became significant when recording holograms of weakly illuminated objects. These recordings consist of density variations in the film caused by exposure to the incident reference and object beams, as well as random transmittance variations caused by the growth of film grain centers during development. If the corresponding spatial frequencies of the signal and the film grain centers are the same, the diffracted light of the hologram reconstruction will appear noisy. The resulting decrease in the signal-to-noise ratio will eventually cause a loss in image resolution, as well as producing a low contrast image. This effect is noted more in the large grained films such as Tri-X and Panatomic-X.

It is desirable to study the properties of this noise source separate from any recorded information or signal. In the last report, a procedure was described in which a piece of film was fogged by exposing it to the incoherent light from a tungsten source. The film was then processed using standard developing procedures. By using incoherent light, a uniformly dense film grain matrix resulted. Exposure to coherent radiation would have resulted in speckling, another noise source, which complicates the grain structure and does represent recorded information on the film.

In order to study the noise properties of the uniformly exposed emulsion, a parallel beam of monochromatic coherent light is passed through the film

grain matrix. Some of the light passing through the film is scattered by the developed grains. In addition to this noise, variations in both the refractive index and the thickness of the emulsion also contribute to the overall scattered light pattern. These additional sources of scattering are inherent in the emulsion and, like the grain noise, are not associated with signal information. Diffraction occurs as the uniformly intense plane, coherent wavefront passes through the gelatin emulsion. The light diffracted at some particular angle emerges as a plane wave. The entire wavefield emerging from the emulsion expands into a spectrum of plane waves encompassing a solid angle of possibly 2 pi sterradians.

By using ideal lenses, the spectrum of plane light waves can be focused to a spectrum of continuous points. This light intensity pattern is similar to the intensity pattern that would be observed in the Fraunhofer diffraction pattern, and can be related back to the size of the localized noise generating centers present in the emulsion. In fact, the detection, measurement, and recording of the diffraction pattern is sufficient to quantitatively analyze the spatial frequency spectrum of the film grain matrix and localized variations of the refractive index and thickness of the emulsion. All three of these parameters contribute to the diffraction pattern if the emulsion is not placed in a liquid gate.

Vander Lugt and Mitchell[4] describe clearly the conventional way in which the scattered light is focused to obtain the diffraction pattern. A stationary lens is placed in the wavefield of the scattered light. Parallel waves are focused in an angular range from 0 degrees to approximately 10 or 20 degrees off-axis. A light detector with a small filtering aperture is then used to measure the intensity variations of the light in the focal plane of the lens. The focal plane may be referred to

as the spatial frequency plane of the lens. The use of smaller f-number lenses only serves to increase the aberrations of the image in the focal plane. This reference has been made to point out the disadvantage of using a stationary lens. In the spatial frequency spectrum analyzer built at the University of Arkansas Graduate Institute of Technology and described in this report, the lens, pinhole spatial filter, and detection system are mounted on a rotating arm which is continuously incremented in a circular arc about the sample. The diffraction pattern of a scattering medium can be scanned from 0 to approximately 80 degrees, and it is not important that the lens being used possess the capability for off-axis imaging. Low cost, simple thin lenses or a cemented doublet, corrected for spherical aberration, can be used.

The construction, operation, and calibration of the spatial frequency spectrum analyzer described in the Renewal Proposal for NASA Grant NGR 04-001-007 of December 2, 1968, which can perform the functions described above is the subject of this report.

Work Performed

A schematic drawing of the Spatial Frequency Spectrum Analyzer described in this report is shown in Figure 5. The light from a HeNe laser is expanded, collimated, and directed so as to be incident upon a sample holder. The light scattered by the sample at some particular angle is focused by a lens onto a pinhole spatial filter. The light passing through the filter is incident upon a detector, the output of which is ultimately displayed on a recorder. The focusing lens, pinhole, and detector are all mounted upon an arm which rotates in

an arc about the sample. This enables the entire scattering spectrum of the sample to be detected and recorded.

Most of the design characteristics of the spectrum analyzer can be made using the generalized diffraction equation

$$d^* = \frac{1}{d} = \frac{2}{\lambda} \sin \left(\frac{C}{2}\right) \tag{1}$$

where C is the angle between two intersecting parallel beams of coherent monochromatic light of wavelength λ which cross in space to form an interference pattern. The pattern which is produced consists of many small planes of localized light variations. The spatial distance d between these planes is often written in terms of its reciprocal d^*. This quantity effectively expresses the number of interference planes in a unit distance of space. Conversely, the diffraction pattern from a grating may be described by a similar equation

$$nd^* = \frac{2}{\lambda} \sin \left(\frac{C}{2}\right) \tag{2}$$

where n is the order number of the diffraction pattern, and C is the angle between two similar orders of diffraction. The diffraction angle C will change if the wavelength of the light is changed. To maintain a 1 to 1 correspondence between the spatial frequency and the diffraction angle, a coherent monochromatic laser source is used in the spatial frequency analyzer. The laser used is a 1 mw HeNe CW laser operating at a wavelength of 6328 A. The output of this laser is a beam approximately 2 mm in diameter. This beam is expanded by means of a collimator which consists of a 20X microscope objective, a 5 micron pinhole aperture which spatially filters out any deviated rays caused by laser mirror imperfections, and a long focal length lens to render the diverging light from the pinhole parallel. The long focal length lens permits

the beam to expand over a relatively long distance before collimation. In this way, a small portion of the expanding beam will be collimated and localized intensity variations are minimized.

For analysis, a sample is placed in an adjustable holder. Adjustments along three orthogonal axes allow for exact positioning of the sample. The sample holder assembly may be seen at the far right of Figure 6. The holder also allows the sample to be rotated 360 degrees about the axis of the incident laser beam. With the holder shown, an area of the sample ½ inch in diameter can be analyzed. The focusing lens can also be seen in Figure 6. It is located just to the left of the sample holder.

Jenkins and White[5] discuss the experimental procedure for simulating the Fraunhofer diffraction pattern in the laboratory using lenses. A lens is placed parallel to the plane of the wave front. Parallel light entering the lens from a wavefield under study is focused to a point in the back focal plane of the lens. Along with this focusing, the intensity of the diffraction pattern increases simply because r has been decreased from some large value to f. When lenses are used, $r = f$.

The entire diffraction pattern cannot be focused with a single lens. The edges of the lens and lens aberrations limit the field of view and distort the image. However, that portion of the pattern which is focused near the optical axis of the lens is a good approximation to the actual diffraction pattern. In this region, the lens suffers little from the lens aberrations. For ideal lenses, the diffraction equation is given by

$$G(l,m,f,t) = \iint_{xy} U(x,y,t) \exp -j \left[\frac{2\pi \sin \left[\tan^{-1} \left(\frac{l}{f} \right) \right]}{\lambda f} x + \frac{2\pi \sin \left[\tan^{-1} \left(\frac{m}{f} \right) \right]}{\lambda f} y \right] dxdy \qquad (3)$$

where U(x,y,t) is the light amplitude distribution in the plane wave-field under study, G(l,m,f,t) is the light amplitude distribution in the focal plane of the lens, and angles A and B are replaced by trigonometric substitution with l and m. These variables are illustrated in Figure 7.

Fraunhofer diffraction has been applied to optical data processing in recent years by several workers[6-11]. These workers used a coherent monochromatic light source and quality lenses to observe a portion of the diffraction pattern. Certain conclusions can be reached if the following properties are considered:

1. The wavelength of the incident radiation is held constant.
2. Small scattering angles are only considered where the obliquity factor is 1.
3. The lens used in forming the diffraction pattern is assumed to possess negligible aberrations over the angular scattering range of interest.
4. The amplitude function U can be separated into a time and space function, that is,

$$U(x,y,t,) = u(x,y)T(t) \qquad (4)$$

When these four properties are considered and the angle of scattering is limited to ±6 degrees, the resulting diffraction equation differs by a factor from the Fourier Integral.

$$G(l,m,f) = \iint_{xy} \frac{u(x,y)}{\lambda f} \exp^{-j} \left(\frac{2\pi l}{\lambda f} x + \frac{2\pi m}{\lambda f} y \right) dxdy \qquad (5)$$

where

$$\frac{1 + \cos \theta}{2} \doteq 1 \qquad (6)$$

and

$$\sin \tan^{-1} \left(\frac{l}{f}\right) \doteq \frac{l}{f} \qquad (7)$$

$$\sin \tan^{-1} \left(\frac{m}{f}\right) \doteq \frac{m}{f} \quad . \qquad (8)$$

From the Law of Conservation of Energy, the total power can be found from either u(x,y) or G(l,m) by either of the two equations below.

$$P_t = \iint_{xy} u^2(x,y)\, dxdy \qquad (9)$$

or

$$P_t = \iint_{lm} G^2(l,m)\, dldm \; . \qquad (10)$$

The overall conclusion which has been made is that the lens is capable of performing a Fourier decomposition of a wavefield into a spectrum of plane waves and that properly designed lenses are capable of doing this Fourier Integration with good accuracy. In this respect, the lens is called a spectrum analyzer.

Monochromatic aberrations can be useful in estimating the focusing aberrations of lenses. The most important of these is spherical aberration. Coma, astigmatism and curvature of the field are in some way affected in off-axis focusing but become negligible for on-axis focusing. Spherical aberration is the only monochromatic aberration which is relatively constant even to off-axis imaging.

From third order theory, Jenkins and White[12] show that the equation for spherical aberration of thin lenses is

$$L_s = \frac{h^2}{\delta f^3} \cdot \frac{1}{n(n-1)} \cdot \left[\frac{n+2}{n-1} q^2 + 4(n+1)\, pq + (3n+2)(n-1)p^2 + \frac{n^3}{n-1} \right] \quad (11)$$

where n is the refractive index of the lens, and p and q are its position and shape factors, respectively, and given by

$$p = \frac{s' - s}{s' + s} \quad (12)$$

and

$$q = \frac{r_2 + r_1}{r_2 - r_1} \quad (13)$$

where s and s' are the object and image distances, respectively; r_1 is the radius of curvature which corresponds to that surface through which on-axis parallel light first passes; and r_2 is the radius of curvature of the second surface.

The variable L_s is a convenient method used to relate the image distance s_h' of any parallel ray passing through the lens at some distance h from its center to image distance s_p' of paraxial rays where h = 0. The quantity L_s is given by

$$L_s = \frac{1}{s_h'} - \frac{1}{s_p'} \quad (14)$$

It is these later rays which are least aberrated by the nature of the spherical surfaces and are those which are used as a reference in measuring the spherical aberration produced by the marginal rays.

Spherical aberration is measured by two distinct quantities, termed longitudinal and lateral spherical aberration. These quantities give a relative measure of the change in the focal length that results using

marginal rays and the amount of lateral displacement that occurs when those rays ultimately cross the paraxial focal plane. Longitudinal and lateral spherical aberrations are defined by the equations

$$\text{Long. S.A.} = s_p' - s_h' \tag{15}$$

$$\text{Lat. S.A.} = (s_p' - s_h') \tan \theta \tag{16}$$

where θ is the angle which a marginal ray makes with the optical axis when it is focused by the lens. Rewriting these equations in terms of L_s, the equations become

$$\text{Long. S.A.} = s_p' \, s_h' \, L_s \tag{17}$$

$$\text{Lat. S.A.} = s_p' \, h \, L_s \tag{18}$$

The lens used in the spatial frequency spectrum analyzer during the period covered by this report was a simple plano-convex lens with a focal length of 1595 mm ± 5 mm. The amount of spherical aberration was calculated for this lens using a sample radius of h = 10 mm, a shape factor of q = 1, a position factor of p = -1, and a refractive index of 1.52. From equations (15) and (16), the Long. S. A. is less than 8×10^{-2} mm and the Lat. S. A. is less than 5×10^{-4} mm. The remaining monochromatic aberrations may be neglected since effectively no off-axis focusing with the lens is made.

The diffraction limit of an ideal lens is the diameter of the airy-disc which is formed when plane waves are brought to a focus by the lens. This limit can be found by evaluating the formula

$$\text{diff. limit} = \frac{1.22 \, \lambda \, f}{r}$$

Where f is the focal length of the lens, r is the radius of the circular aperture used, and λ is the wavelength of the incident radiation. For

the system being described, the limiting aperture is the portion of the sample being illuminated, which is a circle with a radius of ¼ inch. The diffraction limit is therefore found to be approximately 0.197 mm.

Precautions have been taken to maximize the signal-to-noise ratio. Wherever possible, light baffles were placed along the path of the laser beam between the sample and the filtering aperture. These baffles prevented any stray light from directly striking the photomultiplier. Caution was taken in the placement of baffles so that Fresnel diffraction from the edges of the baffles would not cause "ringing" or light intensity variations to exist within the filtering aperture. These light baffles are shown in place in Figure 6.

The focusing lens, light baffles, and photodetector assembly are mounted upon an arm which has for its center of rotation the axis upon which the sample is aligned. Two arms have been made for use on the analyzer and these may be interchanged as desired. The 8 foot arm may be used where long focal length lenses are used or where additional optical components must be added to the system. This long arm suffers from the disadvantage that the total angular scan is limited by the 3 inch track on which the end of the arm rides. A pair of wheels are mounted under the arm to permit smooth and free travel at the end. One of these wheels is an aluminum disc with a groove on the outer edge. An O-ring is fitted tightly about the wheel. A 2 inch fine-tooth gear is mounted on the axis of this wheel and is powered by a smaller 3/8 inch gear on the shaft of a 2 rpm synchronous motor. Figure 8 shows this motor drive arrangement. The extremities of the track limit the angular scan of the arm.

To compensate for the disadvantage of using the long arm, a 3 foot arm is employed to take care of large angular rotations up to nearly 90 degrees which are not possible with the long arm. When the shorter arm is in use, a different method is used to scan the spectrum. A bearing-contained turntable is rigidly mounted on a ½ inch aluminum platform. The arm is then fastened to the turntable. A 1 rpm synchronous motor is used to rotate this arm. Thin piano wire is fastened at both ends to points on the far side of the turntable. With a half twist, the middle of the wire is placed on an aluminum drum having a known diameter. Three slots of different diameter reduce the speed 10:1, 20:1, or 40:1. No track is needed to support the end of the three foot arm. This drive arrangement is shown in Figure 9.

An instrumental frequency spread is always present in measuring the diffraction. Ideally, light rays are focused to a point in the focal plane of the lens and, as a result, a small aperture is needed to filter out rays of other angular orientation. This small aperture does have a finite width, and therefore allows rays of a given angular range to be filtered and detected. This instrumental angular spread of uncertainty in measurement can be converted into an instrumental spatial frequency spread in lines per millimeter by finding the difference in the spatial frequency at the two extreme angles accepted by the receiving aperture. In general, this frequency spread δd^* is dependent upon the scattering angle $C/2$ by

$$\delta d^* = \frac{(C)}{\lambda} \cos \frac{C}{2}$$

where C is the angular width the slit makes with the sample. The quantity C/λ is the maximum possible frequency spread sampled by the instrument.

This relationship does not hold if any of the five monochromatic aberrations of lenses are appreciable. A filtering aperture 0.020 inch in diameter was used during the period covered by this report.

An EMI 9558B photomultiplier tube is used as the primary energy transducer in the optical system. This tube has a 2 inch diameter, flat-faced, pyrex end window with 11 venetian blind dynodes having CsSb secondary emitting surfaces. The photocathode is of the S-20 or tri-alkali (NaKSbCs) type having a quantum efficiency of 6 percent near 6329 A. The typical gain of the dynode section is near 2×10^6. The venetian blind dynode system was selected because the gain drift for such a dynode configuration has been determined to be less than 0.7 percent per period of 24 hours operation. The rise of time of this tube is 8 nsec with a time spread of 16 nsec. The cathode sensitivity of the 9558B is 152 μA per lumen at an overall voltage of 900 V. A maximum overall voltage across the photomultiplier must never be exceeded for this tube. For DC measurements, the typical anode dark current at 900 V is less than 2.5 nA at room temperature of $75^{\circ}F$ compared to the manufacturer's specified current of 1.2 nA prior to shipment from the factory. For highest stability in DC conditions, the manufacturer suggests that the anode current not exceed 10 μA. This condition is always observed when any measurements are made.

Because of the low level signal current involved, a mu-metal shield is wrapped around the tube to reduce any electromagnetic interference. This shield is held at photocathode potential. If this is not done, field interactions with electrons leaving the photocathode occur and electron collection efficiency decreases.

A linear resistor chain of 68K ohms ± 1 percent between all dynodes is used to distribute the potential to the dynodes. A Motorola IN3817 Zener Diode rated 120 V at 2.5 mA with a tolerance of 10 percent is used to stabilize the voltage between the photocathode and the first dynode.

The incident light level on the photocathode is limited by an attenuator box which is mounted in front of the entrance aperture to the tube. Four 2 inch by 2 inch filter slots are present in the box so that glass or gelatin filters can be easily inserted. A painted aluminum cover plate seals off any light entering the photomultiplier through the attenuator box. An Alphax camera shutter is mounted behind the attenuator box to optically isolate the photomultiplier from all external light sources and to provide a fast means of turning off the light to the detector. The pinhole filtering aperture is interchangeable and is mounted on the front of the attenuator box. Figure 10 shows the entire detector assembly.

The power supply of the EMI 9558B is a Hewlett Packard Model 6516A HV DC power supply, which is an all-semiconductor package that can furnish 3000 V at 6 mA. It is designed for applications requiring extreme stability, regulation and insensitivity to ambient temperature variations. The supply has a load regulation of 0.01 percent output voltage change for a full load to no load change in the output current. An Analog Devices Model 310 J Electrometer Amplifier is being used in the current-to-voltage mode to maintain the ideal characteristics of the photomultiplier output. The high input impedance of 10^{12} ohms allows small currents to be measured with large feedback resistors in the circuit. By using this circuitry, the collecting anode is held at virtually ground potential, and the

output impedance is much less than 1 ohm. The output voltage may be as high as 10V which is quite adequate to directly drive almost any recording instrument. Like the photomultiplier, the operational amplifier circuitry requires an additional power supply. An Analog Devices Model 901 DC Power Supply was purchased for use with the amplifier.

The signal current at the photomultiplier output becomes a time dependent quantity whenever the optical bench is rotated. All voltage measuring equipment and the recording instrument must, therefore, respond at the frequency of the information signal. The recording of higher frequency signals may necessitate the use of either a galvanometer recorder or photographing the display on an oscilloscope.

The choice of a recording medium for continuous measurement of diffraction patterns depends on the sweep rate of the detector. The time dependent frequency of a signal appearing at the photomultiplier output is simply the product of the spatial frequency of the optical signal and the velocity of the filtering aperture through the spectrum. This relationship is given by

$$\nu = d*V \tag{19}$$

where ν is the frequency of the electrical signal and V is the velocity of the filtering aperture. The minimum rotational speed of the 8 foot arm is 0.088 degrees per second ± 2 percent. All data taken for this work are made at this speed. Assuming a lever arm of 2000 mm and a filtering aperture diameter of 0.050 inch, the maximum cutoff frequency that can be safely measured is 1.21 Hz. A certain amount of end play is present in the gear teeth of the motors driving the arms. In both of the motor assemblies, an error of ±0.008 degree for the long arm and ±0.0318 degree for the short arm is always present. Oscillatory

motion occurs in the short arm. To dampen this effect when continuous measurements are being made, a spring-loaded nylon-tipped rod gently rides against the turntable. Properly adjusted, no undesired oscillations are observed. The error in the long arm is sufficiently small at the present that no damping is used.

The stability of the laser output power is very important in the detection, measurement, and recording of a diffraction pattern. The output power is measured by removing all samples from the holder and allowing the light from the laser to strike the photomultiplier tube. A sufficient filter is used to attenuate the light to a safe level. The laser is then actuated, and the signal recorded. Figure 11 shows the output power plotted vs. time. The power is sampled once every 30 minutes for 15 minute periods until equilibrium is reached after 90 minutes. A maximum variation of 20 percent at t = 15 minutes reduces to 10 percent after 90 minutes. After 2½ hours of continuous operation, the variations in the output power are limited by a bandwidth of 0.02 Hz of the voltmeter.

In order to evaluate the performance of the spatial frequency spectrum analyzer, a number of tests were performed in which the recorded data could be compared with expected data from specially prepared samples.

The first test was to study the diffraction pattern from a linear grating. The spacing of the grating was measured on a calibrated shadowgraph comparator. The average spatial frequency of the grating measured over 50 grating slits was found to be 150 lines per inch or 5.91 lines per mm with an error of less than 1 percent. From equation (2) the angle of the 10th diffracted order was calculated and found to be 2.14

degrees. This angle was then compared to the diffracted angle of the 10th order scattered beam when the grating was placed in the sample holder of the instrument. This angle was measured by triangulating the positions of the filtering aperture at the 10th and zero orders, and was found to be 2.17 degrees. The result was a difference in angle of less than 2 percent with the calculated angle.

Secondly, it was desired to study the diffraction of light from N identical apertures distributed randomly in a given area. Stone[13] has discussed the scattering distribution criteria for the apertures and concludes from a random walk analysis that the intensity of light at some arbitrary point in the smoothed diffraction pattern is N times greater than the light intensity that is produced by a simple aperture of the same size.

A series of test plates were made in which a known number of uniform size lead BB's were photographed upon a white background. When the photograph was developed, small circular transparent apertures were present on the film. Prior to photographing, each BB was rinsed in an acetone bath, placed on an absorbent paper material, and sprayed with a coat of flat black enamel paint. After drying the BB's were then stirred and repainted. Stirring and repainting 10 to 15 times was sufficiently effective to paint the entire surface of the lead black.

A known number of these BB's were randomly distributed upon a white background and photographed. Kodak High Resolution 649-F plates were used in recording the test images. This medium was chosen because high resolution and low graininess are required to satisfactorily record

0.002 inch BB images. The high contrast characteristics and low graininess of the film permit the recording of apertures with sharp edges. The relatively slow speed of the film does not become a disadvantage in photographing the test scene since no motion of the object occurs. Also, the glass substrate of the plate provides a convenient mounting support for later use.

After the proper focus and exposure had been determined, a series of test plates were made. These plates, being negatives of the test scene, appeared as small transparent apertures on a black field. The test plates were similar, except that the number of BB's within the scene was varied.

Contact copies of these plates were then made. The emulsion of an unexposed 649-F plate was immersed in water, pressed to the emulsion side of a test plate, and exposed through the back of the test plate. Effectively, the complement of the original plate is generated. Exposure and development must be carefully controlled during this copying. The copy process was repeated three times to obtain a high density gradient at the edge of each aperture. After the contact printing had been completed, a series of "best" plates were retained for analysis and the rest discarded. The "best" plates consisted of transparent apertures on a black background and also some negatives of these. Jenkins and White[14] state that if opaque and transparent areas on a screen are interchanged upon another screen, the second screen is the complement of the first. According to Babinet's Principle, the smooth diffraction patterns of the complementary test plates should be identical.

Five of the test plates which were made photographically by the process just described were selected for study. The size of 25 "typical"

scattering centers were measured using a calibrated shadowgraph comparator. The values were then statistically averaged and recorded in Table II. 1.

TABLE II. 1

Diameter Measurements Made

By Using A Calibrated Shadowgraph Comparator

Test Plate Number	Average Size of Apertures (mm)	Standard Deviation (mm)	Cause of Diffraction	Number of Apertures Used
1	0.071	0.00023	Stops	700
2	0.089	0.00048	Stops	3000
3	0.071	0.00023	Apertures	700
4	0.071	0.00037	Apertures	1000
5	0.081	0.00041	Apertures	3000

Along with the average sizes are recorded one standard deviation of these measurements, the nature of the scattering center (aperture of stop) and the number of centers which are present in the circular area of the test plate having a diameter of 3/8 inch. The test plates were singly placed into the laser beam and the diffraction pattern of each was measured. The recorded patterns were then compared to the diffraction pattern of a grating in order to calibrate the spectra. From this, the angle between the first minima was measured and divided by 2. To be certain that the diffraction pattern was symmetric regardless of the orientation of the test plate, each plate was rotated 45, 90, and 180 degrees. Table II. 2 lists the average value for the four orientations. These values are listed under A_{scan} along with their standard deviations.

The calculated angle of the first minima from the average value of aperture stop diameters of Table II. 1, along with their corresponding standard deviations, are given in Table II. 2 under the column $A_{calculated}$. Table II. 3 and Table II. 4 list similar results of test plates which exhibited the presence of a second and third minima in intensity. Poor agreement is observed when the appropriate columns are compared. A second check was used to account for this error. The diffraction pattern of test plate 3 was photographed by placing a 4 x 5 sheet of Panatomic X film in the plane of the filtering aperture. A print of this photograph is shown in Figure 12. Figure 13 is a photographic enlargement of the test plate 3 taken on the shadowgraph comparator. The overall diffraction pattern appeared to be somewhat elliptical. The major and minor axes were then measured and found to be 1.31 inch ± 0.08 inch by 1.08 inch ± 0.08 inch, respectively. These diameters in turn correspond to an elliptical aperture whose size is 0.071 mm by 0.089 mm ± 0.010 mm. This error of about 15 percent is sufficiently large to compensate for the small standard deviation in A_{scan} and $A_{calculated}$.

TABLE II. 2

Calculated and Experimental Angular Values of First Minima

Test Plate Number	$A_{calculated}$ (degrees)	Standard Deviation	A_{scan} (degrees)	Standard Deviation
1	0.62	0.0089	0.52	0.022
2	0.50	0.0012	0.48	0.017
3	0.62	0.0089	0.57	0.034
4	0.62	0.0014	0.61	0.029
5	0.54	0.0012	0.48	0.017

TABLE II. 3

Calculated and Experimental Angular Values of Second Minima

Test Plate Number	$A_{calculated}$ (degrees)	Standard Deviation	A_{scan} (degrees)	Standard Deviation
2	0.91	0.0022	0.88	0.052
3	1.14	0.0016	1.01	0.036
4	1.14	0.0026	1.05	0.036
5	1.00	0.0022	0.90	0.065

TABLE II. 4

Calculated and Experimental Angular Values of Third Minima

Test Plate Number	$A_{calculated}$ (degrees)	Standard Deviation	A_{scan} (degrees)	Standard Deviation
3	1.66	0.0024	1.41	0.072
4	1.66	0.0038	1.42	0.085
5	1.45	0.0032	1.32	0.014

The filtering aperture has been superimposed on Figure 12 to scale to show its size relative to the diffraction pattern and the path that is followed when a recording is being made. The aperture has been intentionally displaced a distance corresponding to three aperture diameters below the center of the diffraction pattern to prevent damage to the photomultiplier by the intense zero order beam.

Previously, it was stated that if N apertures are randomly arranged on a screen (or test plate) the intensity at some arbitrary scattering point in the smoothed diffraction pattern should be N times more intense than that caused by a single aperture. Test plate 5 was arbitrarily

chosen for the determination of its aperture density distribution characteristics, and the results were compared to a random distribution.

The 3/8 inch test plate was enlarged 21 times to 8 inches, and 169 sampling squares 1/2 inch by 1/2 inch were superimposed upon the enlarged plate. The number of apertures contained in each square was then recorded. Table II. 5 has the results of these measurements.

TABLE II. 5

Density Distribution Characteristics
of Apertures in Test Plate 5

Given number of apertures per sampling area n_i	Density of apertures per unit sampling area D $(\text{apertures/inch})^2$	Number of sampling areas having given density N_i
(½" x ½")	(4 x column 1)	
1	4	1
2	8	3
3	12	0
4	16	0
5	20	4
6	24	3
7	28	7
8	32	2
9	36	4
10	40	12
11	44	14
12	48	21
13	52	21
14	56	10
15	60	14
16	64	19
17	68	7
18	72	10
19	76	4
20	80	3
21	84	5
22	88	3
23	92	1
24	96	1

The first column represents the number of apertures found in any one sampling area. The second column lists the corresponding number of apertures per unit, D_i. Figure 14 is a plot of the density distribution characteristics of the last two columns of Table II. 5. The average density $\overline{D}$ of the apertures is given by the equation

$$\overline{D} = \frac{\Sigma N_i D_i}{\Sigma N_i} \quad . \tag{20}$$

The square of the standard deviation from this mean is given by

$$s^2 = \frac{\Sigma N_i (\overline{D} - D_i)^2}{(\Sigma N_i) - 1} \quad . \tag{21}$$

Using these equations and normalizing the average to the original size of the test plate, the results in Table II. 6 are obtained.

TABLE II. 6

Averaged Results of Density Distribution Characteristics of Test Plate 5

Actual area of test plate (0.375 in. diameter)	= 0.110 inch^2 = 71.3 mm^2
Area of test plate after magnification (8 in. diameter)	= 50.3 inch^2 = 32,500 mm^2
Sampling area of magnified test plate (½ x ½ in.)	= 0.25 inch^2 = 38.7 mm^2
Total number of sampling areas investigated	= 169
Total number of apertures on test plate	= 3000
Average value of aperture density on test plate	= 36 apertures/mm^2
Standard deviation of aperture density on test plate	= 12 apertures/mm^2

The scattering theory previously discussed by Stone was studied. A set of plates, described in detail in Table II. 7 were prepared. On each

of the plates only the number of apertures was allowed to vary. The diffraction patterns of each were recorded and relative intensity values of the first maxima were determined. The results are shown in Table II. 7.

The relative intensity of the first maximum is seen to increase as the number of apertures increases from 300 to 700 and from 700 to 3000. There is a discrepancy, however, as the number of apertures increases from 700 to 1000. Plates 8 and 9 were rechecked, but essentially the same results were obtained. Visual examination showed that plate 9 was slightly overexposed. This could partly account for the reduced intensity which was measured.

TABLE II. 7

Dependency of Intensity of First Minima
on the Number of Apertures in the Test Plate

Test Plate	Cause of diffraction	Number of apertures	Relative intensity of first maxima
7	apertures	300	120
8	apertures	700	2500
9	apertures	1000	1300
10	apertures	3000	9000

Blurring of the edges of the aperture could result in a decrease of the average intensity at high spatial frequencies or large diffraction angles of the spectrum of these apertures. This can be likened to the loss of higher diffraction orders from a grating as the lines in the grating become less well defined at their edges. The effect of this blurring can be noted by referring to Tables II. 2, II. 3, and II. 4. Test plates 3, 4, and 5 exhibited spectra out to at least the third minimum. For test plate 2 only the second

minimum could be determined, while only the first minimum was observed for test plate 1. Visual observation of these test plates indicated that the edges of the aperture in plates 3, 4, and 5 appeared to be more sharp than those of plates 1 and 2.

An additional factor that can prevent the diffraction pattern from being exactly as calcuated is a non-uniform incident beam on the sample. Prior to measuring the diffraction patterns of plates 7, 8, 9 and 10, the incident beam was "flattened" or made uniform. This was accomplished by allowing the light from the pinhole of the collimator to expand. The distance over which the expansion occurs allows stretching of the intensity variations in a given aperture. As a result, the wavefront becomes more uniform. The uniformity of the incident beam was measured by removing the focusing lens from the instrument and allowing the light to pass through the empty sample holder and fall directly on the filtering aperture at the end of the movable arm. The photomultiplier then scanned the horizontal intensity profile of the beam in nearly a straight path. An arc of 0.7 degree is traversed when 20 mm of beam is sampled at 1595 mm. This error was negligible compared to a probable error of 1 degree in aligning the photomultiplier normal to the incident beam. Several horizontal scans were made across the aperture and the profile of the entire area was mapped. Of these, the scan which exhibited the greatest fluctuations is shown in Figure 15. Peak variations of 30 percent are observed. Approximately 30 percent variation in intensity in the vertical direction was found when the different scans were compared.

Conclusions:

The basis for continued use of the spatial frequency spectrum analyzer

to related problems of diffraction has been made.

Two basic signal forms were studied and measured using the instrument. In one form, a diffraction grating was used to generate a single frequency optical signal. The angular coordinates of the signal in the diffraction pattern were measured and compared to calculated values using the generalized diffraction equation for gratings. A 2 percent agreement between these values shows that a diffraction grating can be used to calibrate either the angular or spatial frequency axis of the instrument.

In the second form, a continuous spatial frequency signal spectrum was generated using small circular apertures and stops. Angular values of successive minima in their diffraction patterns were measured and compared to the corresponding calculated angular values. A difference of less than 15 percent was observed in the corresponding values. Additional photographic evidence indicated that this large difference could easily have been expected.

The smoothed diffraction pattern of a large number of relatively uniform apertures was detected, measured and recorded. Large photographic errors were present in making the test plates and have prevented any quantitative conclusions from being made. Qualitatively, however, the intensity of the light of the second maxima increased with the number of apertures.

Negligible mechanical and electrical noises were observed during all experiments that were performed. Linear operating conditions for the photomultiplier were found using neutral density filters to reduce the power of the measured beam.

Future Work

Future work with the instrument will primarily involve its use under

conditions similar to those encountered while measuring the diffraction pattern of the aperture test plates that were just discussed. During the continuous measurements referred to in this report, large variations in signal current were observed and scale changes on the recorder were made constantly. To overcome this difficulty, an appropriate feedback system should be built for the photomultiplier so that the output signal is a logarithmic function of the input light power. This logarithmic response may be obtained by varying the overall voltage across the photomultiplier in such a way that output current is constant. It can be shown that the voltage across the tube is a logarithmic function of the gain. Therefore, the signal will simply become related to the applied voltage across the photomultiplier. By so doing, the range of the output signal may be increased from its present range of 10^2, which is the range of the output current in its present form, to 10^4.

This feedback circuit will be useful in later studies on film grain noise which will be underway soon. In brief, it is planned to review those darkroom parameters, such as exposure, exposure time, development time and temperature, density of the photographic emulsion, and developer, which affect the diffraction pattern of developed film that has been previously exposed to incoherent light. In this way no information will be present on the developed film except that of the film grain. The diffraction pattern of the film grain matrix will be detected, measured and recorded in a manner similar to that of the test plates in this report.

Additional uses of the optical spectrum analyzer will be investigated. One such use could be in the measurement of transfer characteristics of any recording medium. These transfer characteristics may be obtained from the recorded diffraction pattern, for which the spectrum analyzer will be utilized.

III. Unconventional Image Storing and Processing

A. Experimental Photographic Processes

J. G. Dodd

Introduction

Use of contrast amplification by partial suppression of the zero-order beam in image formation is limited in practical cases by the system noise level. In photographic emulsions, this noise arises chiefly from scattering by macromolecules characteristic of the emulsion matrix, by "fog" - random unexposed but developed grains -, and by imperfections, such as dust or thickness variations.

Gelatin-silver halide emulsions suffer from the first and second ailments in large degree. The second can be controlled at the sacrifice of film speed. The first, however, is intimately related to the emulsion matrix. The purpose of the present study is to investigate low-noise high-primary quantum efficiency photo processes that might be uniquely suited to contrast amplification.

Systems Chosen for Initial Study

a. Matrices

   1. Low molecular weight gelatin
   2. Polyacryls
   3. Cross-linked Polystyrene
   4. Polyvinyls

b. Processes

   1. Photoreduction of metal ions
   2. Photo-polymerization
   3. Dye reactions.

Work Performed

a. Matrices

(1) Acrylamide polymerizes easily in the presence of H_2O_2. Provided a sufficiently dilute acrylamide-water solution is used to prevent self-heating during polymerization, it is possible to control rather closely the kind of polymer by a combination of amount of activator, polymerization temperature, and time. Several such polymers have been prepared. High activator concentrations and high temperatures encourage low molecular weight chains; polymerization occurs relatively rapidly. Long chains form in the presence of small initiator concentration and low temperatures.

Several such polymers have been prepared. A typical recipe was a 5% by weight solution of acrylamide in water with 0.01% H_2O_2 activator held at 80°C for 48 hours. The resulting solution was very viscous and perfectly transparent. However, there was no tendency to gel. A slide coated with the solution became tacky and finally dried hard and smooth. The coating was water-soluble. Since one of the criteria of a suitable matrix is that it swell (to permit ion migration) but not dissolve, this formulation must be evaluated as unsuccessful.

Tendency to gel is associated with chain length and with cross-linking. Increased chain length can be obtained by polymerization with lower initiator concentrations and lower temperatures. Cross-linking normally requires additives during polymerization. For example, chromium ions are known to induce cross-linking in this class of polymers. Work has begun on development of a formulation that will result in a clear, stable gel.

The reason for pursuing this particular class of polymers is that initial tests show that light scattering is less than in normal gelatin

matrices; this is, therefore, a potentially "quiet" water-permeable emulsion. Of course, since low scattering implies relatively low molecular weights, to produce a gel without significantly degrading clarity will probably require cross-linking. It would be desirable to be able to do this without introducing metal ions which might compete adversely with some photo processes. This problem is now under study.

Development of a satisfactory "quiet" water-permeable gel will permit investigation of a variety of high quantum efficiency metal-inorganic photosensitive processes.

(2) Gelatin scatters light strongly because of the presence of very large macromolecules. It is possible to limit the maximum molecular weight of a gelatin emulsion by filtration. It has been discovered that a hot (80°C) 5% gelatin solution can be filtered through Whatman medium filter paper with a yield greater than 50%.

Slides were coated with this filtered gel, allowed to dry, and tested for Tyndall scattering in a laser beam by visual comparison with slides made from the unfiltered gelatin. It is estimated that the visual scattered intensities compared as 1:10; what this means in photometric terms is not known.

The dried emulsions made from filtered gelatin appeared perfectly clear and uniform. Unfortunately, when placed in cold water these emulsions tended to dissolve. Apparently the high molecular weight fractions held back by the filter paper are responsible for normal gelation. It was found, however, that the gel was stable in a 3% formaldehyde solution. Thus, it seems possible to make a fairly low-noise gelatin emulsion, although it will be rather fragile.

It should be mentioned that the polyacryls decribed under (1) exhibit almost no visible Tyndall scattering. Whether this desirable behavior can be maintained after sufficient cross-linking to permit gelation is, of course, the crucial test. If so, the polyacryl emulsions would be superior for contrast amplification applications.

(3) Styrene polymerized in the presence of divinylbenzene is extensively cross-linked and swells without dissolving in benzene. Since the first two emulsions described are both water-based, cross-linked polystyrene would provide a possible non-aqueous alternative for organic photo-sensitive processes. We have not yet investigated non-aqueous systems.

(4) Polyvinyl alchohol has been used by others for silver halide emulsions and bichromate wash-off relief processes. Tests with PVA in this laboratory have been disappointing; the emulsions show very strong Tyndall scattering. Otherwise, they seem to have no particular advantage. Further investigation is not planned at this time.

b. Processes

(1) The "blueprint" process is based on the photo-reduction of a ferric salt to a ferrous salt and subsequent development by reaction of the ferrous ion with a ferricyanide to produce ferrous ferricyanide (Turnbull's blue). After washing to remove the unreacted ferric salt, the image is oxidized in potassium bichromate to ferric ferricyanide (Prussian blue).

In this laboratory the interest in the blue print process is as a prototype of a high primary quantum efficiency non-amplifying grainless process. Ferric ammonium citrate has been the salt most often used; although ferric chloride is more sensitive, it is also much less stable. Emulsions have been prepared using gelatin, polyacryls, and PVA. The process is compatible with

any of the three. Typical proportions would be 20% by weight of the ferric ion in an emulsion. The developer (usually potassium ferricyanide) is always used separately rather than as an integral part of the emulsion, principally, to provide some development options.

Test slides were made of an electron microscope grid magnified 5x by a 16 mm slide projector; exposure times of 1/2, 1, 2, 4, 8, and 16 minutes gave a series of images of roughly equal density steps, the shortest exposure visible to the eye being the 2 minute exposure. These results did not depend upon the emulsion matrix.

In polyacryl emulsions, a dimensionally stable image has not been obtained because the matrix is not a gel, but a sol.

In gelatin, the image is stable. Examination under a schlieren microscope revealed rather unexpectedly that the image was a strong phase image as well as an amplitude image. In fact, even the 1/2 minute image was visible as a phase object while quite invisible otherwise. Evidently the gelatin matrix participates in a tanning reaction, much like the bichromate process.

Once this was realized, an attempt was made to produce a test slide using filtered gelatin. A 10% formaldehyde-potassium ferricyanide developer was found to preserve the integrity of the emulsion. The slide was exposed through the back to take advantage of whatever adhesion the tanning reaction might produce. Unfortunately, the slide was washed in plain water and once the formaldehyde was washed out of the emulsion, it dissolved. This is obviously an avoidable difficulty.

While the blueprint process was chosen for study because it is simple rather than because of any anticipated intrinsic usefulness, the fact that it can produce strong phase images makes it immediately

of interest in holography. Only the region of spectral sensitivity is really disadvantageous. It may be possible to dye-sensitize the process to the red end of the spectrum; in any case, it could be used now with an argon ion laser.

Work is continuing in an effort to produce a stable phase image in a filtered gelatin emulsion.

(2). In attempts to produce a polyacryl-"blueprint" emulsion it was noticed that the solubility of the emulsion seemed retarded in the vicinity of the exposed and developed image. Using water as the solvent it was not possible, however, to obtain enough differential solubility. One slide, exposed through the back and developed in an alcoholic solution of potassium ferricyanide did show a good relief image; it is possible that a wash-off process based upon this observation might be developed. It is quite possible that considerable internal amplification exists since the cross-linking produced (if that is the insolublization mechanism) is much greater than that of the primary compound.

The principle difficulty with most processes based upon differential solubility is that the difference is usually one of degree rather than kind. Whether that is true of this process is not yet known. Study is continuing to find a more selective solvent. The higher alcohols are logical candidates.

III. B. Phase Holography Using Photographic Media

G. K. Wallace

Introduction

In an ordinarily recorded and processed hologram, amplitude and phase information necessary to reconstruct an image of some object are stored as optical density (amplitude transmittance) variations in the photographic emulsion. These images are usually dim, since the maximum diffraction efficiency of an amplitude hologram is approximately 4%[15].

One means of improving the intensity of a hologram image is to utilize a phase hologram rather than an amplitude hologram. A variety of phase hologram materials are available for use. Shankoff[16] recently reported the use of dichromated gelatin for this purpose. Kodak Spectroscopic Plates, Type 649-F, or Kodak High Resolution Plates can be dichromated for use. Diffraction efficiencies approaching 100% have been reported but with a reduction in emulsion speeds. Another method for producing phase holograms is to convert from an amplitude hologram by bleaching the developed silver grains. A number of methods of bleaching have been reported in the literature[17]. The bleach removes optical density variations and produces a transparent hologram where index of refraction differences and emulsion thickness variations phase modulate the incident reconstruction beam to form the image.

As discussed in the NASA Grant NGR-04-001-007 Report of September 30, 1968, a study of the Wash-Off Relief Method of producing phase holograms is being conducted by this laboratory. It was shown in the above report that the brightness of reconstructed images obtained from Wash-Off holograms

was affected by the recorded spatial frequency as well as the exposure used. Here, additional methods of modifying the photographic emulsion to obtain phase holograms and the results thus far obtained are presented. The study to date has been confined to 35 mm films, since their low cost, ease of handling and processing, and availability make them an ideal medium for "box-camera" holography.

Work Performed

Previous work at this laboratory[18] explored the use of the Wash-Off Relief Method to produce phase gratings. It was noted earlier[18] that several photographically recorded, wash-off relief processed gratings of 25 line pairs/mm possessed unusual light intensity distributions in their various orders. These distributions have been measured and are tabulated in Table III. 1. One grating (exposure = 0.65 microJoules/cm^2) has the ±1 and ±2 diffraction orders with greater intensity than the zero order. In the other grating (exposure = 0.43 microJoules/cm^2), for incident white light, the ±1 diffraction order had suppression of the red component of the light which resulted in the ±1 order being blue-green in color. When red light (6328Å) is incident on the gratings, the ±2 and ±3 diffraction orders are intense and the ±1 order is suppressed. The only experimental difference between the gratings is the exposure. This information is presented for comparative purposes with data presented later in this report. The unusual intensity distributions noted above are also found to occur in phase holograms produced by the Purex Relief Method discussed below.

The use of 35 mm color film was next explored in an attempt to find suitable phase hologram media. Color films are, in general, known to be

TABLE III. 1

FILM: Kodak High Contrast Copy film (35 mm)

TREATMENT: Wash-Off Relief Method

RECORDING: 25 line pairs/mm grating

READ-OUT: Intensity of each order as % of incident monochromatic (6328A) light

EXPOSURE: 0.65 microJoule/cm^2

TOTAL INTENSITY OUT: 90.341%

ORDER NUMBER	INTENSITY OUT:
-6	0.004%
-5	0.027
-4	0.221
-3	1.760
-2	10.000
-1	29.135
0	9.519
1	28.558
2	9.519
3	1.442
4	0.135
5	0.019
6	0.002

EXPOSURE: 0.43 microJoule/cm^2

TOTAL INTENSITY OUT: 44.299%

ORDER NUMBER:	INTENSITY OUT:
-6	0.995%
-5	0.995
-4	1.493
-3	5.973
-2	7.466
-1	1.991
0	9.457
1	0.995
2	5.973
3	3.982
4	2.986
5	1.493
6	0.498

rather limited in resolving power. Films with small ASA numbers were chosen for use since the ASA number (film speed) is usually indicative of resolving power. Gratings were made with the arrangement shown in Figure 16 using Kodak Kodacolor-X (ASA 80), Ektachrome-X (ASA 64) and Kodachrome II (ASA 25) color films. The films were commercially processed (Kodak Processing Laboratory, Dallas, Texas) and are therefore subject to less exacting control than is normally employed in scientific photo-processing procedures.

Since resolving power was limited, a trial grating of $d^* = 13$ line pairs/mm was first formed using Ektachrome-X and Kodachrome II (color positive films) and Kodacolor-X (color negative film). (Color positive films record positive color transparencies; color negative films record a scene backwards in that light and dark areas are reversed from the original scene and the colors are complementary to those in the original scene.) Exposure was varied. Kodacolor-X produced an orange-tinged film (characteristic of the film) with green color where constructive interference occurred and black where destructive interference occurred. This film was therefore useless with the red-light-emitting He-Ne laser. No diffraction pattern necessary for holographic applications was produced.

Ektachrome-X produced only a zero and two first (±) orders and then only for an exposure of 28 microJoules/cm^2. No detectable relief occurred. All other exposures produced negative results (no first or higher orders).

Of the materials used, Kodachrome II produced the best diffraction of light. One obvious reason for this is the fact that Kodachrome II has the highest resolving power of any widely available color film (response about 5% at 100 line pairs/mm[19]).

Kodachrome II used the subtractive process method of recording images[20]. Three separate emulsion layers are used: the top layer is exposed only by blue light, the middle layer is sensitive only to green or blue light, and the bottom layer is exposed only by blue or red light. A yellow (minus blue) filter between the top and middle layers prevents blue light from exposing the middle and bottom layers. The resulting tripack has a blue sensitive top layer, a green sensitive middle layer and a red sensitive bottom layer. In holography using the He-Ne laser, a grating is laid down on the film by alternating constructive and destructive interference of the red (6328A) light. After exposure, the film is developed normally. When the film is exposed to normal exposure values, grains in the developed negative will be reduced to silver in the red sensitive areas (constructive interference); no reduction occurs in the destructive interference areas since no light exists to expose these areas (see Figure 17). After a second exposure and treatment in dye-coupler developers, those areas in each layer where the silver was removed are not dyed. Other areas are dyed either cyan (minus red), magenta (minus green) or yellow (minus blue). (These dyes exert independent control on the primary colors red, green and blue in white light.) In the constructive areas, the top and middle layers will be dyed yellow and magenta respectively; in destructive areas, all three layers are dyed. Now, all silver is removed to obtain a transparency (see Figure 17[20]) with only the dyed layers remaining. Red light or the red component of white light should pass through the constructive areas. Virtually no light passes through the destructive areas. The process described above produces an amplitude grating.

As the exposure is increased, however, different results are obtained. The film becomes transparent in the areas of constructive interference. The destructive interference areas become red. This result is not obvious based on the above explanation of the color exposure process for normal exposure values. Figure 18[20] presents the probable explanation of the observed effects. In the destructive areas of the film the probability exists that, after enough exposure, sufficient light exists to expose the red sensitive layer in the destructive area of the interference pattern. In the constructive areas of the film the intensity of the red (6328A) light is sufficient to expose all three layers. Based on the assumption of Figure 18, the layers corresponding to the constructive areas will not be dyed at all and in the destructive areas the top and middle layers will be dyed yellow and magenta respectively. The increased exposure values can thus be used to produce a phase grating (or hologram) for incident red light since it will pass easily through the constructive and destructive areas.

The effect of exposure on diffraction intensity is shown in Table III. 2. Exposure values of 1.4, 2.8, 5.6 and 14.0 (for a spatial frequency of 13 line pairs/mm) are the amplitude gratings discussed above. The exposure values 28.0, 69.8 and 139.6 are the phase gratings. The differences between the constructive and destructive areas of these phase gratings appear to modulate the incident beam sufficiently to produce a bright first (±) order. The additional data of Table III. 2 for Kodachrome II film shows that the first (±) order beam intensity drops quickly as the spatial frequency increases. While Kodachrome II produced the best results, it is obvious from the data of Table III. 2 that even this film is of limited resolution. Color film of the Kodachrome type (low ASA number, color positive films)

TABLE III. 2

FILM: Kodak Kodachrome II (35 mm) Color Film

TREATMENT: Commercial Development

READ-OUT: Intensity of each order as % of incident monochromatic (6328A) light

EXPOSURE (microJoule/cm^2)	RELIEF (micron)	INTENSITY OUTPUT ZERO ORDER	FIRST ORDER	SECOND ORDER	THIRD ORDER	TOTAL
SPATIAL FREQUENCY:	13 line pairs/mm					
1.4	0	16.9%	0.1%	0%	0%	17.1%
2.8	0	15.8	2.1	0.1	0	20.2
5.6	0	14.2	2.9	0.3	0	20.6
14.0	0	13.3	3.2	0.3	0	20.3
28.0	0.6	8.6	11.2	3.9	0.6	40.0
69.8	0.6	25.4	11.0	1.6	0.2	51.0
139.6	0.1	57.7	0.9	0	0	59.5
SPATIAL FREQUENCY:	20 line pairs/mm					
14.0	---	12.3%	1.5%	0.1%		15.5%
28.0	0.7	9.2	1.3	0.1		12.0
69.8	0.3	16.8	1.5	0.1		20.0
139.6	0.3	44.0	0.9	0		45.8
SPATIAL FREQUENCY:	40 line pairs/mm					
14.0	---	17.8%	0%	0%		17.8%
28.0	0.2	25.9	2.4	0.1		30.9
69.8	0.2	43.0	0.2	0		43.4
139.6	0	52.0	0	0		52.0
SPATIAL FREQUENCY:	80 line pairs/mm					
14.0	---	15.5%	0%	0%		15.5%
28.0	0	27.0	0	0		27.0
69.8	0	58.5	0	0		58.5
139.6	0	59.0	0	0		59.0

but with higher resolution would appear to offer good possibilities in phase holography. However, a high resolution color film to fulfill these basic requirements is not presently available.

A study of a chemical method of relief on Kodak High Contrast Copy Film (35 mm) was begun (see Appendix I). In effect, the hot water Wash-Off Relief Method previously described[18] was replaced with a faster acting Purex (by weight, 6% sodium hypochlorite and 94% inert ingredients) wash treatment at room temperature. Various dilutions of commercial Purex bleach in water were used (1%, 3%, 6¼% and 12½% Purex bleach by volume). The 1% solution gave the best control of the emulsion removing process, since it did not remove the unhardened gelatin as rapidly as the more concentrated solutions. This particular solution was adopted for use in subsequent experiments. Given sufficient time, the Purex treatment will remove all gelatin (both hardened and unhardened). In order to use the Purex treatment to advantage, it is necessary that this removal occur at different rates. From the data in Tables III. 3 and III. 4, some preference appears to exist in gelatin removal rates of hardened (exposed) and unhardened (unexposed) areas. (Note: Although it is generally stated that the Wash-Off Relief Method preferentially removes unhardened gelatin, given sufficient time all emulsion might be removed by this method. Purex treatment time is measured in minutes while the Wash-Off requires hours.)

The relief was measured using a microscope interferometer. Intensity measurements were obtained using the Rotating Optical Spectrum Analyzer developed in this laboratory[18]. Those values of relief indicated by a dash in Tables III. 3 and III. 4 could not be determined since the surface of the emulsion (an insert in one of the legs of the interferometer) scattered the

TABLE III. 3

FILM: Kodak High Contrast Copy Film (35mm)

TREATMENT: Purex Relief Method (1% Solution)

RECORDING: 13 line pairs/mm grating

READ-OUT: Intensity of each order as % of incident monochromatic (6328A) light

BLEACH TIME	RELIEF (microns)	INTENSITY OUTPUT ZERO ORDER	FIRST ORDER	SECOND ORDER	THIRD ORDER	FOURTH ORDER	FIFTH ORDER	SIXTH ORDER	TOTAL
EXPOSURE: 0.6 microJoule/cm^2									
A. M.*	0.05	44.3%	0.1%	0%	0%	0%			44.5%
0 sec	0.20	49.2	1.7	0	0	0			52.6
5	0.21	46.7	1.4	0.1	0	0			49.7
15	0.20	45.1	2.0	0.1	0	0			49.3
30	0.30	41.0	3.7	0.3	0	0			49.0
1 min	0.65	27.9	8.9	1.5	0.2	0			49.1
2	0.59	28.7	10.2	2.1	0.4	0			54.1
4	0.15	52.5	0.2	0	0	0			52.9
8	0	52.5	0	0	0	0			52.5
16	0	53.7	0	0	0	0			53.7
EXPOSURE: 0.9 microJoule/cm^2									
A.M.*	0.20	28.8%	1.1%	0%	0%	0%	0%	0%	31.0%
0 sec#	0.59	19.4	11.5	3.2	0.5	0.1	0	0	50.0
5	0.62	20.9	10.6	2.3	0.3	0	0	0	47.3
15	0.49	8.9	7.4	5.8	2.0	0.4	0.1	0	40.3
30	0.37	19.7	9.1	1.8	0.3	0	0	0	42.1
1 min	0.65	17.9	10.6	2.9	0.5	0.1	0	0	46.1
2	1.18	18.9	9.8	2.0	0.3	0	0	0	43.1
4	1.18	11.2	4.5	2.8	2.3	1.9	1.1	0.5	37.4
8	---	42.4	1.3	0.2	0	0	0	0	45.4
16	0	56.1	0	0	0	0	0	0	56.1
EXPOSURE: 1.8 microJoule/cm^2									
A.M.*	0.12	20.6%	0.7%	0%	0%	0%	0%	0%	22.0%
0 sec#	0.59	15.0	10.9	3.5	0.6	0.1	0	0	45.2
5	0.51	17.1	10.7	2.2	0.3	0	0	0	43.5
15	0.49	19.4	11.0	2.1	0.2	0	0	0	46.0
30	0.44	12.6	11.6	3.1	0.5	0.1	0	0	43.2
1 min	0.59	13.9	10.6	2.4	0.3	0	0	0	40.5
2	---	7.1	8.1	4.9	1.2	0.2	0	0	35.9
4	---	11.5	3.3	1.6	2.4	2.0	1.0	0.4	32.9
8	---	52.9	1.3	0.1	0	0	0	0	55.7
16	0	64.7	0	0	0	0	0	0	64.7

(TABLE III. 3 con't.)

BLEACH TIME	RELIEF (microns)	INTENSITY OUTPUT ZERO ORDER	FIRST ORDER	SECOND ORDER	THIRD ORDER	FOURTH ORDER	FIFTH ORDER	SIXTH ORDER	TOTAL
EXPOSURE: 3.6 microJoules/cm^2									
A.M.*	0.24	9.7%	0.3%	0%	0%	0%	0%	0%	10.3%
0 sec#	0.24	22.5	7.9	1.0	0.1	0	0	0	40.5
5	0.59	10.9	11.0	3.5	0.6	0.1	0	0	41.3
15	0.26	33.1	3.4	0.1	0	0	0	0	40.1
30	0.30	22.5	6.6	0.6	0	0	0	0	36.9
1 min	0.39	27.0	4.3	0.2	0	0	0	0	36.0
2	0.37	14.8	7.2	1.0	0.1	0	0	0	31.4
4	---	7.0	5.3	3.0	0.9	0.2	0	0	25.8
8	---	16.9	4.7	2.8	0.8	0.1	0	0	33.7
16	---	27.5	6.2	1.4	0.2	0	0	0	43.1
EXPOSURE: 8.9 microJoule/cm^2									
A.M.*	0.18	8.3%	0.2%	0%	0%	0%	0%	0%	8.7%
0 sec#	0.37	23.4	12.5	4.2	1.1	0.3	0	0	59.6
5	0.35	22.3	13.2	4.7	1.2	0.3	0.1	0	61.3
15	0.35	21.5	12.8	4.2	1.1	0.2	0	0	58.1
30	0.35	20.8	12.1	3.2	0.7	0.1	0	0	53.0
1 min	0.52	20.4	12.5	4.5	1.4	0.4	0.1	0	58.2
2	0.41	19.6	10.9	2.9	0.6	0.1	0	0	48.6
4	---	13.2	8.9	2.9	0.9	0.3	0.1	0	39.4
8	---	28.7	5.8	1.2	0.3	0.1	0	0	43.5
16	0.53	29.4	4.3	4.6	1.3	0.2	0	0	50.2
EXPOSURE: 17.8 microJoule/cm^2									
A.M.*	0.10	1.0%	0%	0%	0%	0%	0%	0%	1.0%
0 sec#	0.20	34.7	3.2	0.1	0	0	0	0	41.3
5	0.10	30.2	0.6	0.3	0	0	0	0	40.[illegible]
15	0.20	30.2	5.5	0.3	0	0	0	0	41.8
30	0.10	37.7	1.1	0	0	0	0	0	39.9
1 min	0.16	32.5	32.5	0.2	0	0	0	0	40.1
2	0.22	23.4	5.7	0.6	0.1	0	0	0	36.6
4	---	13.6	4.6	0.7	0.1	0	0	0	24.4
8	---	21.9	3.6	0.3	0	0	0	0	29.7
16	---	26.0	2.9	0.7	0.2	0.1	0	0	33.8

*Ordinary or amplitude grating

#Dichromate bleached grating

TABLE III. 4

FILM: Kodak High Contrast Copy Film (35 mm)

TREATMENT: Purex Relief Method (1% solution)

RECORDING: 26 line pairs/mm grating

READ-OUT: Intensity of each order as % of incident monochromatic (6328A) light

BLEACH TIME	RELIEF (microns)	INTENSITY OUTPUT ZERO ORDER	FIRST ORDER	SECOND ORDER	THIRD ORDER	FOURTH ORDER	FIFTH ORDER	TOTAL
EXPOSURE: 0.2 microJoule/cm^2								
A.M.*	0	53.6%	0.1%	0%	0%	0%		53.8%
0 sec#	0.06	66.1	0.2	0	0	0		66.5
5	0.06	55.8	0.1	0	0	0		60.0
15	0.06	51.2	0	0	0	0		51.2
30	0.06	51.2	0.1	0	0	0		51.4
1 min	0.13	46.5	0.9	0	0	0		48.3
2	0.22	46.5	5.6	0.3	0	0		58.3
4	0.06	55.8	0.2	0	0	0		56.2
EXPOSURE: 0.3 microJoule/cm^2								
A.M.*	0	51.9%	0.4%	0%	0%	0%		52.7%
0 sec#	0.07	50.0	0.7	0	0	0		51.4
5	0.11	50.0	0.5	0	0	0		51.0
15	0.04	51.8	0.1	0	0	0		52.0
30	0.20	50.0	0.7	0	0	0		51.4
1 min	0.07	48.2	1.5	0	0	0		51.2
2	0.30	34.5	5.9	0.4	0	0		47.1
4	0.12	42.7	0.7	0	0	0		44.1
EXPOSURE: 1.0 microJoule/cm^2								
A.M.*	0.15	8.8%	0.6%	0%	0%	0%	0%	10.0%
0 sec#	0.52	10.4	11.5	1.9	0.2	0	0	37.6
5	0.44	21.4	9.1	0.7	0	0	0	41.0
15	0.52	9.9	14.4	2.9	0.2	0	0	44.9
30	0.52	9.1	11.2	2.0	0.2	0	0	35.9
1 min	0.44	1.1	11.0	4.5	0.7	0.1	0	33.7
2	0.26	14.4	5.9	0.5	0	0	0	27.2
4	---	3.9	0.9	5.1	3.0	0.8	0.1	23.7
8	0.15	5.9	10.4	3.6	0.5	0	0	34.9

(TABLE III.4 (con't.)

BLEACH TIME	RELIEF (microns)	INTENSITY OUTPUT ZERO ORDER	FIRST ORDER	SECOND ORDER	THIRD ORDER	FOURTH ORDER	FIFTH ORDER	TOTAL
EXPOSURE: 1.8 microJoule/cm^2								
A.M.*	0.20	0.7%	0%	0%	0%	0%		0.7%
0 sec#	0.59	6.5	10.4	2.4	0.3	0		32.7
5	0.30	10.2	9.5	1.7	0.2	0		33.0
15	0.52	8.6	10.2	2.1	0.2	0		33.6
30	0.44	11.5	8.9	1.4	0.1	0		32.3
1 min	0.44	10.9	8.3	1.3	0.1	0		30.3
2	0.52	8.3	9.9	2.0	0.2	0		32.5
4	0.52	8.1	9.1	1.8	0.2	0		30.3
8	---	5.4	7.7	1.7	0.2	0		24.6
16	---	1.7	6.1	2.2	0.4	0		19.1
EXPOSURE: 4.6 microJoule/cm^2								
A.M.*	0.06	0.3%	0%	0%	0%	0%		0.3%
0 sec#	0.44	15.2	5.9	0.5	0	0		28.0
5	0.30	16.4	6.1	0.6	0	0		29.8
15	0.22	19.4	4.8	0.3	0	0		29.6
30	0.18	21.8	2.7	0.1	0	0		27.4
1 min	0.24	15.8	5.2	0.4	0	0		27.0
2	0.20	19.1	4.2	0.3	0	0		28.1
4	---	13.9	3.9	0.3	0	0		22.3
8	---	7.7	5.2	0.7	0	0		19.5
16	---	3.0	5.5	1.3	0.1	0		16.8
EXPOSURE: 9.2 microJoule/cm^2								
A.M.*	0.10	0.1%	0%	0%	0%	0%		0.1%
0 sec#	0.24	24.3	5.3	0.3	0	0		35.5
5	0.30	22.1	6.8	0.5	0	0		36.7
15	0.27	25.1	5.5	0.3	0	0		36.7
30	0.27	24.3	4.3	0.2	0	0		33.3
1 min	0.27	24.7	5.1	0.3	0	0		35.5
2	0.30	22.1	5.5	0.3	0	0		33.7
4	---	15.3	4.5	0.3	0	0		24.9
8	---	10.2	4.3	0.4	0	0		19.6
16	---	5.3	6.4	1.2	0.1	0		20.7

*Ordinary or amplitude grating

#Dichromate bleached grating

light used by the interferometer to read-out relief. The longer Purex treatment times combined with long exposure values turned the emulsion crystalline in appearance and changed the transmission and reflection properties of the emulsion. The Purex Relief Method (for 1%, 3%, 6¼% and 12½% solutions) produces additional relief (over and above that obtained by dichromate bleaching) only for short exposures. The longer exposures (greater values of original optical density) will actually have less relief after Purex treatment. The best relief was obtained by dichromate bleaching of gratings with middle exposure values.

It is preferable to concentrate as much light as possible into the ±1 order, since this is the usual location of images in holograms. In general, the ±1 order was found to be stronger than the ±2 and higher orders. (The sole exception is seen in Table III. 4, exposure 1.0 microJoule/cm^2, Purex treatment 4 minutes. This emulsion has a crystalline appearance described above.)

While the highest efficiency (greatest % intensity in ±1 order) found in Tables III. 3 and III. 4 is 14.4% (Table III.4, exposure 1.0 microJoule/cm^2, Purex treatment 15 seconds), the Purex produces little additional intensity in the ±1 order, in the higher exposure values, above that produced by dichromate bleaching. In the lower exposure values (0.2, 0.3, and 0.6 microJoule/cm^2) Purex does produce significant increases in intensity in the ±1 order. The best results were obtained for a Purex treatment of 2 minutes.

TABLE III. 5

Intensity Values with a Purex Treatment of 2 Minutes

Exposure		±1 Order Intensity	
(microJoule/cm^2)	A. M.	Dichromate	Purex
0.2	0.1%	0.2%	5.6%
0.3	0.4%	0.7%	5.9%
0.6	0.1%	1.7%	10.2%

Table III. 5 shows that, for the low exposure values, the Purex treatment produced good ±1 order intensity values. An increase of 102 times in the intensity of Purex treated gratings over that of the ordinary amplitude gratings and of 6 times in intensity of Purex gratings over dichromate gratings occurred at an exposure of 0.6 microJoule/cm^2. Greater increases in intensity of Purex treated gratings over dichromated gratings occurred at 0.2 and 0.3 microJoule/cm^2 (28 times and 8 times as intense, respectively) exposures. The Purex treatment appears to have fine possibilities in recovering very low intensity images that occur at short exposures, thus effectively increasing film speed. No results have as yet been obtained at spatial frequencies above 26 lines/mm. This is a severe limitation in recording off-axis holograms.

As with the Wash-Off Relief gratings described earlier in this report, unusual light intensity distributions were found to occur in Purex treated gratings. For one 26 line pair/mm Purex treated grating (see Table III. 4, exposure 1.0 microJoule/cm^2, Purex treatment 1 minute) the zero order is almost completely absent and the ±1 and ±2 orders appear more intense. Several instances where the zero and ±1 orders are about equal in intensity can be found. These are Purex treated gratings with medium values of exposure (0.9, 1.0, 1.8, and 3.6 microJoule/cm^2). Equal amounts of relief do not give similar diffraction intensities.

While no general relation appears to exist between diffraction intensity and relief, the lower exposure values seem to have increasing intensity of the ±1 order for increases in relief. It appears that some other factor such as changes of index of refraction are affecting the intensity distributions.

Conclusions

Available color film does not appear to have sufficient resolution for use in holography. Higher resolution color film, if such should become available, could prove to be an efficient hologram recording medium.

The Purex Relief Method is a faster relief method than the hot water Wash-Off Relief Method, although it too is limited at present to low spatial frequencies.

For short exposures, relief and ±1 order intensity increase after Purex treatment. For the longer exposures, the ±1 order intensity after Purex treatment remains about the same as or less than that obtained by the dichromate treatment alone. It therefore appears possible to increase the effective film speed by underexposing and using the Purex treatment. Increasing the effective film speed should enable one to use very short exposure times combined with sufficient laser intensities to capture transient events.

It is possible to place light in selected order (or suppress it from those orders) by using the Purex treatment.

Future Work

All of the techniques investigated to date for controlling emulsion relief have been characterized by a maximum spatial frequency capability that is inadequate for most hologram applications. It appears at this time that no solutions to this resolution problem are forthcoming in the immediate future.

A study of the Wash-Off Relief method on holographic image resolution and brightness will be continued as a thesis topic. The holograms used will

be recordings of a National Bureau of Standards Resolution Test Chart. Various parameters of the Wash-Off Relief Method such as spatial frequency, exposure, film type, wash time, and wash temperature will be studied in order to determine their effect upon the reconstruction image resolution and brightness. Comparative studies of amplitude, dichromate bleach, and wash-off relief versions of the same hologram will be presented. This work is being undertaken in order to determine the optimum values of reconstructed image brightness and resolution.

If sufficient manpower were to become available, work could continue in several areas. These include the use of the Purex Relief Method to improve the effective speed of the photographic emulsion, and the use of other reactions to produce and control emulsion relief. It is felt, however, that other projects in progress show more chances of success and would find greater use in their application. Therefore, no other work is planned at this time. This topic is open to development as a student thesis, and, should additional methods or improvements in present techniques come to light, this portion of the project will be re-activated.

IV. Characterization of Turbulent Flow by Optical Methods

M. K. Mazumder and D. L. Wankum

Introduction

A laser Doppler velocity meter has the essential features of an ideal instrument to measure the structure of a turbulent fluid flow. There are, however, some problems associated with this technique which need to be solved before this instrument can be effectively employed in a non-stationary localized fluid flow measurement. Of these, the finite instrumental spectral broadening (δf) of the signal and low signal-to-noise ratio are probably most important.

The conventional method of electronic processing of the Doppler signal requires that the inherent frequency spread be minimum. Compared with a FM signal used in communication, the Doppler signal form a non-stationary flow field contains a continuous spectrum of carrier frequency in a range $f_c \pm \frac{1}{2} \delta f$ with the modulation component $\Delta f \cos \omega_m t$. Unless δf is small, frequency to voltage conversion becomes a serious problem.

Further, the accuracy of measurement of the effective frequency spread (Δf) due to the temporal velocity fluctuations is limited by the inherent instrumental spread (δf). For instance, the intensity of turbulence at the center of a pipe is about 3% of the mean velocity of the fluid at the onset of turbulence. Instrumental spread of 1% and above may give rise to a significant error. The amplitude of the Doppler signal depends on the scattering angle and characteristics and concentration of the scattering centers present in the fluid medium. These quantities are not always controllable and often the intensity of the scattered beam is low. This

condition and inefficient spatial filtering to eliminate the unwanted scattered light falling on the photocathode may cause a poor signal-to-noise ratio.

Previous studies[21] on a laser Doppler velocity meter show that the symmetrical system of heterodyning is preferable in the characterization of turbulence. It has the advantage of: (1) low instrumental frequency spread because of complete elimination of the frequency spread due to the uncertainty in the scattering angle, (2) high signal-to-noise ratio, (3) simple optical alignment, and (4) there is no effect of the fluid density fluctuation in the path of the scattered beam. A complete system design to measure the structure of turbulence depends on the statistical parameters that are to be measured, such as the correlation function, energy spectrum, etc. To obtain the joint probability-density-distribution function, simultaneous measurements of velocity at two points are required. The present report outlines the experimental set-up, briefly indicating some of the problems being encountered. Data on the measurement of the velocity profile at a point located at the center of the duct are presented.

Work Performed

(a) System layout:

Figures 19 and 20 show schematically the system layout for the measurement of turbulence structure. An aluminum duct having a cross sectional area of 10 sq cm and a length of 170 cm is used as an air tunnel. At the center of the duct, lucite windows (38 cm x 6 cm x 3 mm) are provided on the four sides. A blower is used at the downstream end of the duct and the flow region up to a well-developed turbulent flow. In the present set-up the maximum velocity to be used will be nearly 0.2 M. At this velocity $\Delta\rho_{air}/\rho_{air}$ will be

around 2%. Turbulence producing grids are placed at the upstream of the duct and their size will be varied to generate desired turbulence scales. Water mist is used as the scattering aerosol.

A symmetrical heterodyning system is used for the measurement of the Doppler signal. For a convenient physical layout of the transmitting and receiving optics and to reduce the scattered lights from the windows falling on the photocathode, a 90° scattering angle is chosen as shown in Figure 19. For simultaneous measurement of velocity at two points, two measuring systems are used. Any one of the 3D velocity components can be measured at any one of these points. The receiving optics consist of a spatial filter to collect scattered light only from the sampling volume where the two incident beams cross. The photomultipliers used are RCA 7265 tubes. Two preamplifiers having a voltage gain of 200 and bandwidth of 30 MHz are used and their outputs are fed to the frequency discriminators.

(b) Frequency to voltage conversion

Frequency to voltage conversion of the Doppler signal presents a problem. This is particularly due to the wide dynamic range of the center frequency (f_c) of the Doppler signal, its associated instrumental spread δf, and large frequency deviation (Δf_u) arising from velocity fluctuations. The center frequency of the Doppler signal in a symmetrical system (Figure 19.)

$$f_c = \frac{2U}{\lambda_o} \sin \frac{\theta}{2} \tag{22}$$

and the signal frequency spread (due to the transmission aperture broadening)

$$\delta f_a \doteq \frac{4U}{\lambda_o} \sin \frac{\alpha}{2} \cos \frac{\theta}{2} \tag{23}$$

or

$$\frac{\delta f_a}{f_c} \doteq 2 \sin \frac{\alpha}{2} \cot \frac{\alpha}{2} \tag{24}$$

$$\doteq \frac{2d}{D} \cdot \frac{F}{R} \cdot \tag{25}$$

The parameters F, R, d and D are shown in Figure 19.

Since $F \leq R$, the maximum broadening will be $\frac{2d}{D} \times 100\%$. In this case, δf_a is referred to as the maximum signal width derived on the assumption that the laser beam intensity is constant across the transmission aperture. This, however, gives a conservative value of δf_a. The total frequency spread depends also on other factors, such as finite sampling volume, finite signal lifetime, etc. In practice, d is fixed by the laser beam spot size and D can be increased to reduce the spread. This increase in θ would result in higher f_c and Δf_u and would require a larger dynamic range of the discriminator. The sampling volume decreases with the increase of θ. Reflection loss from the optical windows increases with θ. An optimum set-up would therefore depend on the above factors. Experimental studies on frequency to voltage conversion using a pulse counting type FM discriminator with a wide linear range are in progress. Other conventional FM detectors are being studied along with the required preconditioning of the signal. Initial work shows some promising features of the above methods. Further work is being continued.

(c) Results

Table IV. 1 shows typical values of SNR and instrumental spread. The spread is small when $\sin \theta/2$ is large and $\sin \alpha/2$ is minimum.

TABLE IV. 1

Typical values of $\frac{\delta f}{f_c}$ x 100% and SNR (db)

sin θ/2	sin α/2	$\frac{\delta f_{\text{half power}}}{f_c}$ x 100%	SNR (db)
0.0750	0.0075	3.8%	31
0.1398	0.0143	4.3%	28
0.1500	0.0028	0.8%	30
0.2436	0.0143	1.4%	30

The data presented here on fluid flow are being carried out with arbitrarily chosen values of θ (sin θ/2 = 0.1398) and α (sin α/2 = 0.0143). Later experiments will employ optimum values of these angles.

The power spectrum of the Doppler signal from laminar flow as well as from turbulent flow of low intensity was observed in the spectrum analyzer display. Figures 21 and 22 show the spectrum analyzer output recorded by a potentiometric recorder. The frequency spread increases considerably when the Reynolds number increases from a laminar flow to a turbulent flow region. This, however, does not immediately tell the actual contribution from the velocity fluctuations, since the instrumental spread δf also increases with the mean velocity $\overline{U}$ (Equation 23). To examine the actual velocity spread, instrumental frequency spread was measured with the same parameters but having the scattering particles moving with a constant velocity equal to the mean fluid velocity $\overline{U}$. This was done using a surface scattering disc rotated by a synchronous motor. Table IV. 2 shows the total frequency spread for different Reynolds numbers and the figures are compared with the expected instrumental spread. As the Reynolds number increases, Δf becomes larger compared with δf. At $R_e \geq 16{,}600$, Δf measurement

becomes difficult with the spectrum analyzer due to the large velocity fluctuations and consequently high modulation index. Figures 23a, 24a, 25a, and 26a show the photographs of the power spectrum of the Doppler signal fluid flow system, whereas Figures 23b, 24b, 25b and 26b are from a surface scattering disc driven by a constant speed motor.

TABLE IV. 2

Total Frequency Spread of Different Reynolds Numbers

Fluid flow ($\sin \theta/2 = 0.1398$, $\sin \alpha/2 = 0.0143$)

mean velocity (cm/sec)	R_e	f_c	total frequency spread (Δf)	instrumental frequency spread (δf)
37.4	762	170 KHz	19 KHz	17 KHz
332.0	5300	1.5 MHz	390 KHz	100 KHz
595.0	10600	2.7 MHz	705 KHz	120 KHz
818.0	16600	3.7 MHz	1.2 MHz	154 KHz

Table IV. 3 shows the effect of turbulence-producing grids. The distance between the grid and the point of measurement was arbitrarily chosen as ten times the diameter of the duct. Square mesh (#6) was used with a rod diameter of 0.035 in. Since the turbulence characteristics depend on the grid size used, these parameters will be controlled in later experiments.

TABLE IV. 3

Effect of Turbulence-Producing Grids

R_e	f_c	Δf with grids	Δf without grids
5300	1.5 MHz	350 KHz	180 KHz
10600	2.7 MHz	705 KHz	212 KHz

Future Work

(1) the optimization of system parameters

(2) design and testing of signal processing equipment and establishing a satisfactory frequency to voltage conversion system.

(3) calibration of the system using a well controlled fluid flow device

(4) turbulence studies on the free submerged jet (rectangular and round nozzles)

(5) generation of near isotropic turbulence using a rectangular wind tunnel of 6' x 6' cross section and data acquisition and signal processing for the determination of statistical parameters describing turbulence structure.

APPENDIX I

PUREX RELIEF METHOD

The Purex Relief Method was performed as follows:

(a) Expose film normally but through the back. The more heavily exposed regions will then be nearest the film base, and proper relief of the image is then possible.

(b) Develop exposed film using the manufacturer's recommended developer. Development times are specified in the Kodak Manual for each particular film and these times were found to be satisfactory. Kodak D-19 developer was used.

(c) The stop bath is a one-minute wash in running water. An acid stop bath should not be used. As in normal film processing, all steps should be performed at the same temperature and preferably at 68°F or less.

(d) The film is fixed in a non-hardening fixer (for convenience Kodak F-24 fixer was used). The film is next washed in running water for ten minutes to clear it of any soluble residues.

(e) After drying at room temperature, the emulsion is "set-up" and one can proceed with the dichromate bleaching step. The dichromate bleach is prepared as follows:

Solution A.	Ammonium dichromate	15 g
	Sulfuric acid (conc.)	3 cc
	Water	2250 cc
Solution B.	Sodium chloride	34.5 g
	Water	2250 cc

Equal parts of solutions A and B are added together for use. Treatment is

terminated when the black image is completely reduced. Dichromate selectively hardens the emulsion in proportion to the image optical density.

(f) The film is again washed for ten minutes in running water. Purex bleach (by weight, 6% sodium hypochlorite and 94% inert ingredients) is added to water

Purex bleach	1 cc
Water	99 cc

The emulsion is first dried as in step (e) and then treated in the Purex bleach solution above for 2 minutes. While 2 minutes treatment generally produced the best results, it is suggested that, in order to obtain the optimum brightness, one should treat identical frames with 5, 15, 30 and 60 second washings in the Purex bleach solution.

APPENDIX II

SNR AND SPECTRAL BROADENING IN TURBULENCE STRUCTURE MEASUREMENT USING A CW LASER*

M. K. Mazumder and D. L. Wankum

University of Arkansas

Graduate Institute of Technology

Department of Electronics and Instrumentation

Little Rock, Arkansas

Abstract

A symmetrical method of optical heterodyning of the Doppler shifted signal has been developed possessing minimal instrumental spectral broadening and high SNR. These advantages can be gainfully employed in measuring turbulence structure using a CW laser. The method employs two beams incident on the moving scatterer. The Doppler signal frequency is independent of the scattering angle and the signal possesses no receiving aperture broadening. Typical values of signal-to-noise ratio are around 30 db for a signal strength of 3×10^{-9} watts. Optical alignment is simple. Relative merits of this technique compared to the local oscillator heterodyning method are briefly described.

Introduction

Recently, considerable work has been reported in the field of laser Doppler velocity measurement[22-29] due to its variety of potential

applications, such as measurement of "clear air" turbulence in the troposphere, propulsion studies, exhaust flow configurations on rocket bases, thermonuclear plasma research, etc. Although a laser Doppler velocity meter has several advantages over a hot wire anemometer, it has major limitations in certain aspects. Among these, the Doppler signal frequency or wavelength line width and signal-to-noise ratio (SNR) are probably most important.

Until now, localized fluid flow measurements using a CW laser employed beating of the scattered beam with a reference beam which is usually a portion of the incident beam[22-25]. Often this is referred to as local oscillator heterodyning. There is a considerable uncertainty in the scattering angles due to the finite sizes of transmission and receiving apertures. This results in a frequency spread of the Doppler signal which is typically around 10 to 15% of the center frequency[26]. In non-stationary localized fluid flow measurements, it is desirable to have a minimum instrumental spectral broadening. Signal line width should be small compared to the effective bandwidth arising from the velocity fluctuations. As an example, the intensity of turbulence at the center of a pipe is about 3% of the mean velocity of the fluid at the incipient turbulent flow[36]. Further, any conventional method of electronic processing of the Doppler signal requires that the inherent frequency spread be minimum. Compared with a FM signal used in communication, the Doppler signal from a non-stationary flow field contains a continuous spectrum of carrier frequency in a range $f_c \pm \frac{1}{2} \delta f$ with the modulation component $\Delta f \cos \omega_m t$. Unless δf is small, frequency voltage conversion becomes a serious problem.

The amplitude of the Doppler signal depends on the characteristics and concentration of the scattering centers present in the fluid medium. These quantities are not always controllable and often the intensity of the scattered beam is low. This may cause a low signal-to-noise ratio. Theoretical and experimental studies on signal-to-noise ratio and instrumental spectral broadening of the Doppler shifted signal have been made under the present work. Different geometrical configurations of optical heterodyning using a CW laser are briefly described.

Doppler Shift and Instrumental Broadening

When a monochromatic beam of light is incident on a moving particle, the Doppler shift of the scattered light wave can be expressed by

$$f_D = \frac{1}{2\pi} (\vec{K}_s - \vec{K}_o) \cdot \vec{V} \qquad \text{(A1)}$$

where V is the instantaneous velocity of the particle with respect to a frame of reference and K_o and K_s are wave vectors representing the incident and the scattered waves. If $\vec{i}_o$ and $\vec{i}_s$ are the unit vectors in the direction of propagation of the two waves, and λ_o and λ_s are the wavelengths of the incident and scattered radiation respectively, and since V<<C, where C is the velocity of light,

$$\lambda_o \approx \lambda_s$$

$$|\vec{K}_s| = |\vec{K}_o| = K_o = \frac{2\pi n}{\lambda_o}$$

$$f_D = \frac{1}{\lambda_o} (\vec{i}_s - \vec{i}_o) \cdot \vec{V}$$

where n is the index of refraction of the medium.

Let us consider that a cone of light is focused on a moving particle at O having velocity components U, V, W and the receiver with an aperture area A is used to obtain the scattered signal, as shown in Figure 27. In a local oscillator heterodyning process, a scattered beam from a moving object is mixed with a part of the incident beam to generate the Doppler signal. A variation of this method has been used by Goldstein and Hagen[24]. From Eq. (A1), the center frequency of the Doppler shifted signal is a function of the scattering angle Ψ and velocity components U, V, W, and can be expressed as

$$f_c = \frac{U}{\lambda_o} \sin \Psi + \frac{V}{\lambda_o} \cos \Psi + \frac{W}{\lambda_o} \tag{A2}$$

and the frequency spread due to finite apertures of the optics,

$$\delta f_a = \delta f_{\Delta\phi} + \delta f_{\Delta\Omega} ,$$

where

$$\delta f_{\Delta\phi} = \frac{2V}{\lambda_o} \sin \Psi \sin \frac{\alpha}{2} + \frac{2\sqrt{(V \sin \Psi - U \cos \Psi)^2 + W^2}}{\lambda_o} \sin \frac{\alpha}{2} \tag{A3}$$

$$\delta f_{\Delta\Omega} = \frac{2\sqrt{U^2 + V^2}}{\lambda_o} \sin \frac{\Delta\theta}{2} \tag{A4}$$

The convergence angle α can be made small. The major contribution is from the solid angle $\Delta\Omega$ subtended by the receiver area on the light scattering point. The choice of angle Ψ depends mainly on the operating frequency range of the photomultiplier and signal processer. If the intensity of the scattered lobe is low, the receiving aperture area needs to be increased for larger signal strength. Increasing $\Delta\theta$ to increase signal strength will result in larger δf_a. The minimum value of $\Delta\Omega$ or $\Delta\theta$ will be determined by the detector sensitivity. The frequency of the Doppler

signal is proportional to the velocity, but both direction and magnitude cannot be resolved unless measurements at additional scattering angles are taken[25].

Figure 28 shows a heterodyning system developed by Bond which will be referred to as symmetrical system type I. In this process, instead of using the reference beam, two scattered beams are mixed to generate the signal. The sine curve of Figure 28 shows the Doppler shift plotted against the scattering angle for constant velocity component U. Here the center frequency f_c is sensitive only to the velocity component U which is coplaner to the two scattered beams and perpendicular to the bisector of the angle Ψ subtended by the two beams at the scattering center. The locations of the two apertures are symmetrical about the incident beam and the Doppler shifts across the apertures are within the linear portion of the curve. Spatial superposition of these two beams gives the same difference frequency across the photocathode surface and results in cancellation of the aperture broadening. Elimination of the aperture broadening will not be complete if the aperture sizes are large since the constraints that the Doppler shift across the aperture should be linear will not be satisfied.

In both the above techniques, heterodyning efficiency is highly dependent on the beam alignment which imposes a rather stringent requirement on the mechanical rigidity of the system.

These limitations can be overcome if a heterodyning system is used employing two incident beams[30], as shown in Figure 29, designated as symmetrical system type II. The scattered beam from the moving particles directly generates the desired signal. The process actually involves

heterodyning of the wave vectors scattered from the two incident beams. The resulting difference frequency can be shown to be the same at all points in the scattered lobe. No further beam mixing is necessary. The difference frequency f_c is given by

$$f_c = \frac{2U}{\lambda_o} \sin \frac{\theta}{2} \tag{A5}$$

and is independent of the scattering angle or the spatial position and area of the receiving aperture. This implies that there is no signal broadening due to receiving aperture, i.e.

$$\delta f_{\Delta\Omega} = 0 \quad . \tag{A6}$$

The receiving aperture area can be increased to increase the signal strength to the desired level without any increase in signal line width. The only aperture broadening will be due to the transmission aperture.

$$\delta f_a = \delta f_{\Delta\phi} = \frac{4\sqrt{U^2 + V^2}}{\lambda_o} \sin \frac{\alpha}{2} \cos \frac{\theta}{2} \tag{A7}$$

Here, δf_a is quite small due to the small value of $\alpha/2$. This system is suitable for measurement of any desired velocity component. Alignment is simple, particularly when a single lens is used for transmission.

Of all the sources of instrumental spectral broadening in the symmetrical system, the transmission aperture, finite scattering volume and finite signal lifetime need special attention. The transmission aperture is generally small, limited by the laser beam diameter. There is probably an optimum size of this aperture since reducing the angle α would effectively increase the sampling volume. Due to the spatial velocity gradient of the flow field, a large sampling volume would cause spectral broadening. Again, an extremely small sampling volume, if

attainable, would be undesirable due to reduced particle transit time. The expected nature of variation of δf_a versus transmission aperture diameter D_α is shown in Figure 30.

If the scattering center concentration is so low that the signal is not continuous in time, the minimum possible line width will be inversely proportional to the lifetime τ of the signal, which is the amount of time that a particle remains in the sampling volume. The frequency spread can be expressed as

$$\frac{\delta f_\tau}{f_c} \triangleq K \sin\frac{\alpha}{2} \cot\frac{\theta}{2} \tag{A8}$$

for a one-dimensional velocity. K is a constant. In most practical cases the aerosol concentration that produces a signal of considerable SNR is sufficiently high to contain a finite number of scattering centers in the sampling volume at any given instant of time. It is interesting to note that when the signal is continuous in time, the ratio of the transmission aperture-line width $\delta f_{\Delta\phi}$ to the center frequency f_c is given by (from Eqs. (A5) and (A7) and assuming V = 0)

$$\frac{\delta f_{\Delta\phi}}{f_c} \triangleq 2 \sin\frac{\alpha}{2} \cot\frac{\theta}{2} \tag{A9}$$

The similarity of Eqs. (A8) and (A9) may result in two different physical explanations of the same experimental data if both of the causes are present. This ambiguity was removed in one experiment by using a sand-blasted aluminum disc as a surface scatterer to insure that $\delta f_\tau = 0$. The frequency spread agreed well with Eq. (A8) and is shown in Figure 32. Pike et. al[31] investigated the broadening of the Doppler signal

due to the finite lifetime of the signal. Apparently, they did not consider the aperture broadening effect, and the interpretation of their data is questionable.

Signal-To-Noise Ratio

Signal-to-noise ratio in ideal photo mixing has been investigated by several workers[32-35] and their studies reveal two important aspects: (1) it is possible to operate a photomultiplier as an ideal receiver, i.e. SNR at the output will be limited by that of the incident light falling on the photocathode, and (2) if the signal bandwidth is very small it should be possible to detect a signal below the Noise Equivalent Power (NEP) of the detector.

In the heterodyning systems described above, the signal-to-noise ratio can be expressed as

$$SNR \doteq \frac{i_s^2 R}{4KT\,\delta f + 2q\langle i_d\rangle \delta f R + 2q\langle i_b\rangle \delta f R + 2qi_{dc}\,\delta f R + a\frac{e_n^2}{R}} \qquad \text{(A10)}$$

where i_s is the signal current through the load resistor R. The first four terms in the denominator represent thermal noise, dark current noise, stray light noise and shot noise, respectively. The last term represents the inherent noise in the signal, which determines the maximum possible signal-to-noise ratio attainable and needs to be considered only when the signal power P_s is quite large.

In the local oscillator heterodyning method, thermal noise, stray light noise and dark current noise can be made insignificant compared

to the shot noise in the photomultiplier by increasing the reference beam intensity. Under this condition,

$$SNR \simeq C\ (\nu_o,\ \varepsilon,\ \eta)\ \frac{P_s}{\delta f_L} \tag{A11}$$

where the constant C depends on laser frequency ν_o, quantum efficiency ε, and heterodyning efficiency η. The quantity δf_L is the instrumental frequency spread of the signal in the local oscillator heterodyning.

In the symmetrical heterodyning system type II noise supression is done by increasing the signal power P_s. This is achieved by increasing the receiving aperture area. The signal-to-noise ratio in this case is

$$SNR \simeq C\ (\nu_o,\ \varepsilon,\ \eta)\ \frac{P_s}{2\delta f_s} \tag{A12}$$

where δf_s is the instrumental signal line width of the symmetrical system. In most laboratory scale applications, $2\delta f_s$ will be smaller than δf_L, resulting in a SNR value higher or equal to the level obtained in the former system, depending on the relative values of δf and signal power. The loss in heterodyning efficiency due to beam misalignment is negligible in this symmetrical method.

A typical Doppler spectrum will display Doppler shift around "zero frequency" in addition to the signal at f_c and its higher harmonics. The Doppler spectrum around zero frequency may have two adverse effects in signal processing. First, it might set the lower limit of the dynamic range in the measurement of one of the velocity components and secondly there may be some deterioration of SNR of the signal at frequency f_c if the effective bandwidth of the zero-frequency-signal encompasses

a large frequency range. This is possible if one velocity component fluctuates while another is being measured. For example, if measurements are taken on U, while V has a fluctuating component such that

$$V = \bar{V} + V_o \sin pt \cdot$$

The Doppler spectrum around the "zero-frequency" due to the component V can be written as

$$f_V = \frac{2\bar{V}}{\lambda_o} \sin \frac{\alpha}{2} + \frac{2V_o \sin pt}{\lambda_o} \sin \frac{\alpha}{2} \qquad \text{(A13)}$$

and the output

$$e_v = e_{\bar{v}} + A \sum_{n=2,4,6}^{\infty} J_n (M) \cos npt \qquad \text{(A14)}$$

where (M) denotes the product of the coefficients and A is a constant. Equation (A14) indicates that effective bandwidth can become large and may produce appreciable noise in the signal frequency range.

Experiments and Results

Experiments were carried out on the heterodyning systems discussed above. A one-dimensional velocity measurement system using back-scattered light from a rotating disc was used employing a 50 mW He-Ne laser. The disc was painted with fairly uniform 20μ diameter white pigment particles and was driven at a constant rpm by a synchronous motor. The velocity of the scattering point could be adjusted from 10 to 30 meters per second. The detector used was a RCA C70038D photomultiplier and had a dark current 2nA at room temperature. A 50Ω load resistor was used and the output was fed to a spectrum analyzer through a wide band amplifier.

Experimental data on instrumental spectral broadening are plotted in Figure 31 for the two systems. The signal line width of the symmetrical system type II does not increase with the size of the receiving aperture. In local oscillator heterodyning, the frequency spread δf increases with aperture diameter. A major contribution to the frequency spread of the symmetrical system type II came from the transmission aperture. Figure 32 shows the variation of $\delta f_{\Delta\phi}$ with the transmission aperture diameter D_α. The local oscillator heterodyning system will show similar variation except that the minimum spread will be higher due to large $\delta f_{\Delta\Omega}$. The diameter of the aperture at the incident beam was kept at 4 mm in both systems during all other experiments.

The signal-to-noise ratios are plotted in Figure 33 for the two systems against signal strength. All other parameters, such as α and $\Delta\Omega$, were kept constant. In the local oscillator heterodyning system, the reference beam intensity was adjusted each time to maximize the signal-to-noise ratio.

Symmetrical system type II is advantageous over type I while retaining the desirable features of the latter system. Our discussion was therefore primarily limited to the local oscillator system and the symmetrical system type II. Table A1 lists some values of SNR and δf for the three heterodyning configurations. These values depend greatly on the intensity of the scattered beam near the receiver aperture and on the system parameters used. If the intensity is high, small values of $\Delta\Omega$ can be used and all three systems will give comparable values of SNR and δf. However, the two-incident-beam method is preferable because of its less critical optical alignment procedures. If the scattered light intensity is

low, but signal strength can be increased by employing large values of $\Delta\Omega$, symmetrical system type II would be again a preferred choice since δf_a would be minimum in this case. In cases where the distance between the scattering centers and the receiver is large and the intensity is low, a reasonably large receiver aperture area will not make a large $\Delta\Omega$ and consequently δf_a will not be significant. Here, local oscillator heterodyning would be a preferred method for heterodyning.

TABLE A1

Typical Values of SNR and δf for the Three Different Systems of Heterodyning*

System Used	$\delta f/f_c$		SNR	
	$\sin\frac{\alpha}{2} = 0.0075$ $\sin\frac{\theta}{2} = 0.075$	$\sin\frac{\alpha}{2} = 0.0028$ $\sin\frac{\theta}{2} = 0.15$	$P_s = 10^{-8}$W	$P_s = 2.2 \times 10^{-7}$W
Local Oscillator	20.0%	20.0%	17db	29db
Symmetrical System Type I**	3.1%	0.8%	12db	33db
Symmetrical System Type II	3.8%	0.8%	31db	33db

* $\Delta\Omega = \pi/8600$ steradians; $D_A = 8.5$ mm

** For large values of $\Delta\Omega$, symmetrical system type I is expected to have larger values of $\delta f/f_c$ compared to symmetrical system type II

Conclusion

The advantage of the symmetrical heterodyning can be employed as long as signal power can be appreciably increased by increasing the receiving aperture area. Conversely, local oscillator heterodyning is advantageous when aperture broadening of the signal is insignificant for scattering

sites located at large distances.

---

*This paper was presented at the 1969 IEEE Conference on Laser Engineering and Applications, Washington, D. C., May 26, 1969; and has been accepted for publication in Applied Optics.

REFERENCES

1. G. S. Ballard, J. Appl. Phys.; 39; 4846 (1968).

2. G. S. Ballard, Univ. of Arkansas Progress Report, NASA Grant NGR 04-001-007, Sept. 30, 1968, p. 1.

3. J. Upatnieks and C. Leonard, Appl. Opt.; 8; 85 (1969).

4. A. Vander Lugt and R. H. Mitchell, J. Opt. Soc. Am., 57; 372 (1967).

5. F. A. Jenkins and H. E. White, "Fundamentals of Optics", McGraw-Hill Book Co., Inc., New York, N. Y. , p. 169 (1957).

6. J. Stone, "Radiation and Optics", McGraw-Hill Book Co., Inc., New York, N. Y., p. 156 (1963).

7. A. R. Shulman, "Principles of Data Processing for Engineers", Goddard Space Flight Center, Greenbelt, Md., Preprint X-521-66-434, August 1966.

8. B. R. Brown and A. W. Lohmann, Appl. Opt., 5; 976 (1966).

9. A. Kozma and D. L. Kelley, Appl. Opt., 4; 387 (1965).

10. A. Vander Lugt, IEEE Trans. on Info. Theory, 10; 139 (1964).

11. P. Croce, Revue d' Optique; 35; 642 (1956).

12 Ref. 5, p. 130.

13. Ref. 6, p. 115.

14. Ref. 5, p. 353.

15. J. N. Latta, Appl. Opt.; 7; 2409 (1968).

16. T. S. Shankoff, Appl. Opt.; 7; 2101. (1968).

17. For example, J. Upatneiks and C. Loenard, Appl. Opt.; 8; 85 (1969).

18. Ref. 2, p. 27

19. Private communication, Eastman Kodak Co., April 16, 1969.

20. Kodak Data Book, "Kodachrome Films for Miniature and Movie Cameras", 5th Ed., pp. 47-48.

21. M. K. Mazumder and D. L. Wankum, "SNR and Spectral Broadening in Turbulence Structure Measurement Using a CW Laser", accepted for publication in Applied Optics.

22. Y. Yeh and H. Z. Cummins, Appl. Phys. Letters; 4; 176 (1964).

23. J. W. Foreman, W. W. George, and R. R. Lewis, Appl. Phys. Letters; 7; 77 (1965).

24. R. J. Goldstein and W. F. Hagen, Phys. Fluids; 10; 1349 (1967).

25. J. D. Fridman, R. M. Huffaker and R. F. Kinnard, Laser Focus; 4; No. 21, 36 (1968).

26. D. T. Davis, ISA Transaction; 7; 43 (1968).

27. E. X. Raymond, Jr., "Study of Techniques for Detection and Measurements of Clear Air Tubulence", DDC Report No. AD 63625, January 1966.

28. R. T. H. Collis, Science J.; 4; 72, February 1968.

29. R. L. Bond, "Contribution of System Parameters in the Doppler Method of Fluid Velocity Determinations", Ph.D. Dissertation, Univ. of Arkansas, 1968, NASA Acc. No. N68-27651.

30. M. K. Mazumder, University of Arkansas Progress Report for NASA Grant NGR-04-001-015, June 30, 1968, NASA Acc. No. X69-10039.

31. E. R. Pike, et al, J. Sci. Instr., Series 2, 1 (1968).

32. M. E. Monroe, DDC Report No. AD 474465, October 1965.

33. B. M. Oliver, Proc. I.R.E. (Corr.); 49; 1960 (1961).

34. H. A. Hans and C. H. Townes, Proc. I.R.E. (Corr.); 50; 1544 (1962).

35. M. Ross, "Laser Receivers", John Wiley & Sons, New York, 1966.

36. H. L. Dryden, Ind. & Eng. Chem.; 31; 416 (1939).

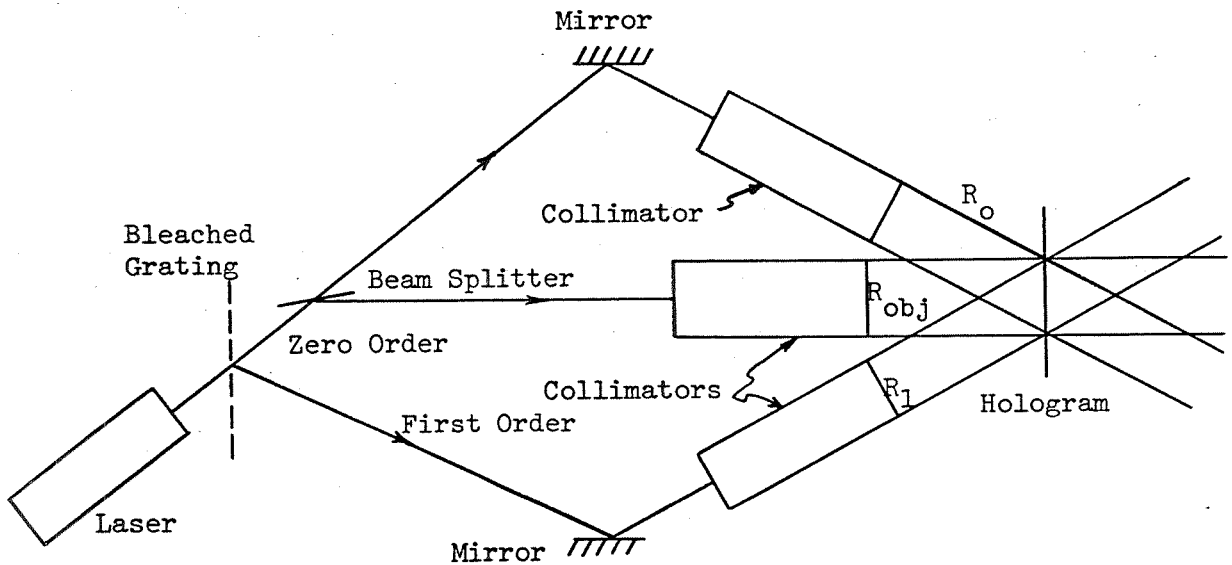

Figure 1

Optical Arrangement for Recording a Double Exposure Hologram
with Separate Reference Beams

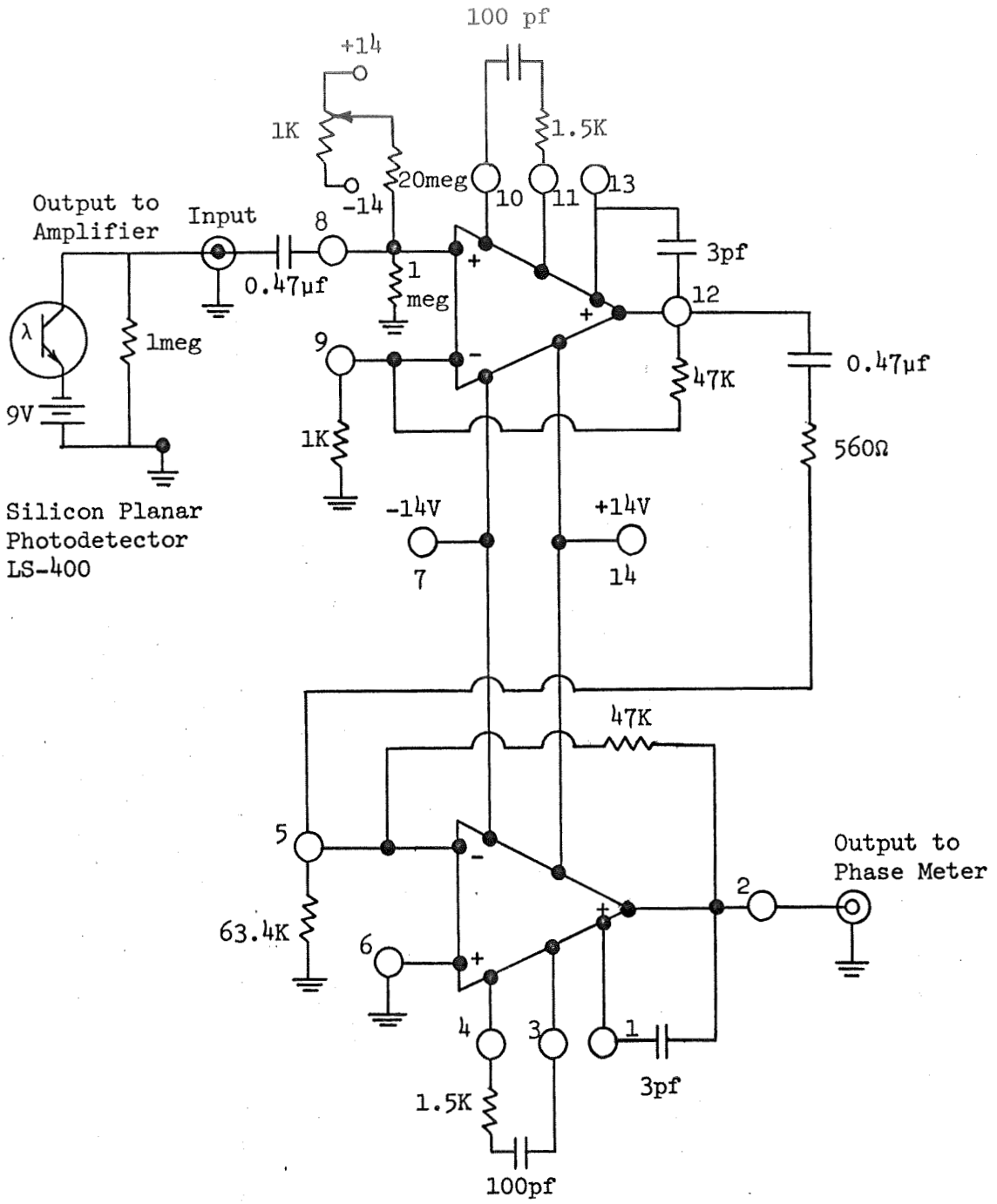

Figure 2

Detector-Amplifier Circuit Diagram

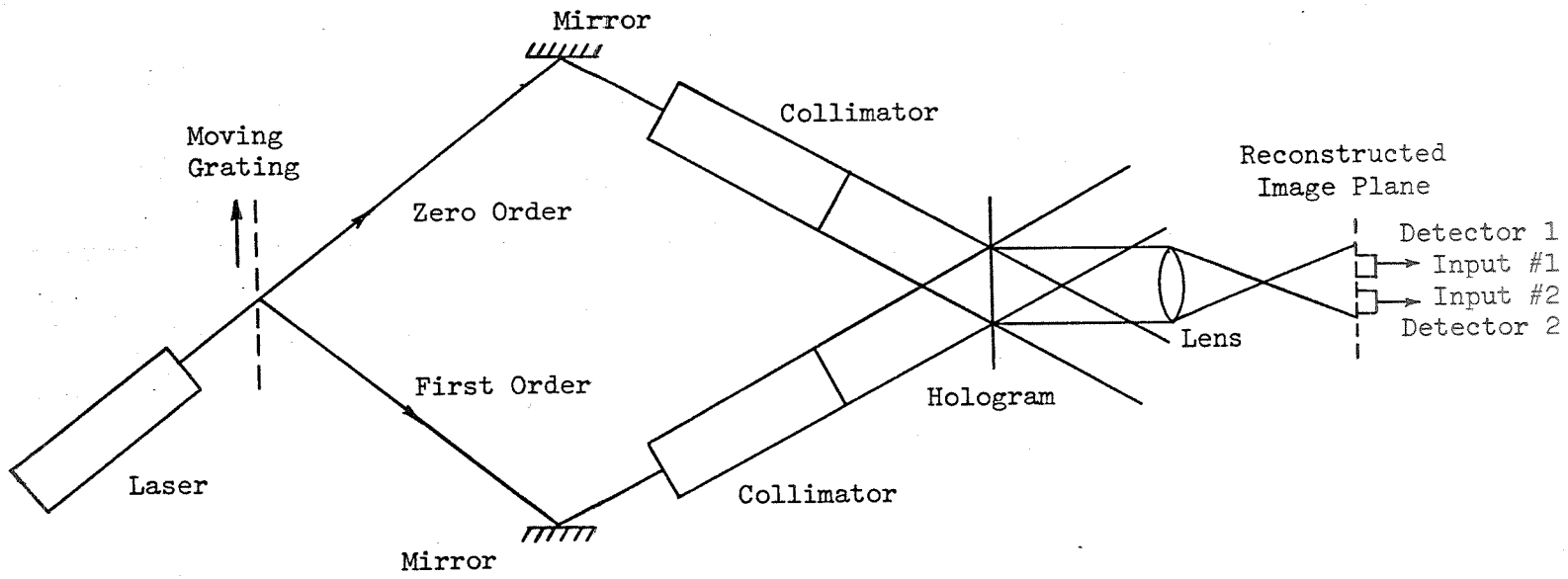

Figure 3

Method of Measuring Small Phase Variations in a Holographically Recorded Test Scene

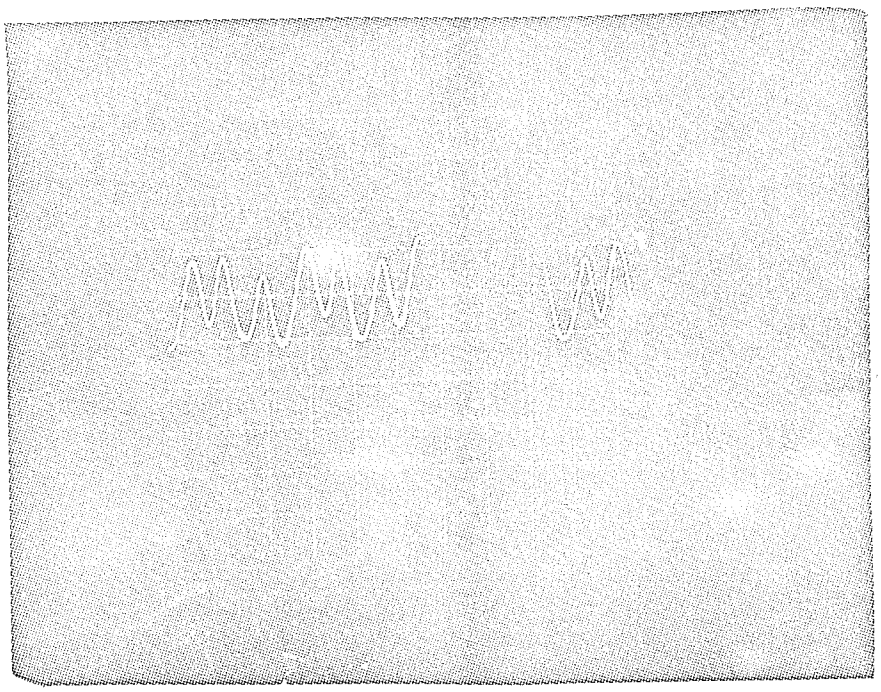

Figure 4

Output Signal With Grating in Motion From One Detector

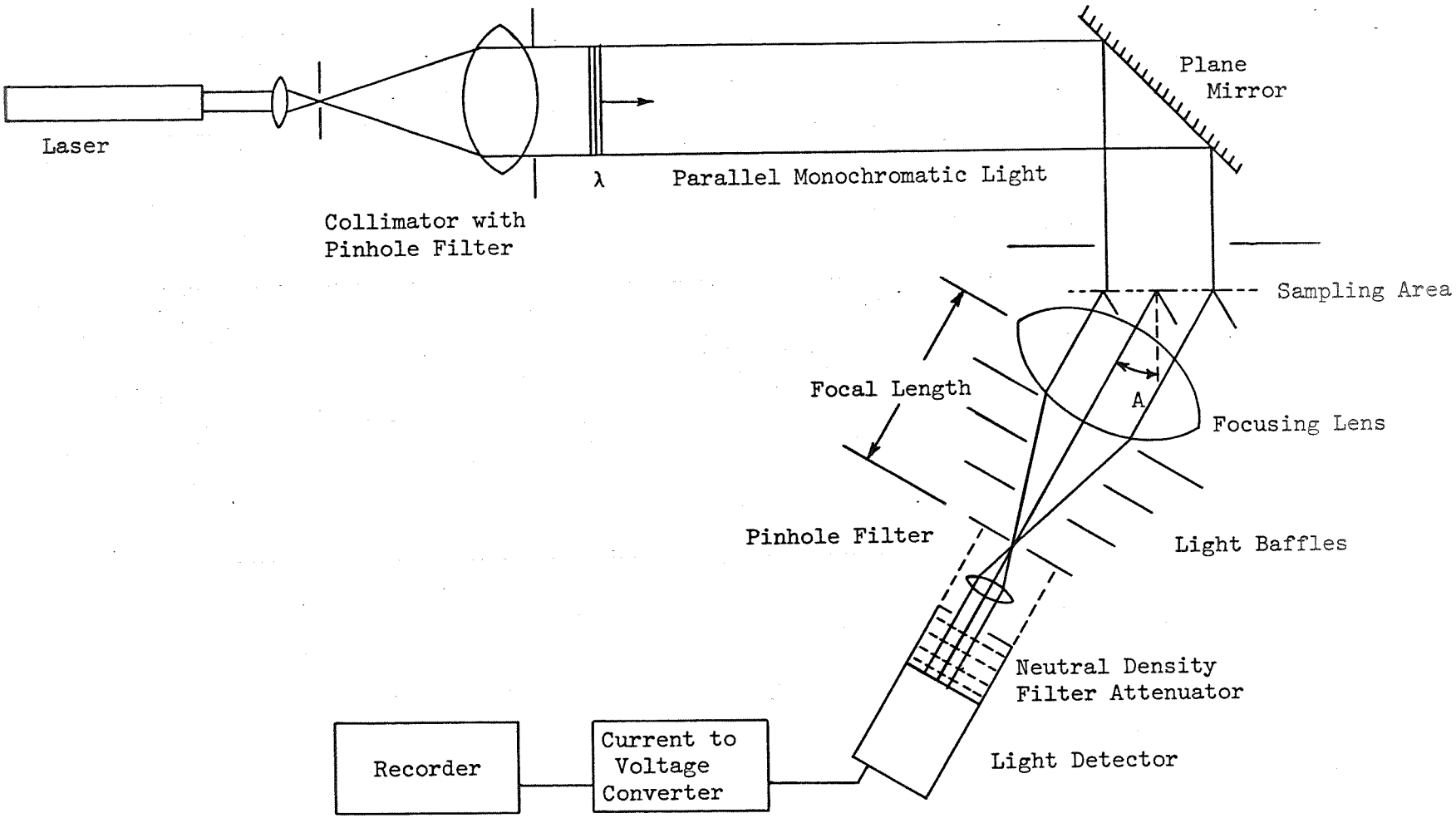

Figure 5

Diagram of the Spatial Frequency Spectrum Analyzer

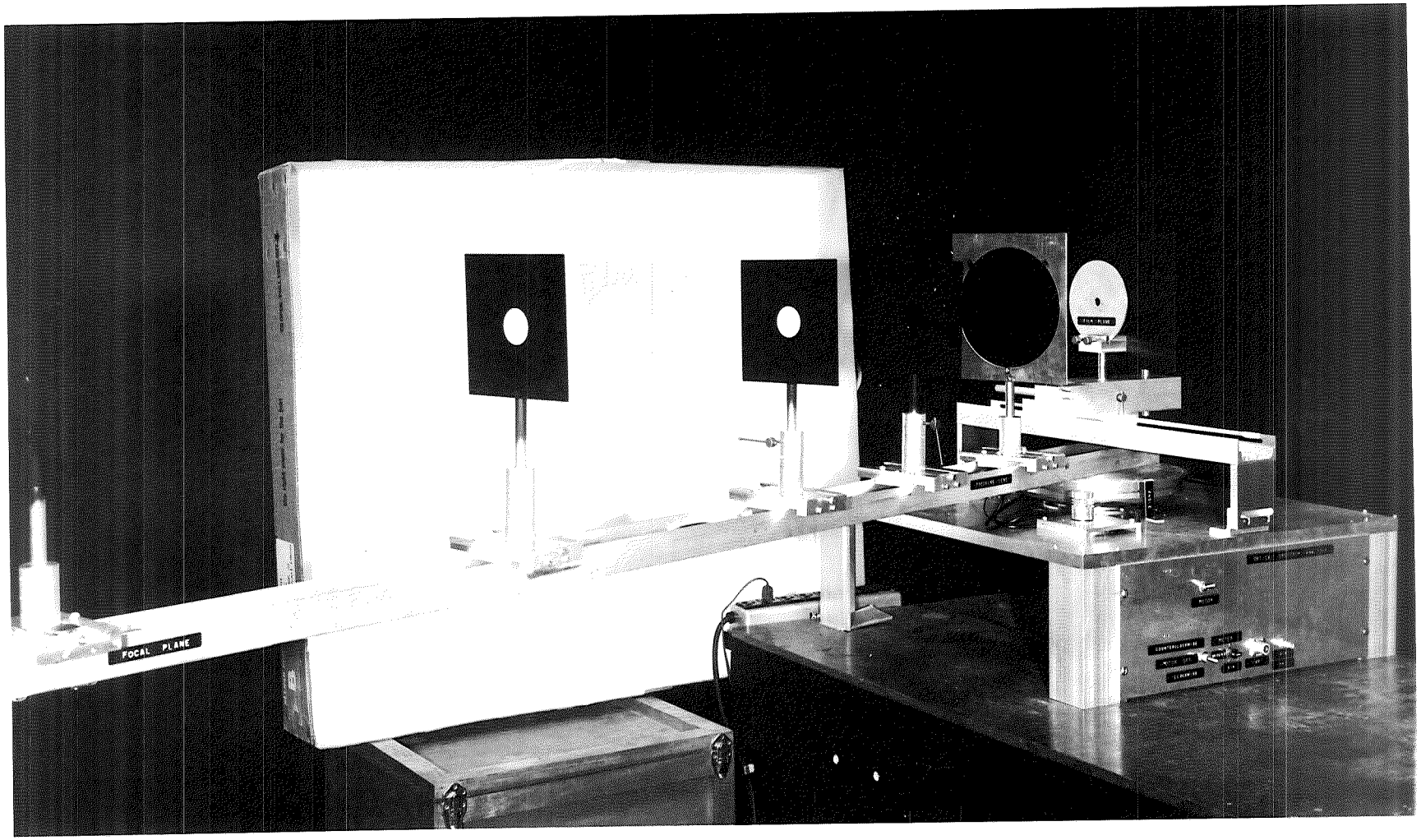

Figure 6. The Optical Spectrum Analyzer Showing Sample Holder, with Lens and Light Baffles In Position On 8' Rotating Arm

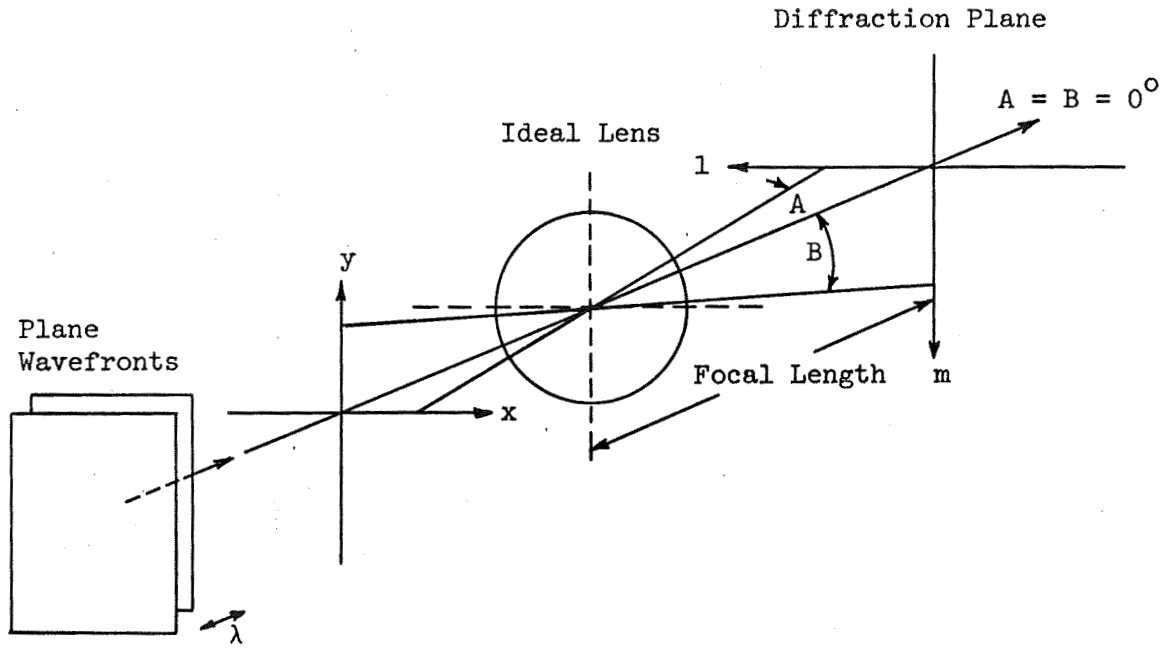

Figure 7

The Space Coordinate System Used in Describing the Angular Dependent Diffraction Pattern When an Ideal Lens Is Present

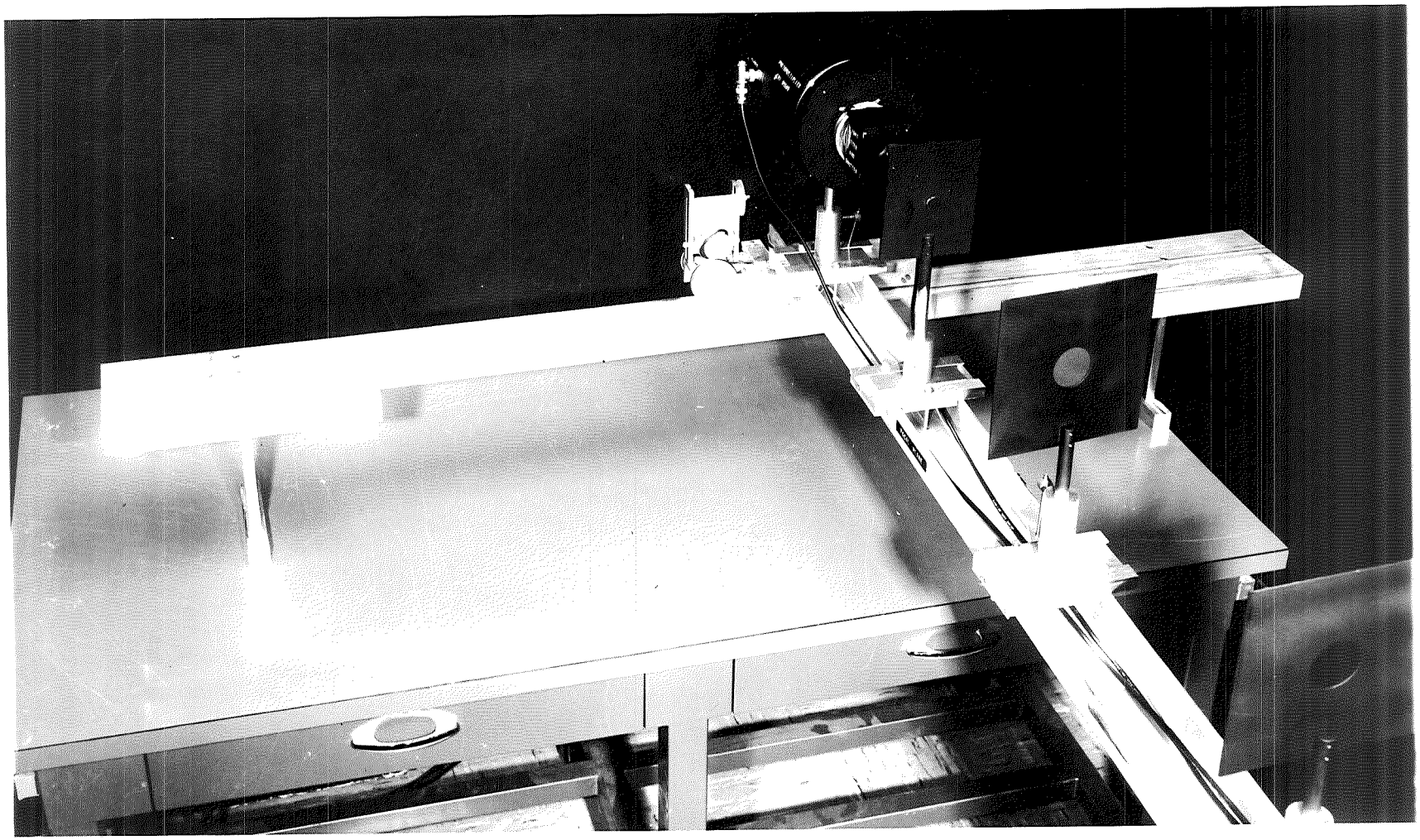

Figure 8. Motor Drive Of Long Optical Bench As It Rides On Track

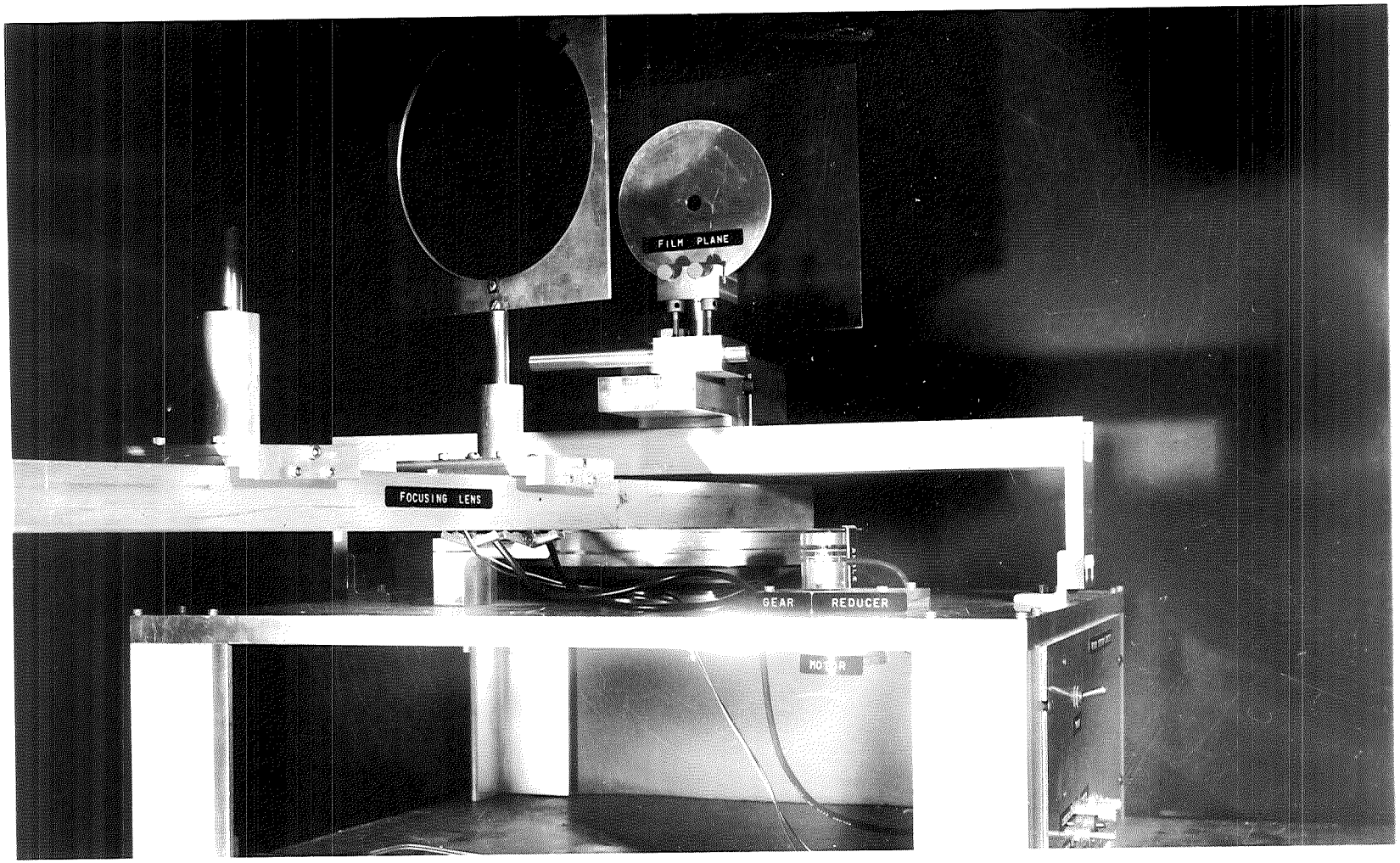

Figure 9. Side View Of Spectrum Analyzer Showing Motor Drive Assembly Used With Short Arm

Figure 10. The Photomultiplier, Shutter and Attenuator Box Used In The Optical System.

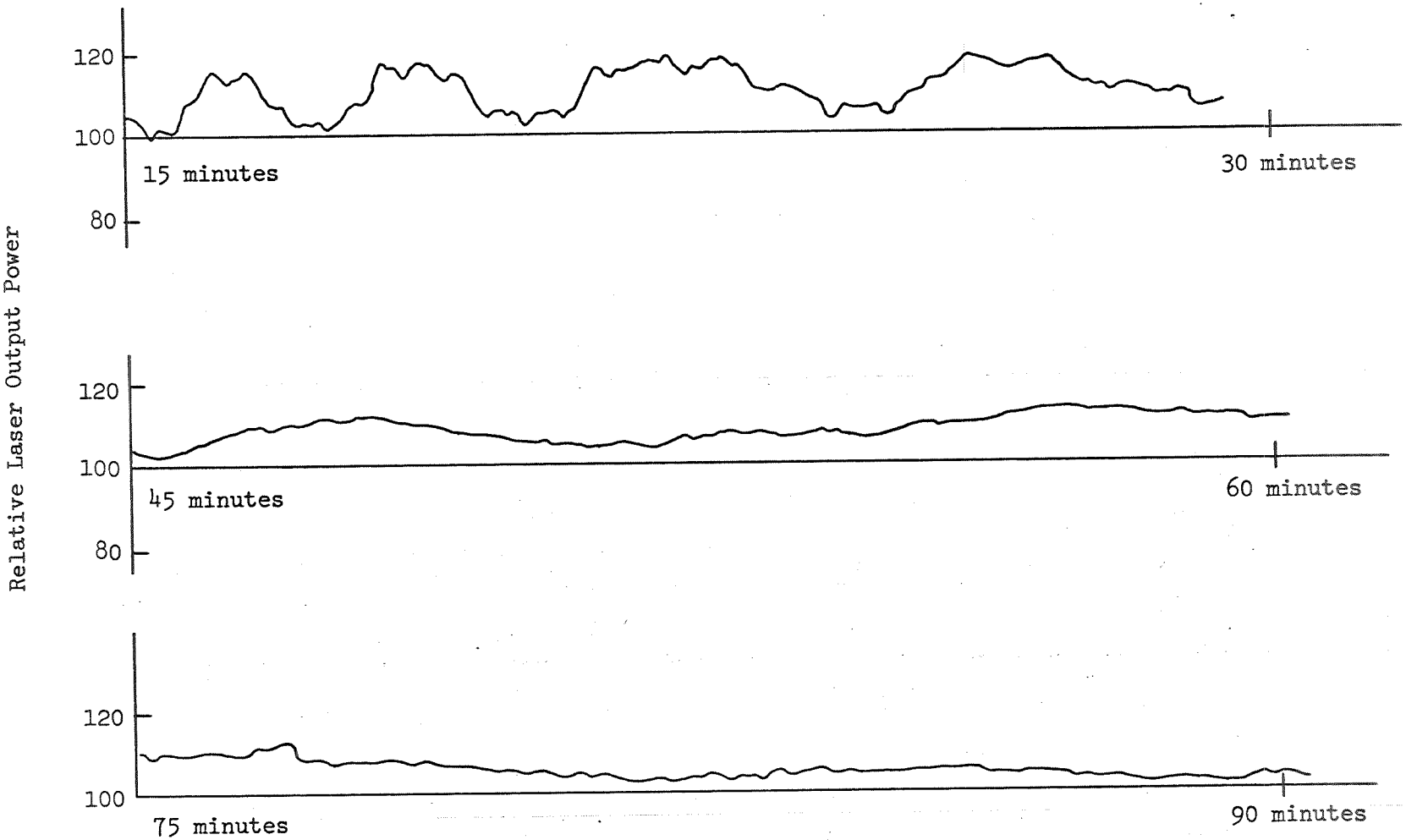

Figure 11

Output Laser Power Recording for Alternate 15 Minute Periods During the 90 Minutes After Turn On

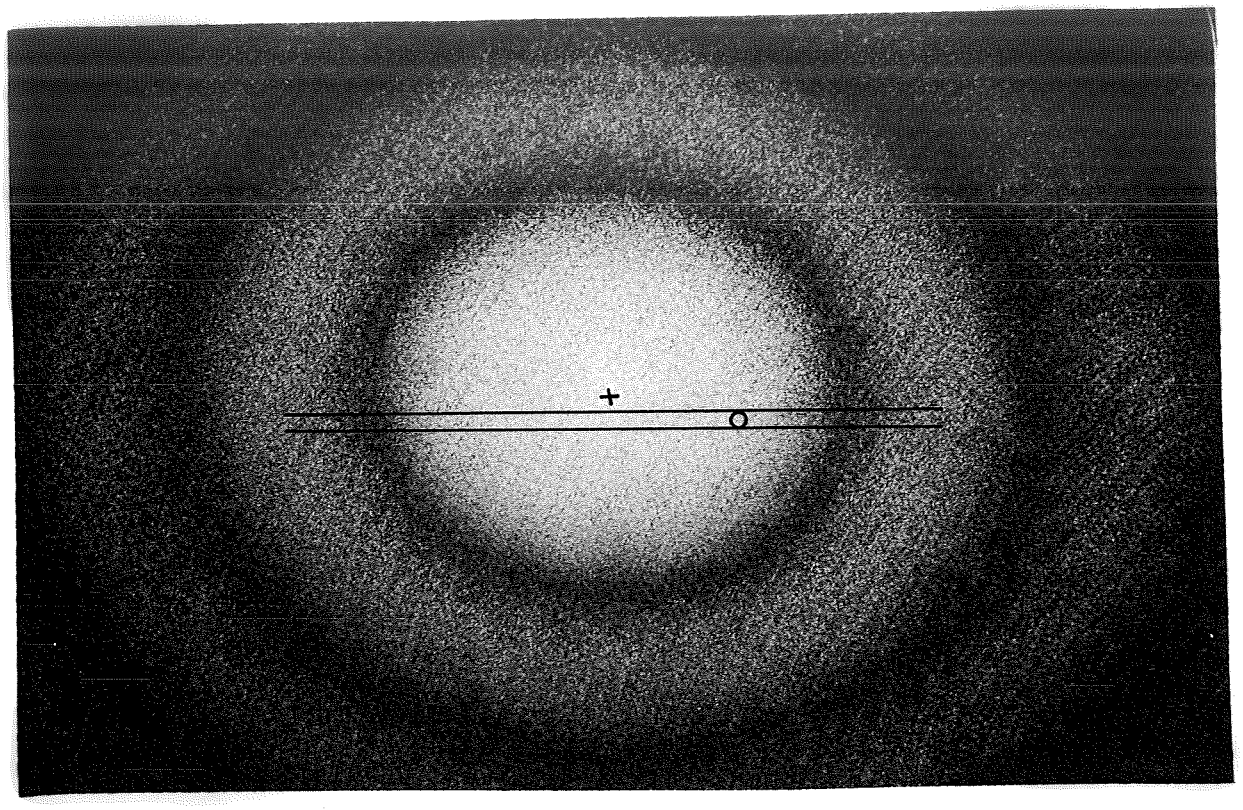

Figure 12. Diffraction Pattern of Test Plate 3
With Filtering Aperture Superimposed

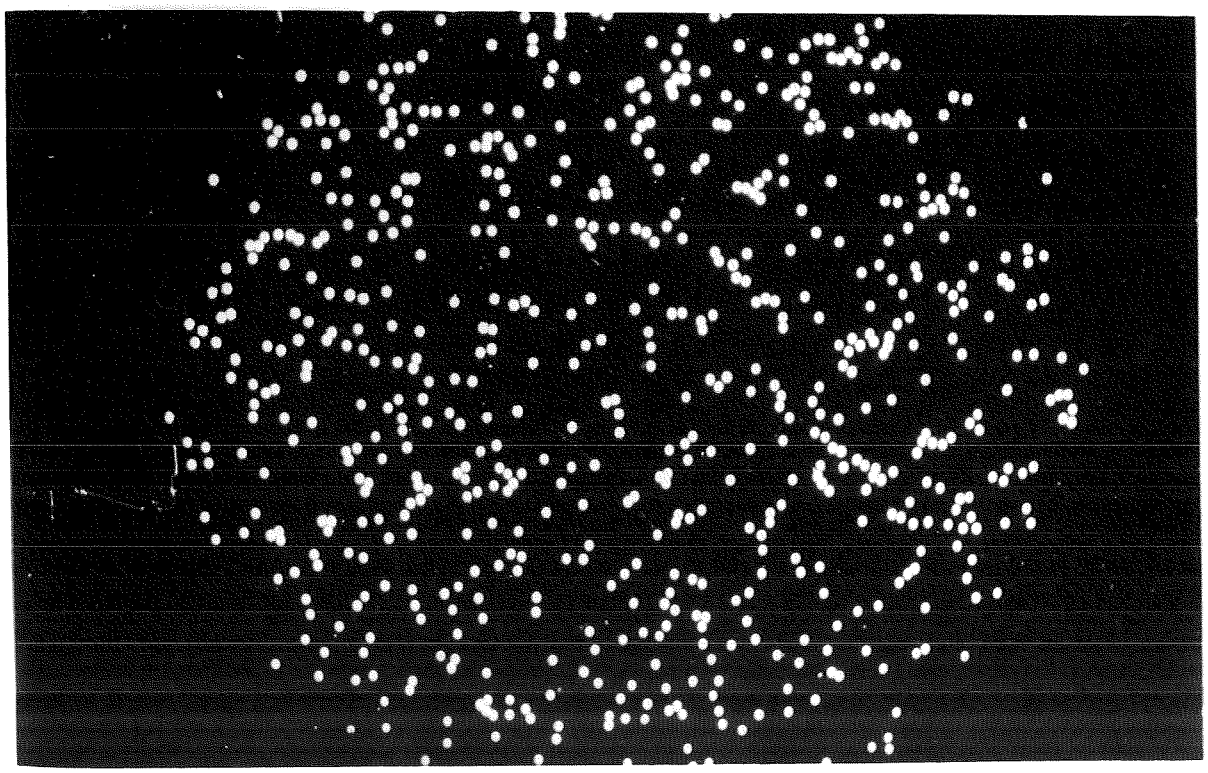

Figure 13. Enlarged View of Test Plate 3

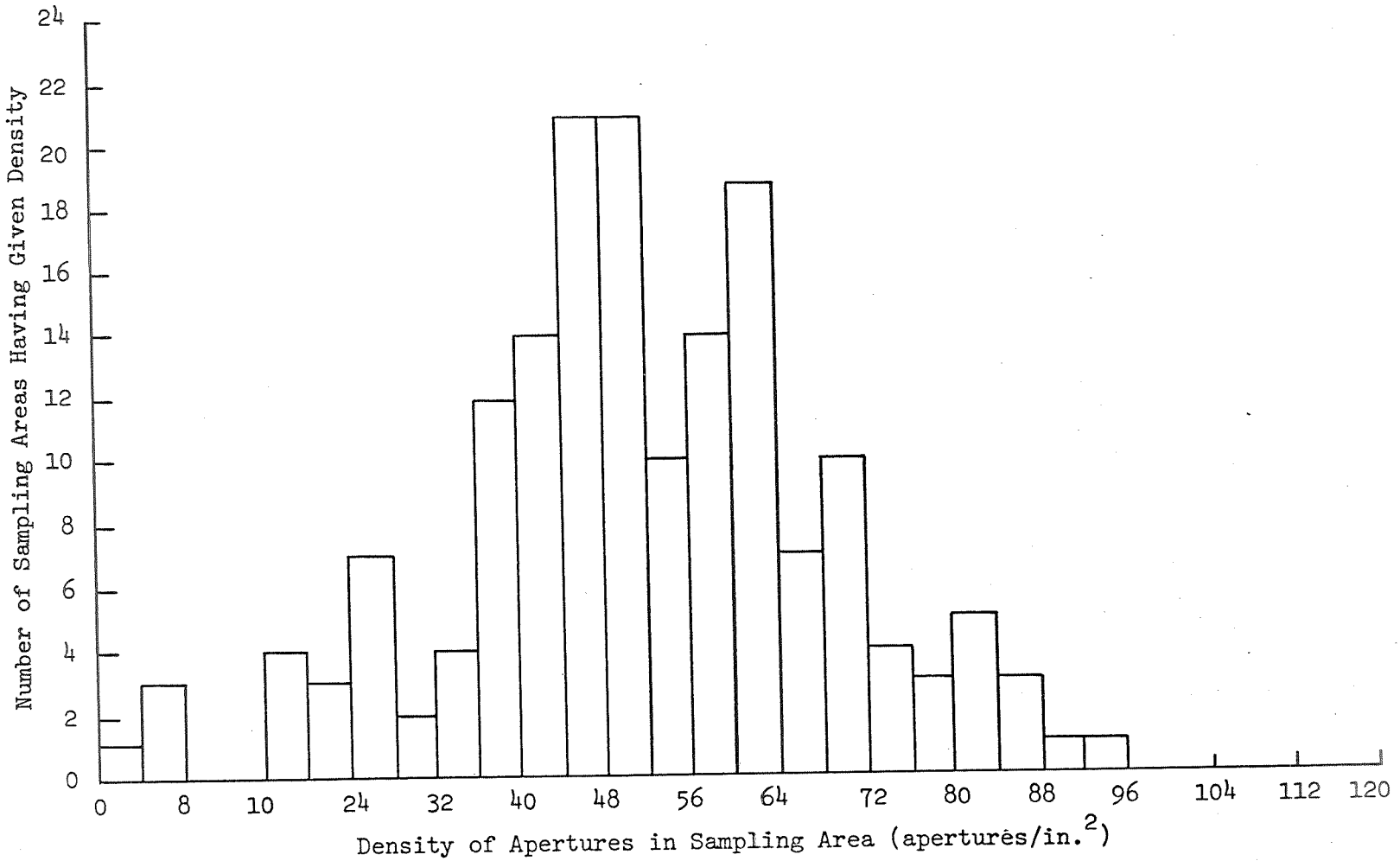

Figure 14

Density Distribution Characteristics of Apertures in Test Plate #5

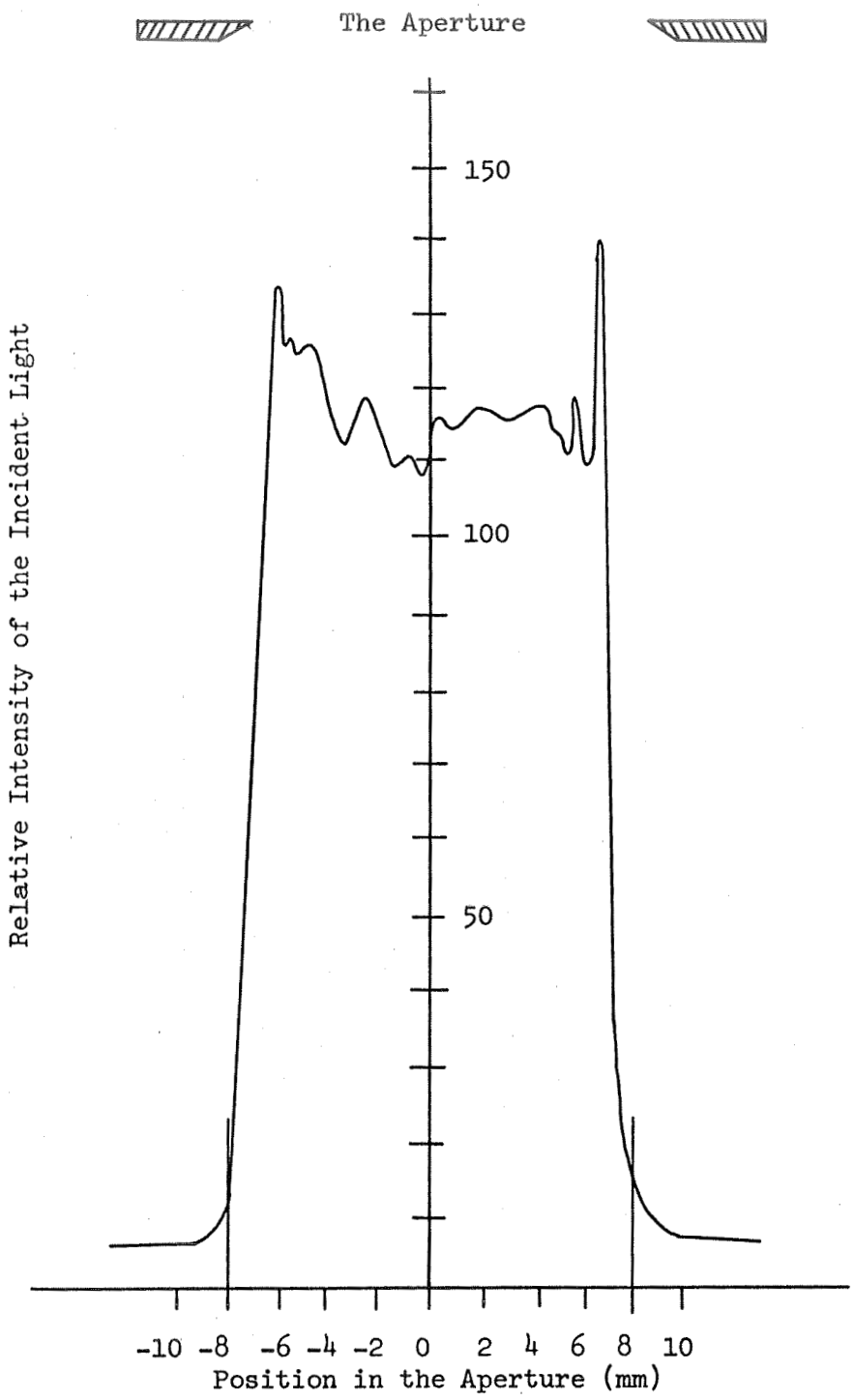

Figure 15

An Experimental Plot of Intensity Variations of the Incident Light at Different Positions on the Sample

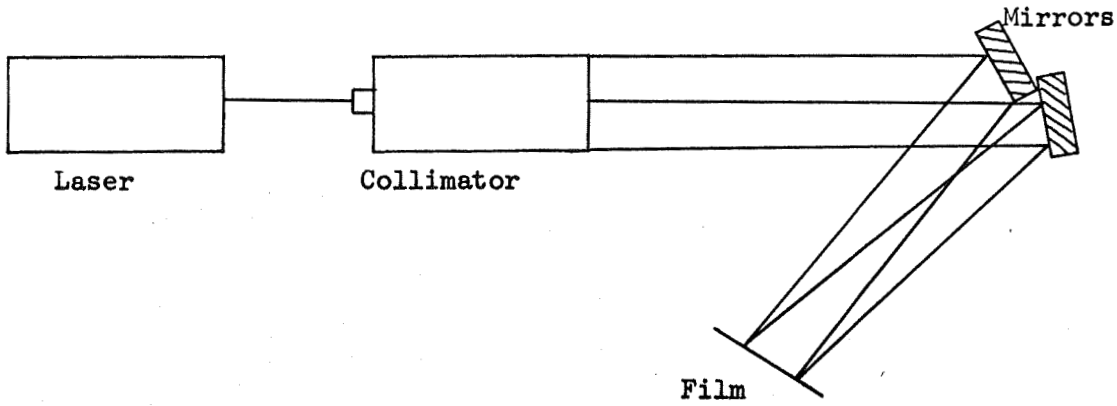

Figure 16

Experimental Arrangement for Making Gratings

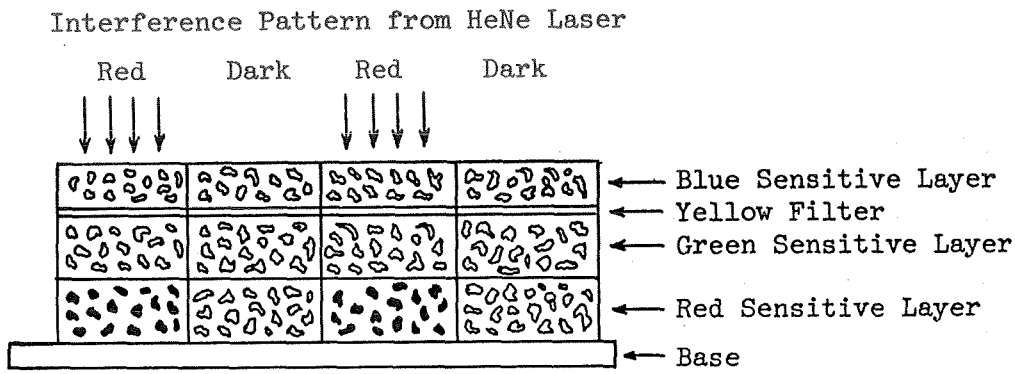

Cross section of color film after the silver halide grains exposed to the constructive interference lines have been developed

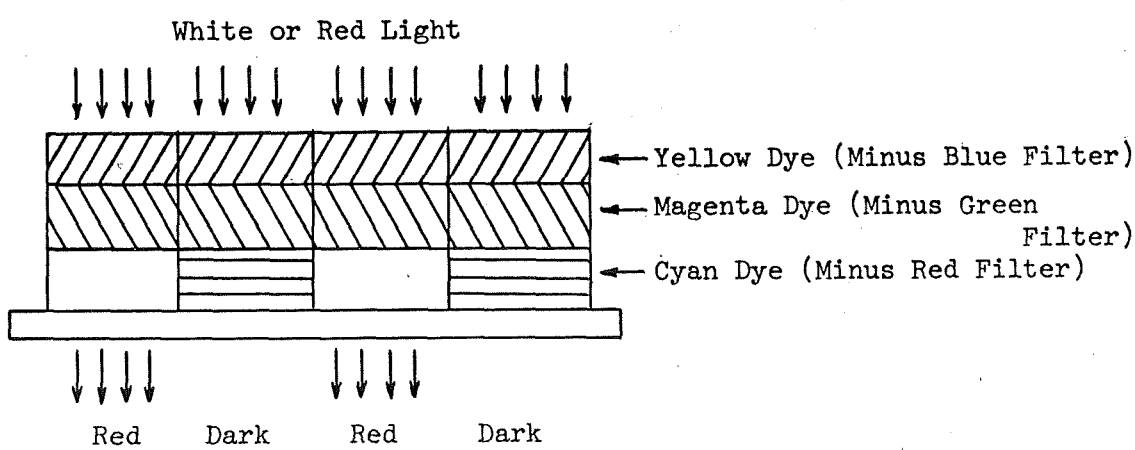

Cross section of color film after complete processing

Figure 17

A Properly Exposed Interference Pattern Recorded on Color Film

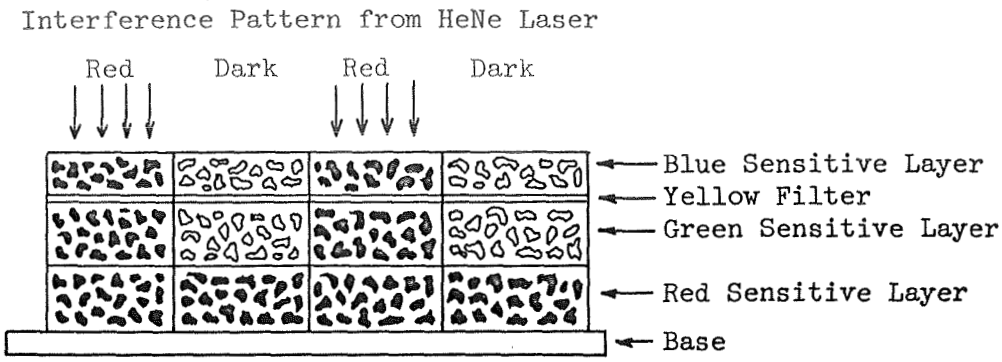

Cross section of overexposed color film after the silver halide grains have been developed

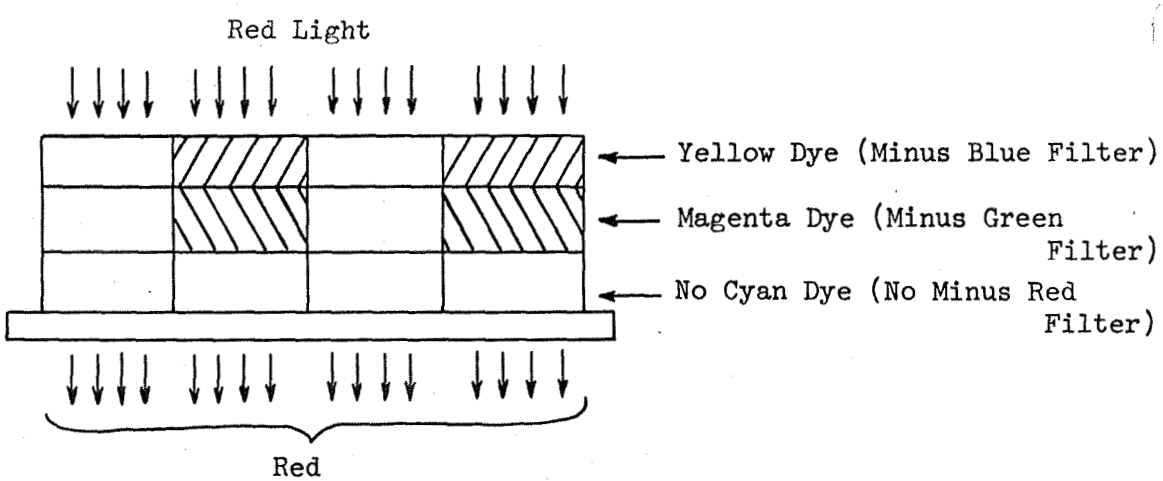

Cross section of overexposed color film after complete processing

Figure 18

Overexposed Interference Pattern Recorded on Color Film

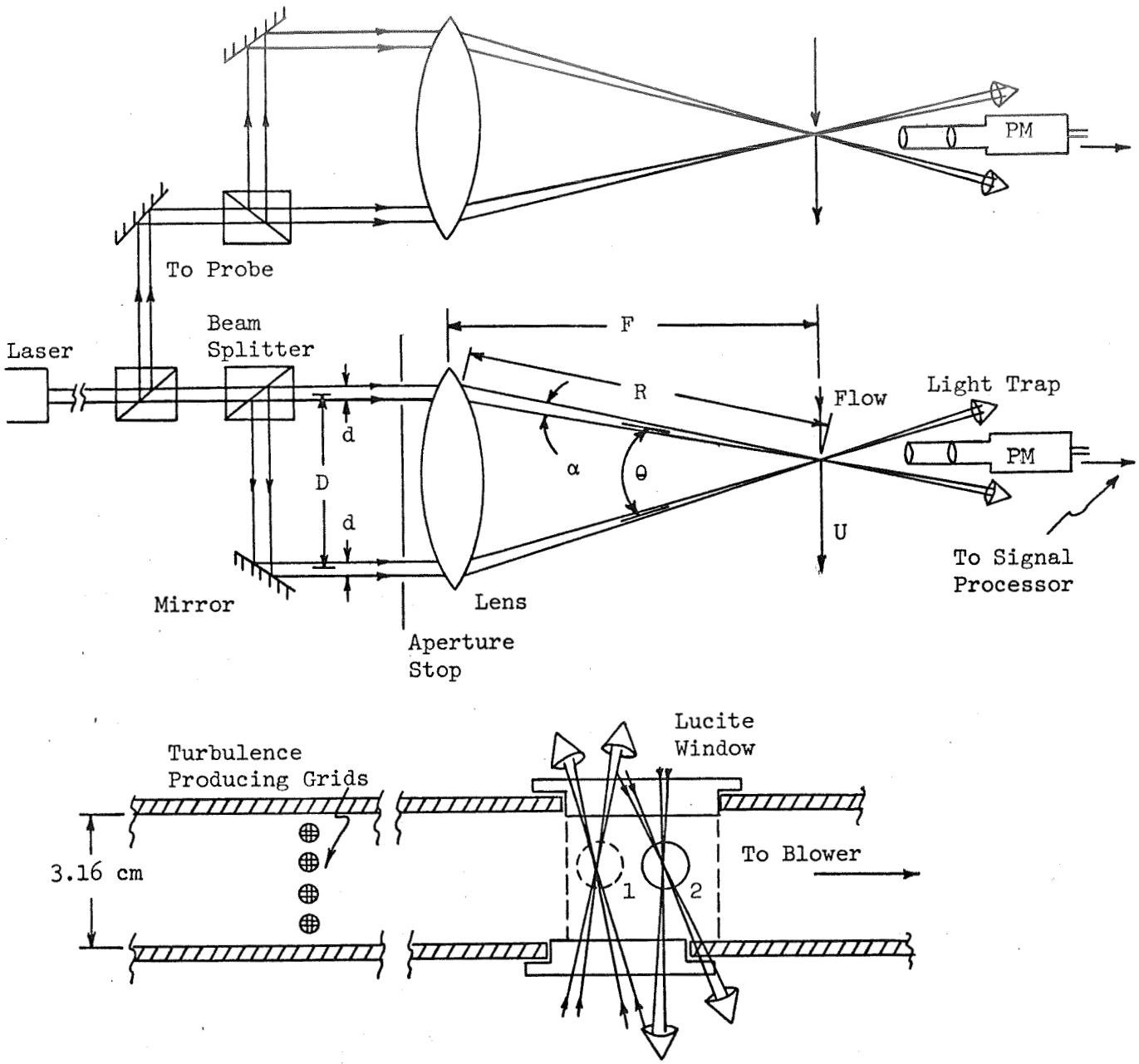

Figure 19

Layout of the Optical System

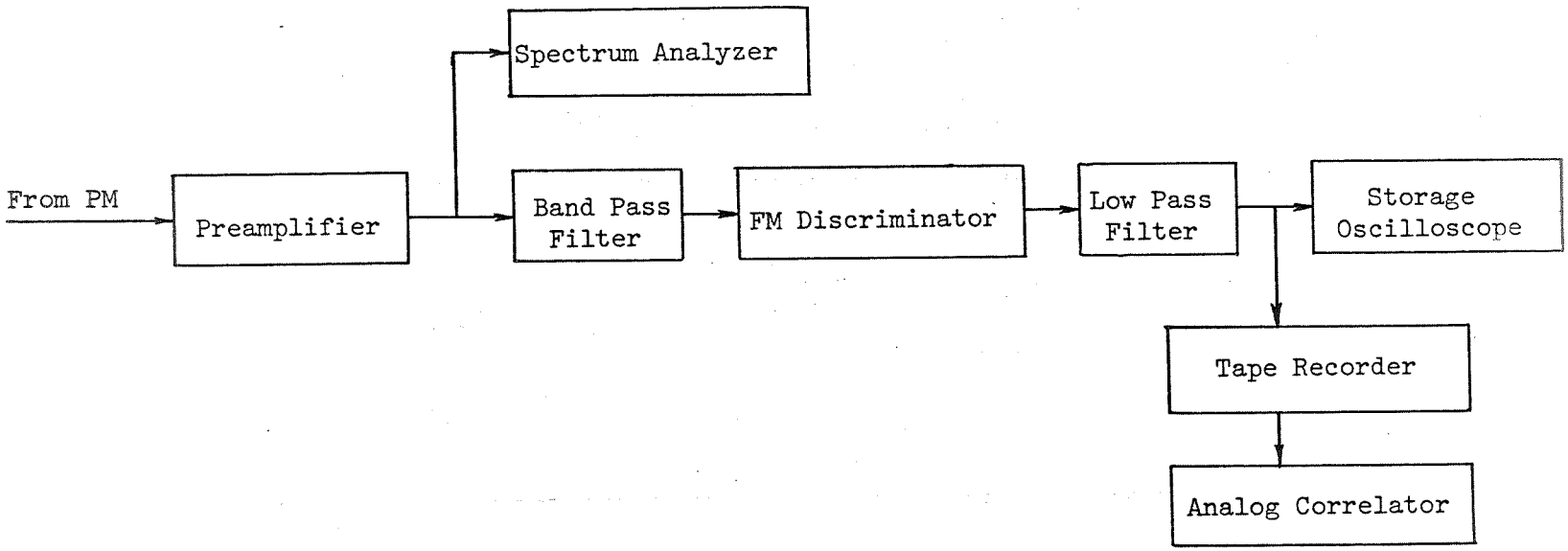

Figure 20

Present Arrangement of Electronic Processing Equipment

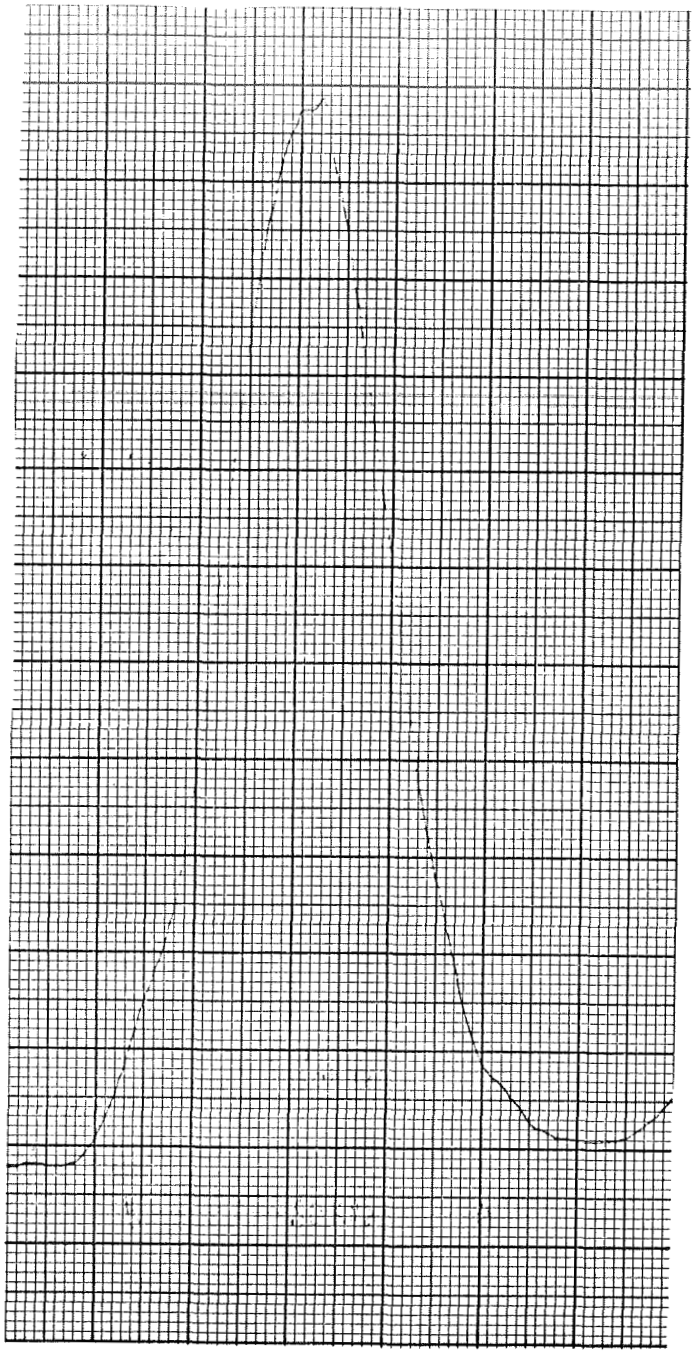

Figure 21

Laminar Flow (R_e = 632)

The frequency spread is entirely due to instrumental spread, most of it is from the spectrum analyzer itself.

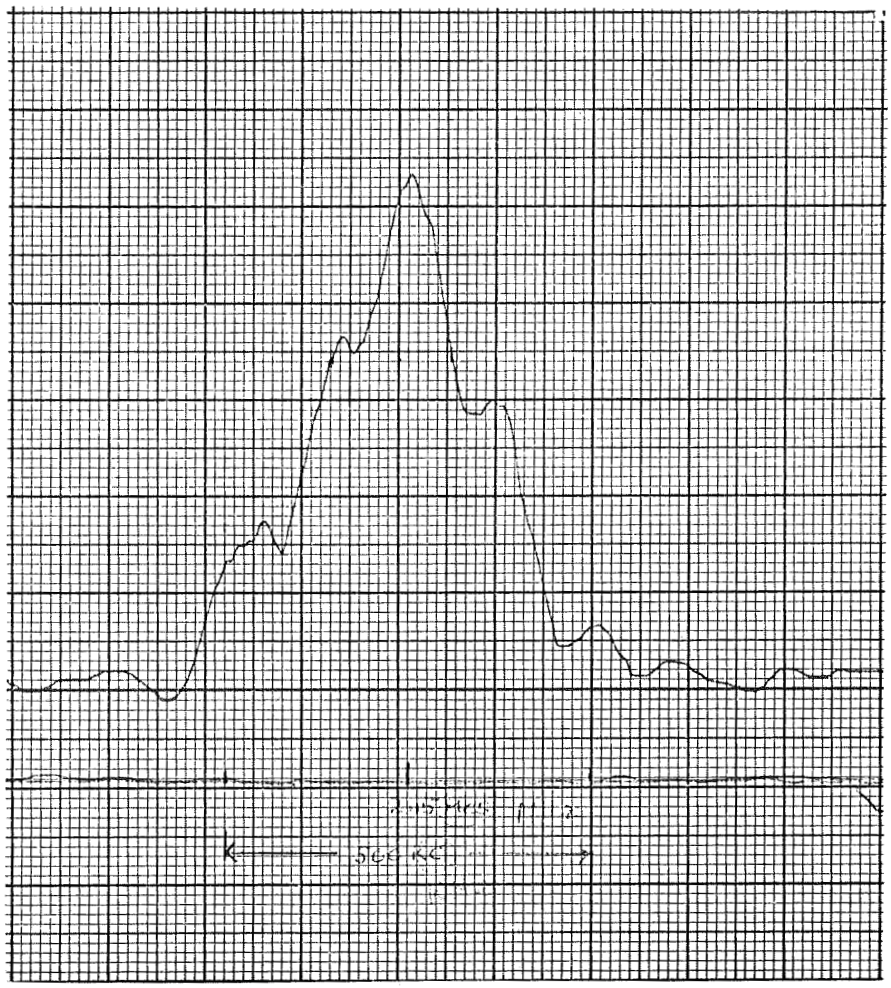

Figure 22

Turbulent Flow (R_e = 9800) Power Spectrum

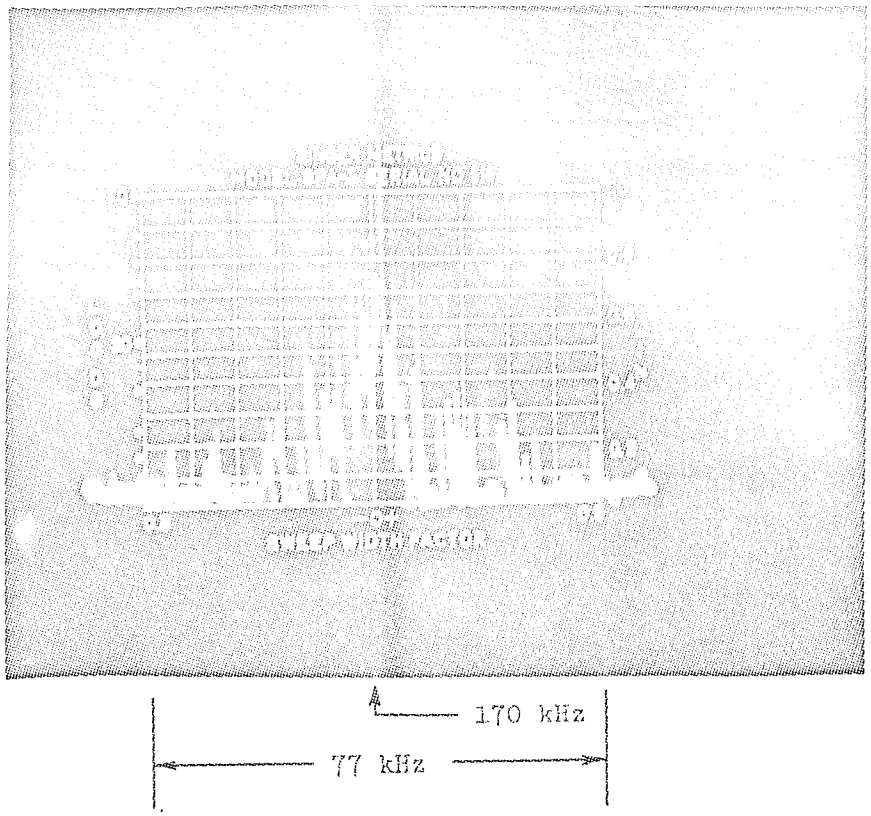

Figure 23a

Observed Power Spectrum of Fluid Flow, R_e = 762, $\bar{V}$ = 37.4 cm/sec

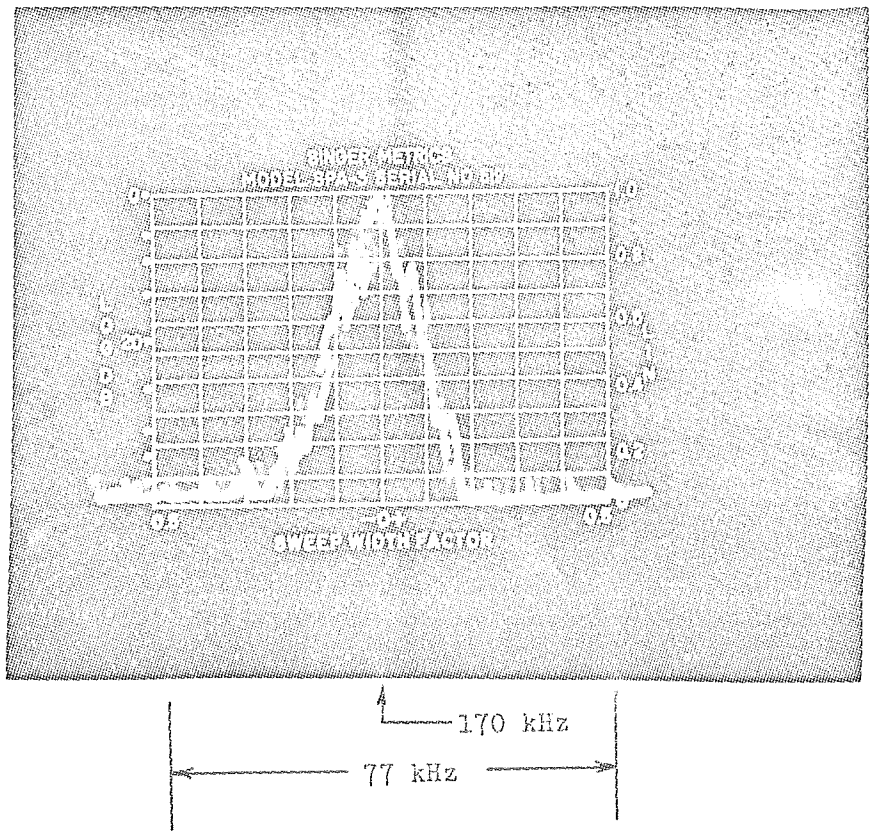

Figure 23b

Power Spectrum Obtained with Surface Scatterer, V = 37.4 cm/sec

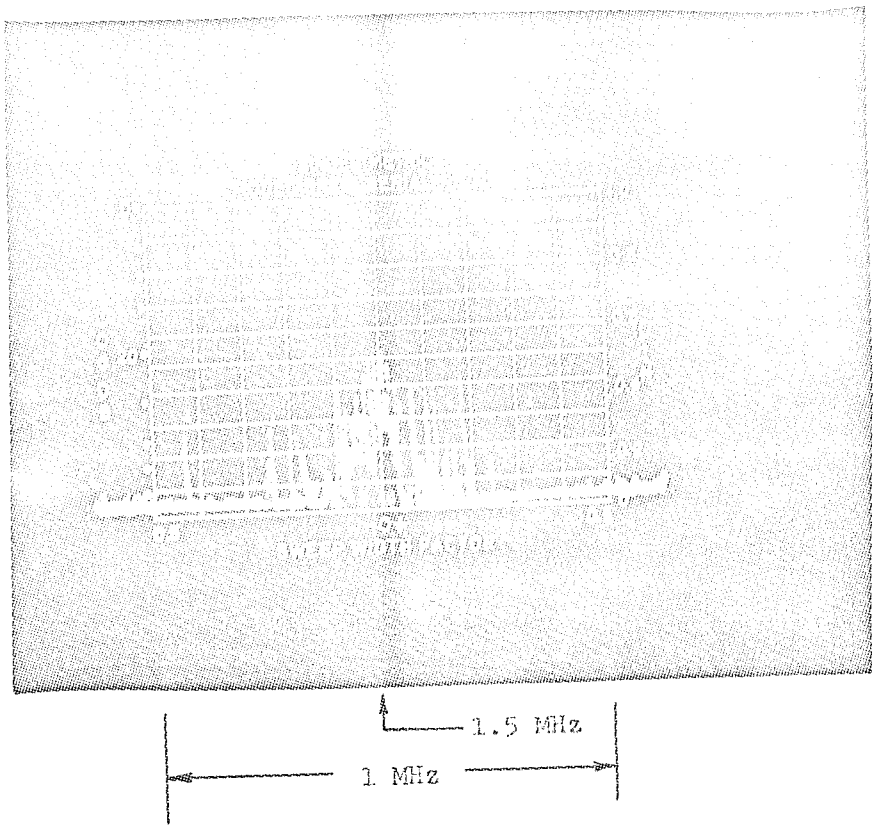

Figure 24a

Observed Power Spectrum of Fluid Flow, R_e = 5300, $\bar{V}$ = 332 cm/sec

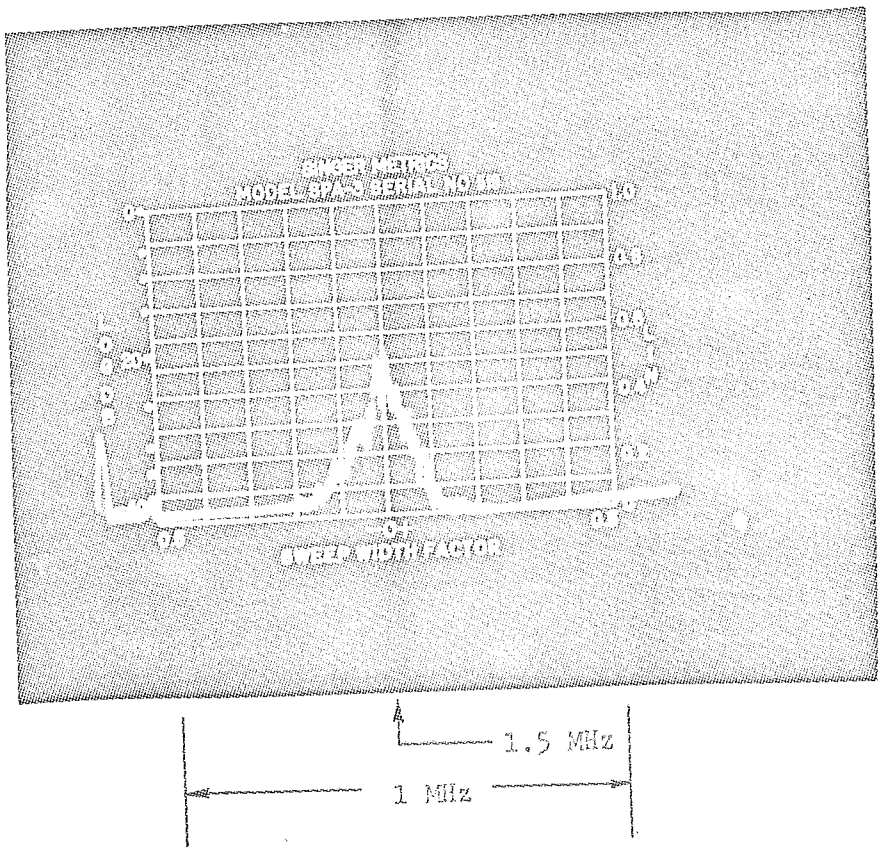

Figure 24b

Power Spectrum Obtained with Surface Scatterer, V = 332 cm/sec

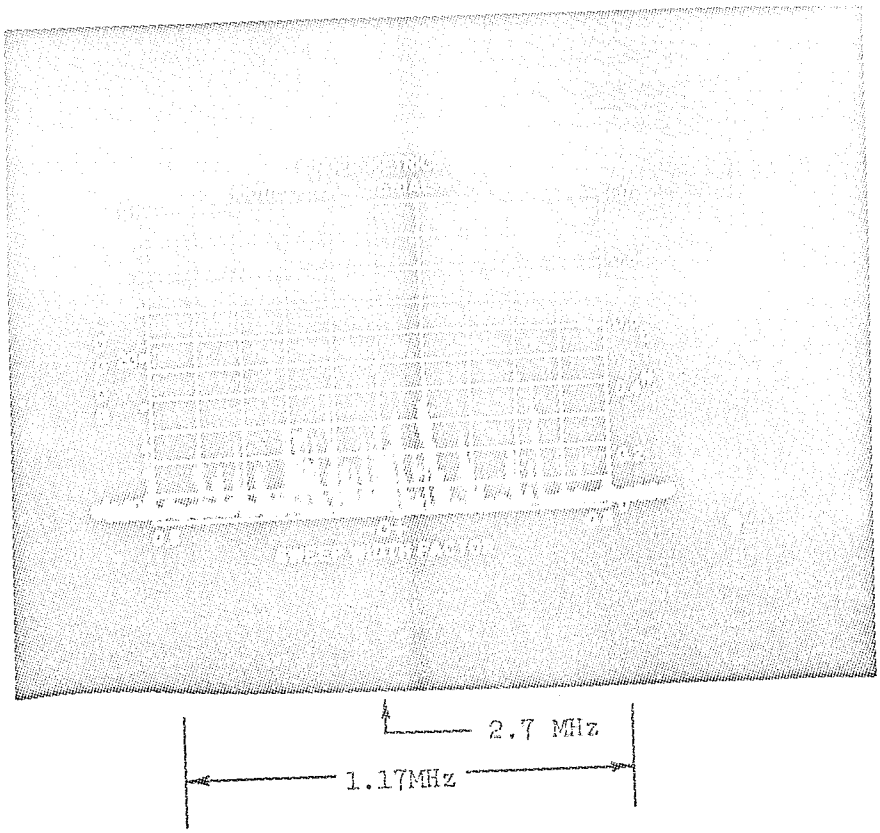

Figure 25a

Observed Power Spectrum of Fluid Flow, R_e = 10,600, $\bar{V}$ = 595 cm/sec

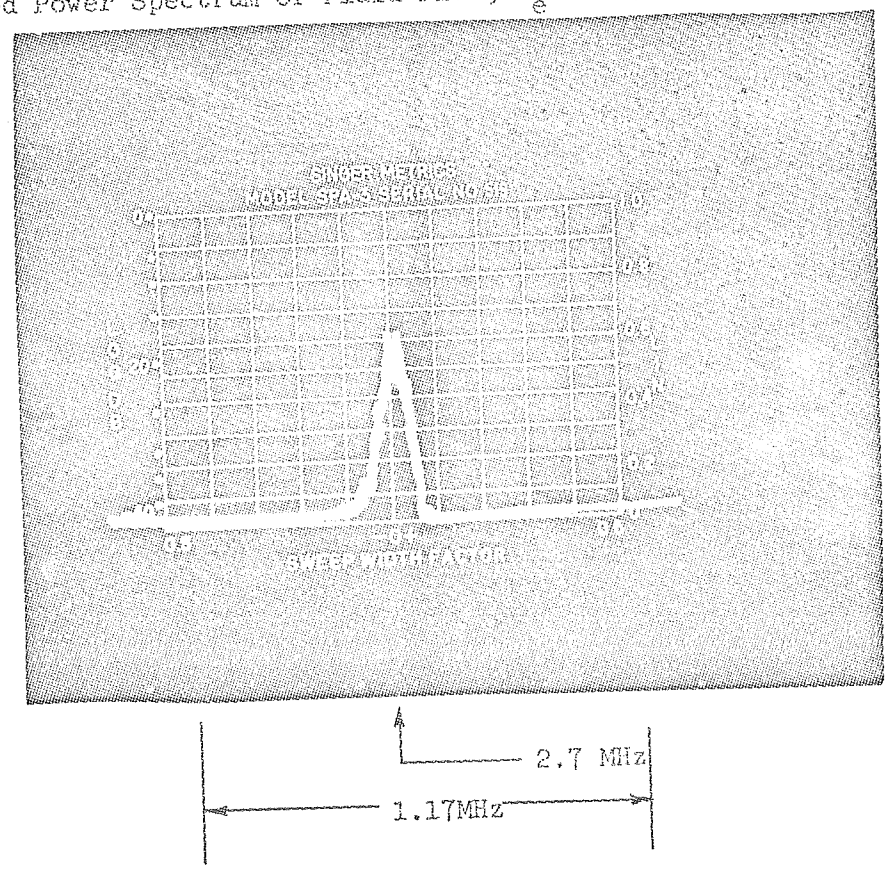

Figure 25b

Power Spectrum Obtained with Surface Scatterer, V = 595 cm/sec

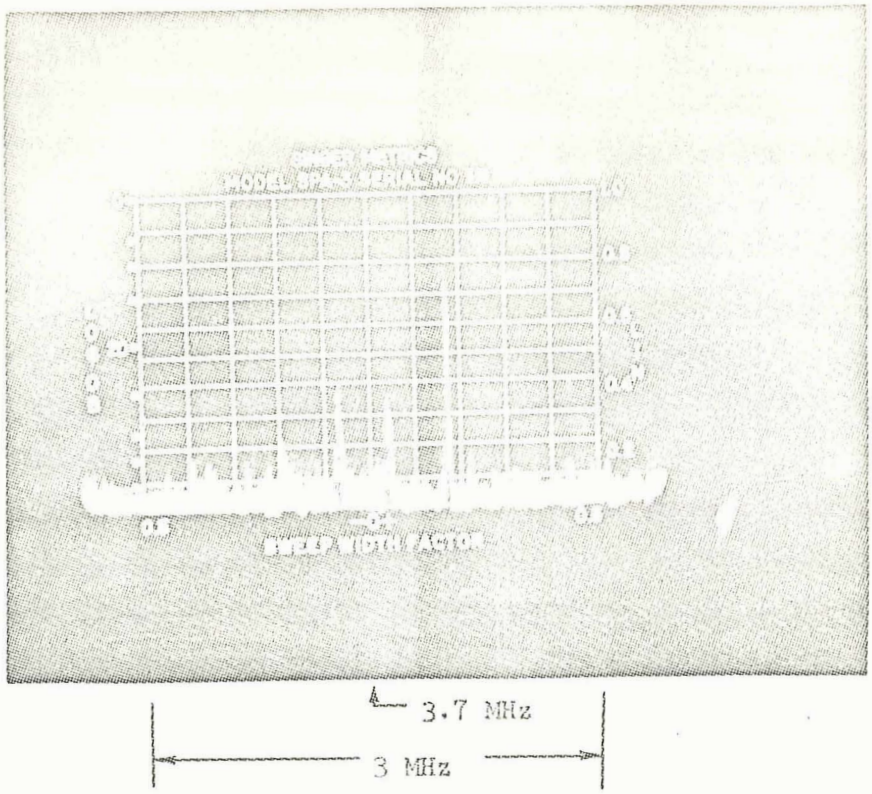

Figure 26a

Observed Power Spectrum of Fluid Flow, R_e = 16,600, $\bar{V}$ = 818 cm/sec

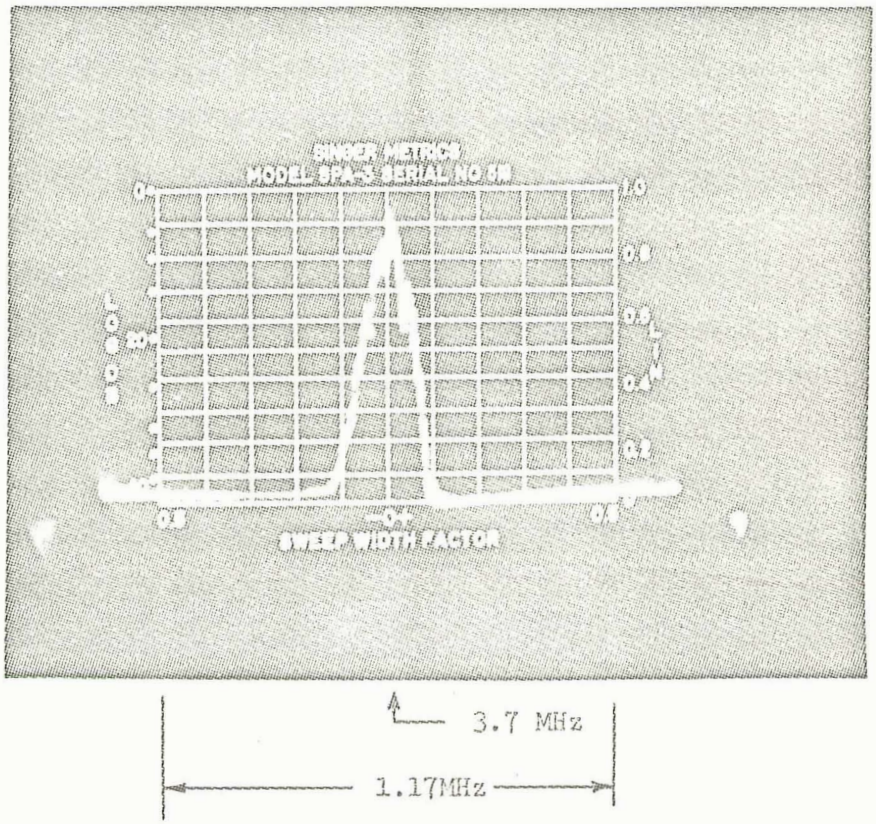

Figure 26b

Power Spectrum Obtained with Surface Scatterer, V = 818 cm/sec

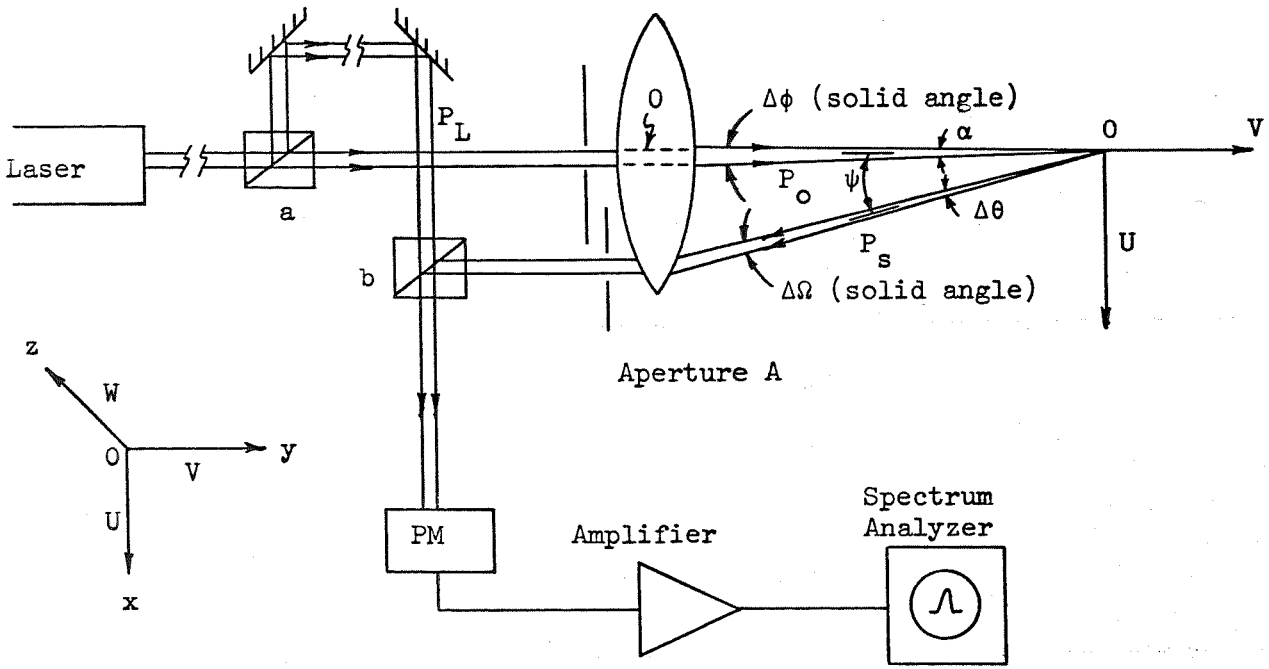

Figure 27

Local Oscillator Heterodyning

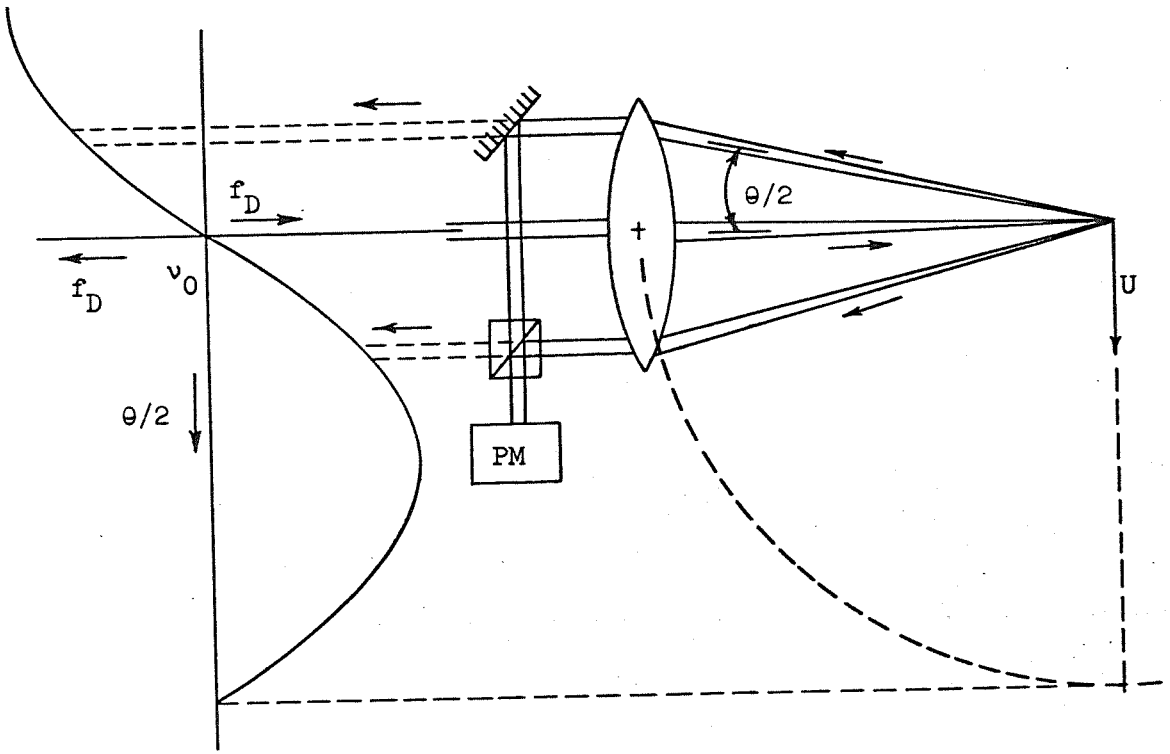

Figure 28

Elimination of Aperture Broadening by Superposition of Two Symmetrically Located Scattered Beams

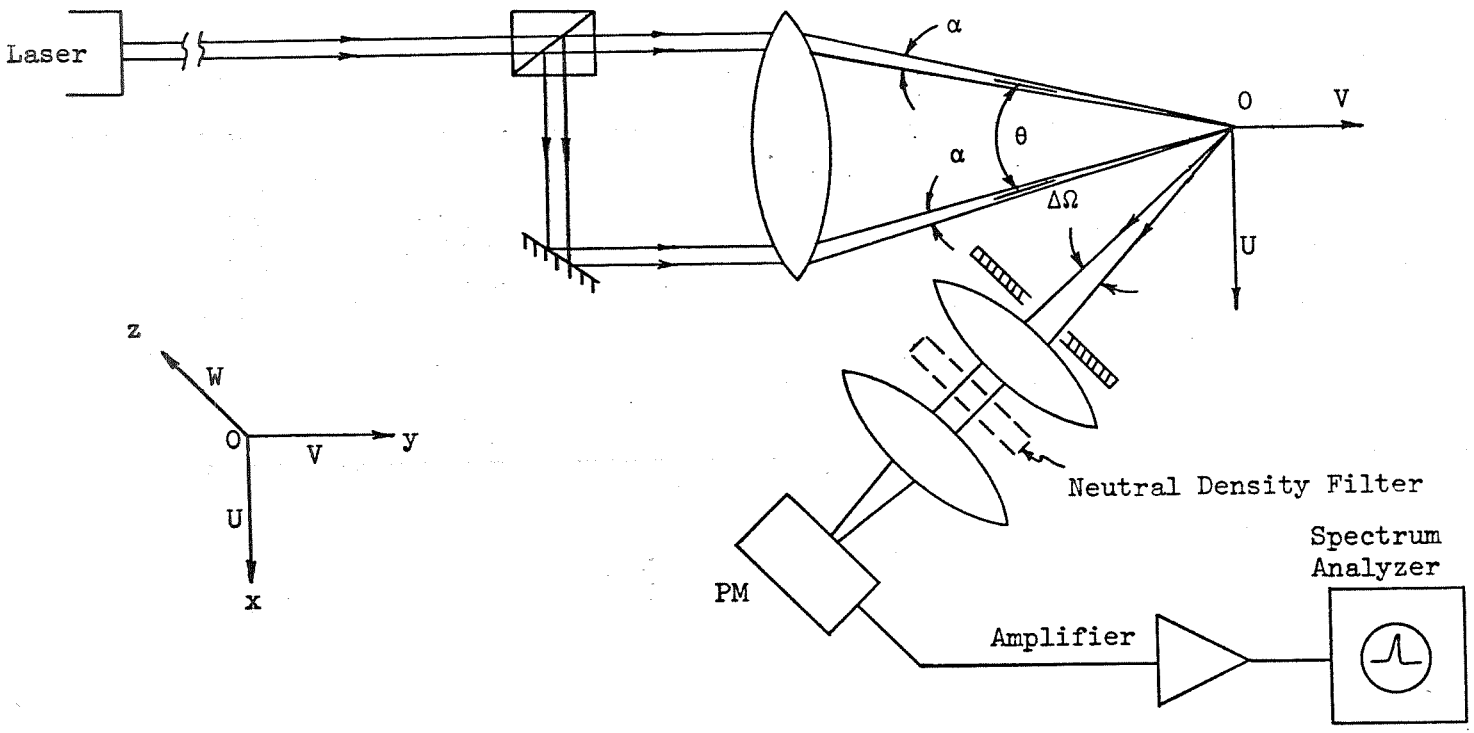

Figure 29

Symmetrical Heterodyning System

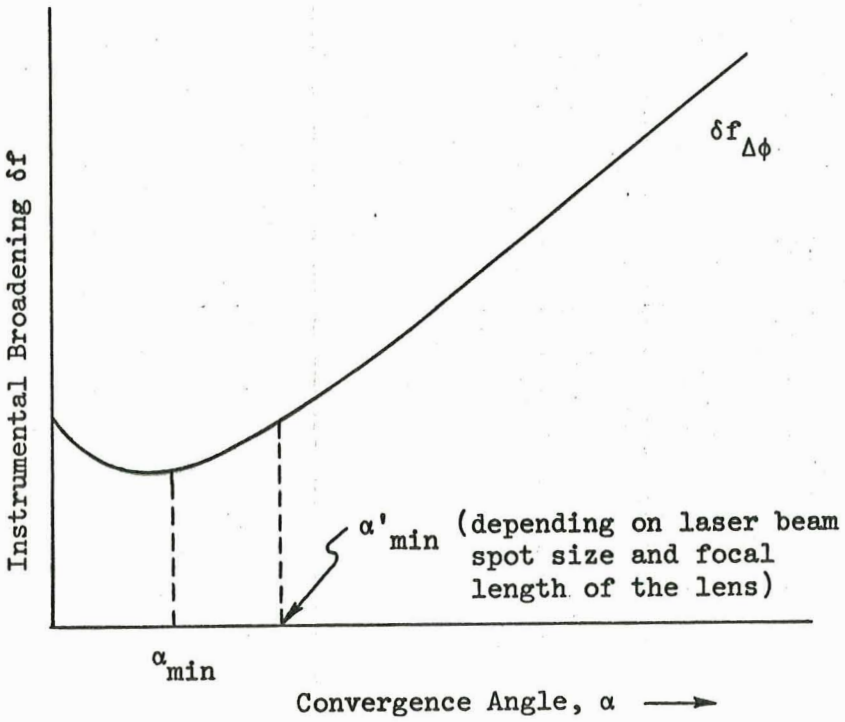

Figure 30

The Expected Nature of the Variation of Frequency Spread (δf) with Convergence Angle (α)

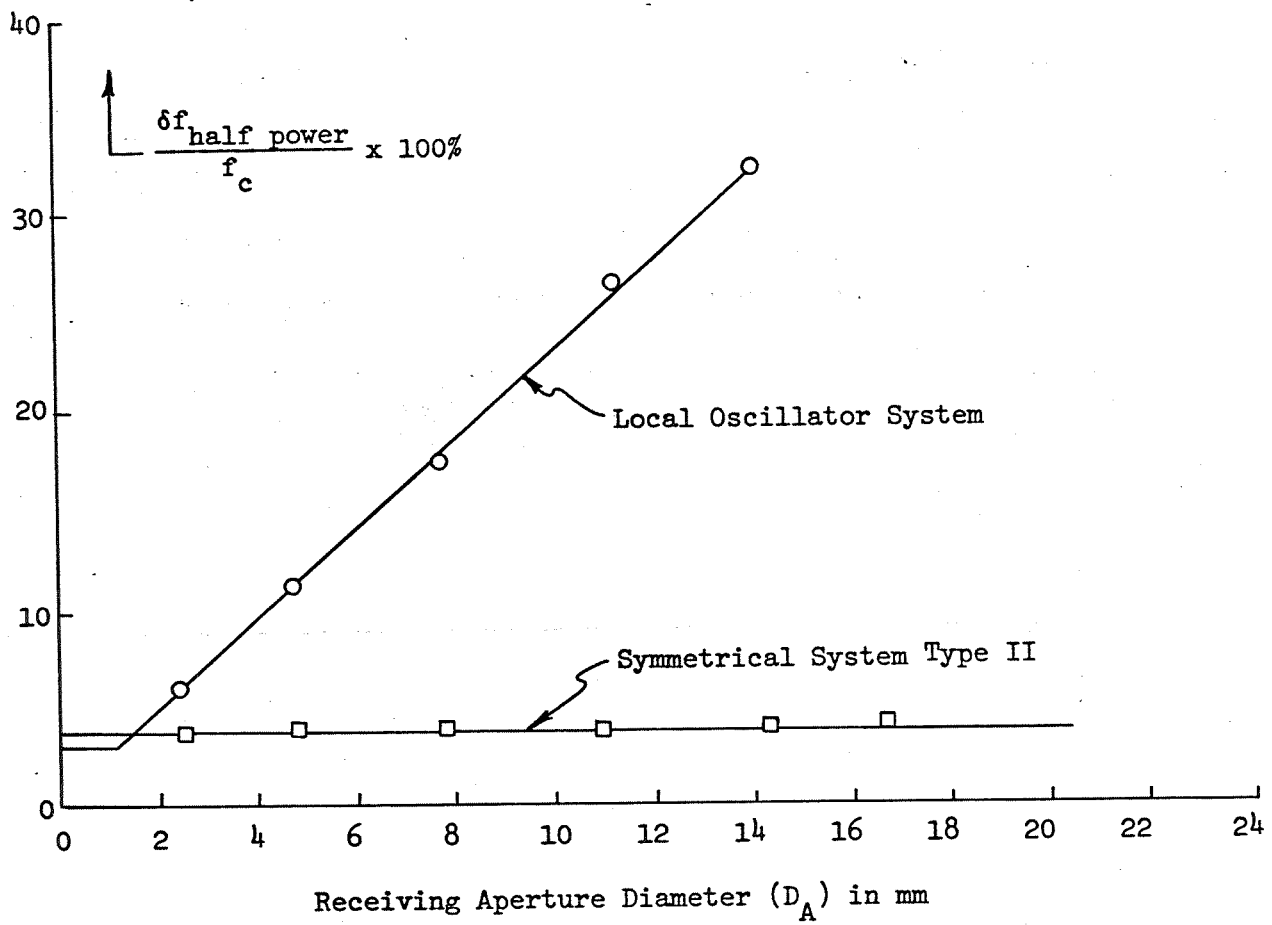

Figure 31

Instrumental Broadening (δf_a) Versus Receiving Aperture Diameter

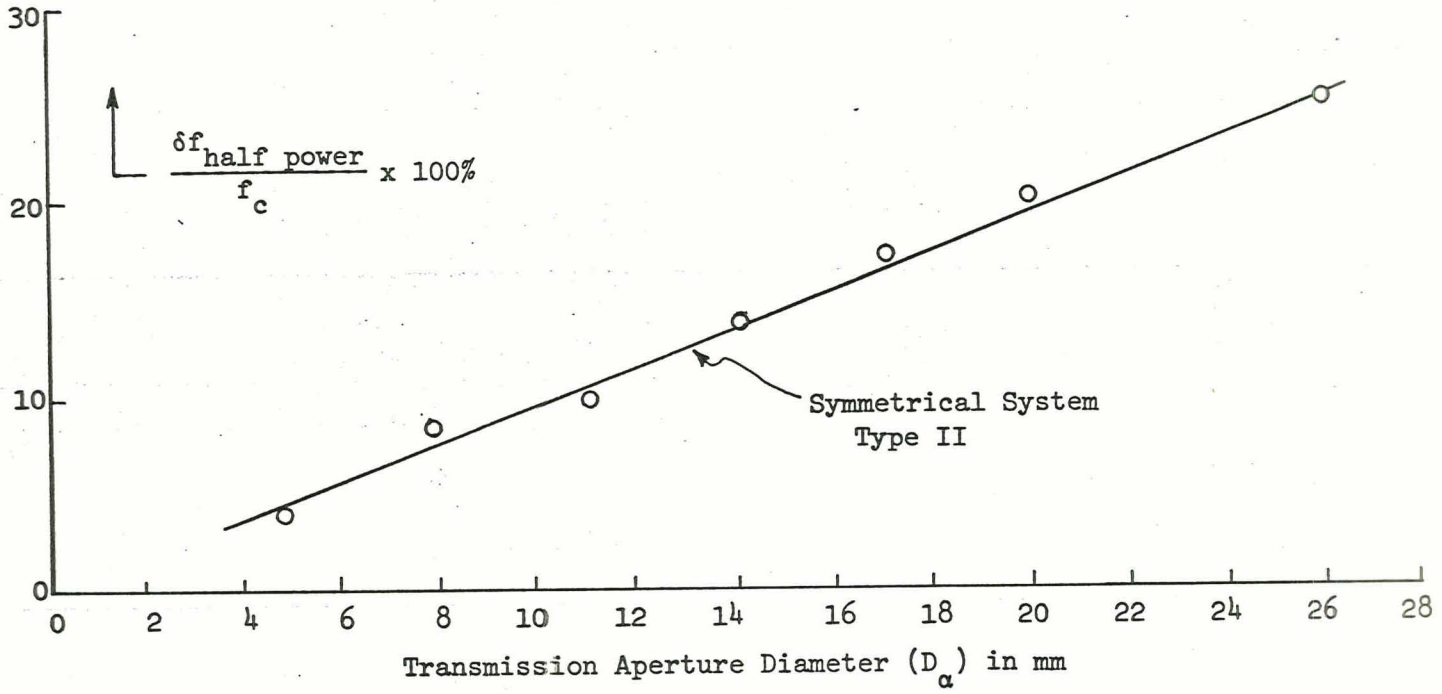

Figure 32

Instrumental Broadening (δf) Versus Transmission Aperture Diameter

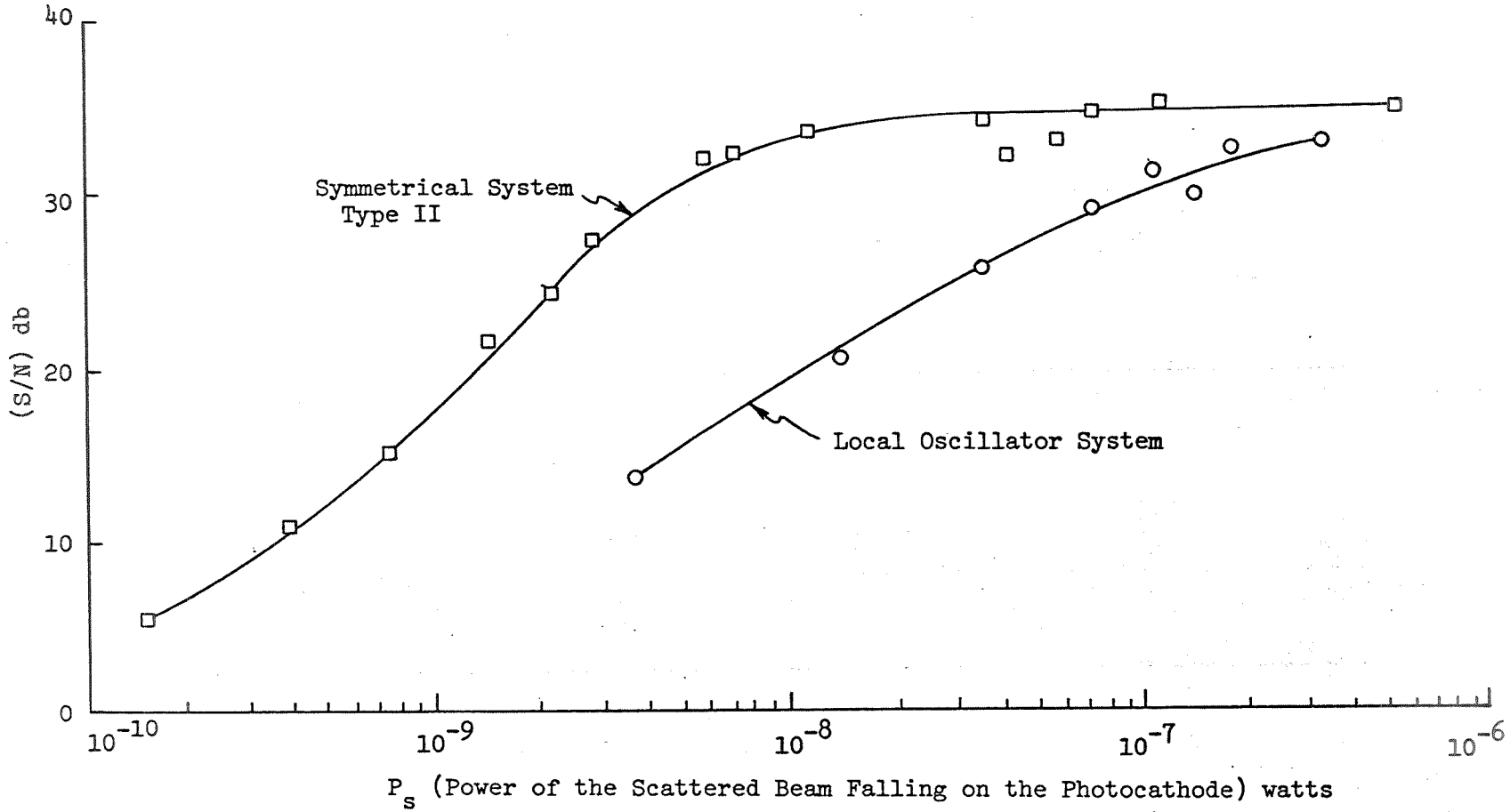

Figure 33

Signal-to-Noise Ratio Versus Signal Power for the Two Different Heterodyning Methods